Aspects of Two-Phase Critical Flow of Water in Short Nozzles under Flashing Conditions

by

Gordon M. Thomson, B.Sc.

Thesis presented for the degree of Ph.D.

Faculty of Engineering,

The University of Glasgow

November 1972.

ABSTRACT

The phenomenon of choking or mass limiting flows of two-phase mixtures is well known. The particular case of choking two-phase flow in which mass transfer takes place between phases is designated two-phase critical flashing flow, and has been the subject of many theoretical and experimental investigations.

In this work, experimental and theoretical studies are described for critical flashing flows of water at temperatures between 120 ^{o}C and 140 ^{o}C with maximum system pressures of 10 bar.

A simple model for turbulent heat transfer is developed from the Reynolds Flux model by introducing a second parameter into the descriptive equations. This revised flux model is adapted for prediction of rates of evaporation and condensation from the surface of water jets, exposed to large variations of surface pressure for short time intervals (of order 1 millisecond). The predictive equation, for evaporation rates, is shown to be applicable to experimental situations similar to these found in certain types of critical flashing flow.

A new model of critical two-phase flashing flow is developed using this method of predicting evaporation rates.

by comparison with experimental data, the model is shown successfully to predict rates of critical flashing flow of water, in nozzles, in cases where the flow is subcooled upstream of the nozzle entrance.

For the experimental tests, initially subcooled water at temperatures up to 140 ^{o}C and pressures up to 7 bar was discharged to atmospheric conditions through test nozzles. The choking condition was obtained by varying the upstream pressure while maintaining constant downstream conditions.

The test nozzles were metal with circular cross-sections and consisted of one of three simple forms of converging entrance before a parallel section at the throat. The nozzles formed a set having lengths of 50 mm, 75 mm, 100 mm and 125 mm for each of two throat diameters of 12.5 mm and 25 mm. Nozzles were made with three different entrances for each length and diameter. Data are reported for critical flashing flow rates of water in this set of nozzles. By using one single set of nozzles on the same apparatus, the effects of variation of critical flow rate with Length/Diameter ratio could be examined with greater certainty than has previously been the case for low pressure critical flashing flows. Pressure profiles of the flow within the nozzles are reported showing the variations of pressure profiles with nozzle length and entrance profile at the choked condition. Measurements of dissolved air in the water used in the experiments are also included.

The experimental data are compared with the assumptions made in deriving the theoretical model and with the predictions made from the theoretical model.

ACKNOWLEDGEMENTS

The work described in this thesis could not have been completed, without assistance from many sources.

In particular, the author wishes to record his thanks to Professor R. S. Silver, Mr. J. R. Tyldesley and other members of Staff, in the Department of Mechanical Engineering at the University of Glasgow, for their help, guidance and encouragement.

The author is grateful to Mr. I.D. Cameron, Superintendent of Engineering Services, and his staff in the Engineering Department Workshops for the construction of the experimental apparatus. Thanks are especially due to Mr. A. Ritchie for assistance in the operation of the apparatus.

The work was financed by the Science Research Council.

References

Annexe A - Previous papers incorporated in Thesis

Annexe A1 "Reynolds Flux and Danckwerts Surface Renewal Theory",
G.M. Thomson and R.S. Silver.

Annexe A2 "An Approach to the Calculation of Equilibration Rates in Flashing Flows",
G.M. Thomson.

Notes on Units, Notation and Organisation

These general notes are intended to explain the notation used in describing the various parts of the thesis.

Units The units used throughout are S.I. units, with certain exceptions. The unit of pressure of magnitude 100 kN/m^2 is designated as the "bar", and in many cases the centimetre has been used in preference to the millimetre. In many drawings of the experimental rig the dimensions are expressed in inches. These drawings are revised copies of those used in construction.

Designation of Figures etc. The numbers assigned to figures, tables, and photographs are defined as follows. The first number is the chapter number and the second number is the number of the figure etc. in the chapter. These second numbers are assigned serially and bear no relation to the section of the text to which the figure refers e.g. Fig 3.3 refers to section 3.5. The numbers of corresponding figures and tables or photographs may not correspond but they are normally physically situated together. Figures etc are placed at the relevant parts of the text, where possible.

Figures etc. in Annexes are not numbered.

Numbering of Equations. When an equation first appears in the text it is numbered serially in the chapter. This serial number is prefixed by the chapter number. If an equation appears in several chapters it retains its original number e.g. equation (3.10) appears in chapter 3 and chapter 4 as "equation (3.10)".

Notation The symbols used in the various equations to denote certain parameters are listed below. In general these are the conventional symbols, where the same letter is used for two different parameters in common practice e.g. ν for viscosity and specific volume, this practice is continued where no confusion could arise.

NOTATION

A = Area

C = Discharge Coefficient

C_D = Concentration

c_p = Specific Heat

D = Diameter

F = Friction Force

f = Friction Factor

G = Mass flow rate per unit area (Specific flow rate)

h = Heat transfer coefficient

h_{fg} = Enthalpy difference between liquid and vapour (at saturation)

K = Slip Ratio

k = Conductivity

L = Overall length (of nozzle)

Le = Lewis number

M = Mass transfer/unit time

$\dot{m}$ = Mass flux (Mass transfer/unit time per unit area)

P,p = Pressure

Pr = Prandtl number

$\dot{q}$ = Heat flux

R = Universal Gas Constant

r = Radius

s = Entropy

T = Temperature

t = time, (exposure time)

u = Velocity

W = Mass flow rate

x = quality

Y = distance (from nozzle entrance)

α = Voidage

β = Equilibration constant

δ = Entity size parameter

G = Mass flux (Reynolds Flux)

Θ = Temperature difference

ρ = Density

τ = Exposure time

$\phi(t)$ = Entity age distribution

ν = Specific volume, viscosity

Suffixes

C = Critical flow (sonic velocity)

D = For diffusion

E = Equilibrium value

f = For liquid phase

g = For gas phase

i = Instantaneous

o = At coordinate o (wall)

t,τ = At time t, τ

y = At coordinate y.

PREFACE

In this thesis experimental and theoretical studies of critical flashing flows of water will be described. The work is principally concerned with those mass limiting or critical flashing flows in short nozzles where the flow is subcooled liquid water upstream of the nozzle and is discharged to a region where the local pressure is less than the saturation pressure corresponding to the liquid bulk temperature. Within the nozzle or flow passage, mass transfer (flashing) takes place.

The study of such flows has considerable value both as a part of some general thermodynamic research programme and also as a contribution to that body of knowledge used by the engineering designer.

In the general research case; the problem of predicting rates of mass transfer between phases in flows of this type is not yet completely solved. This particular problem forms part of the more general problem of the prediction of rates of equilibration in flashing mixtures. Hence additional experimental evidence on these critical flashing flows offers further tests for any theoretical treatment of equilibration rates.

For more concrete engineering design problems, a knowledge of critical flow rates of flashing mixtures is often of considerable value. Typical examples of real situations in which critical flashing flows of initially subcooled water are found include such varied systems as feed-water heater drains, and certain types of soap flake production machinery. In these cases the maximum pressure in the system is only slightly greater than atmospheric and discharges are at pressures less than atmospheric pressure.

Over the last twenty years, much effort has been devoted to critical flashing flows of water and other fluids, to assist the design of safety mechanisms in nuclear reactors. In this case the flows are at high pressures and temperatures.

The work which follows has been principally orientated towards the problem as a part of the research programme carried out in the Mechanical Engineering Department of the University of Glasgow.

Chapter 1 - Introduction and Review of Previous Work

1.1 Introduction

This thesis describes an experimental and theoretical study of certain aspects of two-phase critical flashing flow. The work examines the limiting mass flow rate for the discharge of initially subcooled liquid from some vessel to a region where the local pressure is below the saturation pressure corresponding to the bulk temperature. In this particular work only the case of short nozzles of circular cross section is considered, for systems in which the maximum pressure is less than 10 times atmospheric. Short nozzles are defined here as those for which the ratio of overall length to throat diameter is less than 12.

The theoretical and experimental studies which form the main part of this thesis are presented from Chapter 2 onwards but in this first chapter some of the previous experimental and theoretical studies of other authors will be reviewed and discussed, thus illustrating the problems in making predictions for two-phase critical flashing flows. The next section is a brief presentation of the concepts most frequently used in discussing two-phase critical flows. These concepts are all used in the various references reviewed in sections 1.3 and 1.4 but in section 1.2 no individual attribution is given.

1.2 Two-Phase Flashing Flows

The problems which arise in the analysis of critical two-phase flashing flows are, of course, merely part of the difficulties experienced in the prediction of two-phase single component flows. These in turn form only a small part of the complex subject of two-phase flows. Thus the prediction of two-phase critical flashing flows are subject to many of the difficulties found in the prediction of more general two-phase flows.

Among the more important general effects frequently affecting the description of two-phase flows are the flow pattern of the phases and the velocities of the phases. Many aspects of the general problem have been reviewed by various authors, for example Wallis (1).

The development of this section begins by introducing simple two-phase flow equations.

For the case of uni-directional two-phase flow in any passage, general equations may be written, e.g.

Liquid Continuity $\quad W_f \nu_f = (1 - \alpha) A U_f \quad .....(1.1)$

Vapour Continuity $\quad W_g \nu_g = \alpha A U_g \quad .....(1.2)$

Momentum $\quad - A dp = d(W_g U_g + W_f U_f) + dF_w \quad .....(1.3)$

where A is the passage cross section for the flow

$\left.\begin{matrix}\nu_g \\ \nu_f\end{matrix}\right\}$ specific volume of $\begin{cases}\text{vapour} \\ \text{liquid}\end{cases}$ α void fraction - cross section occupied by vapour

$\left.\begin{matrix}U_g \\ U_f\end{matrix}\right\}$ mean velocity of $\begin{cases}\text{vapour} \\ \text{liquid}\end{cases}$ $\left.\begin{matrix}W_g \\ W_f\end{matrix}\right\}$ flow rate of $\begin{cases}\text{vapour} \\ \text{liquid}\end{cases}$

dF_w = Friction force on element at wall.

The total flow rate in the passage is $W = W_f + W_g$

$$W = (1 - \alpha) A \frac{U_f}{\nu_f} + \alpha A \frac{U_g}{\nu_g} \quad .....(1.4).$$

The total mass flow rate per unit area is denoted by G where

$$G = \frac{W}{A} = (1 - \alpha) \frac{U_f}{\nu_f} + \alpha \frac{U_g}{\nu_g} \quad .....(1.5).$$

A useful parameter is frequently used in the expression for G in place of the void-fraction (α). This is the quality (x) and is expressed as $x = \dfrac{W_g}{W_g + W_f}$. In many flow situations the quality is more easily found than the void fraction. Using equations (1.1) and (1.2) to express the void-fraction in terms of quality and substituting for α in (1.5), a new expression for the mass flow rate is found

$$G = \frac{U_f}{\nu_f} \left[(1 - x) + x \frac{U_f}{U_g} \frac{\nu_g}{\nu_f} \right]^{-1} \quad .....(1.6).$$

The ratio $\frac{U_f}{U_g}$ is greater than one for most flows and conventionally, this ratio is known as the slip ratio; denoted by K, i.e.

$$K = \frac{U_g}{U_f} \qquad \ldots\ldots(1.7).$$

Normally $K \geq 1$. Writing equation (1.6) with substitution for K.

$$G = \frac{U_f}{V_f}\left[(1 - x) + \frac{x}{K}\frac{V_g}{V_f}\right]^{-1} \qquad \ldots\ldots(1.8).$$

G is therefore expressed in terms of the quality, the slip ratio and the velocity of the liquid phase. The velocity of the liquid phase must be found in terms of the pressure gradient for a particular flow.

If $dF_w = 0$ in equation (1.3), as will be the case for flows at high velocities in short passages, then (1.3) may be written as

$$-dP = G\, d\left[xU_g + (1 - x)U_f\right]$$

$$\text{i.e.} \quad -dP = G\, d\left[U_f(xK + (1 - x))\right] \qquad \ldots\ldots(1.9).$$

From equations (1.8) and (1.9) it is clear that the prediction of two-phase flow rates requires a knowledge of, not only pressure gradients and densities of the phases as in the single phase flow case, but also of the quality and of the slip ratio. Further, in some cases, it may be necessary to have a knowledge of the flow pattern in order that any frictional effects can be assessed.

When the case of flashing flows is considered, the problem of prediction is further complicated. Consider the case of a two-phase mixture initially in a state of thermodynamic equilibrium between the phases. If this mixture is to flow through some passage, then it must be accelerated from rest by a pressure gradient. In these circumstances the local pressure may drop below the saturation pressure corresponding to the bulk temperature of the mixture. This is an unstable thermodynamic state and equilibrium can only be restored by a phase change which increases the vapour fraction in the flow.

The proportion of the liquid volume which must evaporate in order to restore thermodynamic equilibrium may be calculated, as for example by Silver (2).

Let h_{fg} be the difference in the enthalpy h_f of the liquid phase and the enthalpy h_g of the vapour phase at the same temperature and pressure.

The specific heat of the liquid at constant pressure is denoted by C_{p_f} and of the vapour by C_{p_g}. The difference between the saturation temperature and the bulk temperature of the mixture is ΔT.

Now the entropy of mixture of vapour and liquid with mass fraction x is

$$S = S_f + x\left(\frac{h_{fg}}{T}\right) \qquad .....(1.10).$$

Differentiating (1.10) and assuming no gain or loss of heat in the liquid vapour system. On rearranging terms.

$$dx = -\frac{\Delta T}{h_{fg}}\left[C_{p_f} + xT\frac{d}{dT}\left(\frac{h_{fg}}{T}\right)\right] \qquad .....(1.11).$$

Using the Clausius-Clapeyron relation to eliminate $\frac{d}{dT}\left(\frac{h_{fg}}{T}\right)$ in (1.11).

$$dx = -\frac{\Delta T}{h_{fg}}\left[C_{p_f} + x(C_{p_g} - C_{p_f})\right] \qquad .....(1.12).$$

If C_{p_g} and C_{p_f} are of the same order as is frequently the case e.g. for water substance, and the quality is low (say $x < 0.1$), then (1.12) may be approximated as;

$$\Delta x_E \doteqdot \frac{C_{p_f}\,\Delta T}{h_{fg}} \qquad .....(1.13).$$

where Δx_E denotes the change in quality if thermodynamic equilibrium is restored between the phases.

However mass transfer between phases proceeds at a finite rate and if the change in pressure on the mixture took place over a short time interval then the possibility exists that the phases will not achieve thermodynamic equilibrium. A metastable state of this type would be most likely to exist in a system with a high pressure gradient and flow velocity, and these conditions are those which are associated with critical flows.

The possibility of lack of equilibration can be allowed for by introducing a parameter β, the equilibration constant, defined by

$$\beta = \frac{\Delta x}{\Delta x_E} \qquad .....(1.13).$$

where Δx is the change in quality for the particular system. Clearly $\beta \leq 1$.

Certain parameters of the flow will affect the value of β for a particular system. Among these are, the pressure gradient and the velocities of the phases. β will also depend on the flow pattern, since the rate of vapour evolution will be partly controlled by the area of the surface between the phases. Thus any model of flashing flow must include either some assumption of flow pattern or assume complete thermodynamic equilibrium between phases at all points, an identical assumption to that of infinite mass transfer rate between phases. As an example of the effect of flow pattern consider a low quality flow. If the flow consisted of a very large number of small vapour bubbles dispersed in the liquid phase then the area of surface would be much larger than for a flow with the same quality but with the phases completely separated. Consequently, all other conditions being the same, the bubbly flow would have a larger value of β than the separated flow.

From the above discussion certain requirements for models of two-phase flashing flow can be identified. All such models will present the mass flow rate per unit area in the form of (1.8), and hence must include some prediction procedure for both quality and slip ratio. These quantities need not be correlated but if an equation of the form (1.8) is used to predict the mass flow rate then the effects of variations in these two quantities interact.

For any constant value of mass flow rate (G) in equation (1.8) there exists a set of differing pairs of values of slip ratio and quality, each pair predicting the same value of the mass flow rate. The variation of slip ratio required to predict a constant mass flow rate for varying quality is shown in Figure 1.1. Figure 1.1 shows the values of quality and slip ratio required to predict a constant mass flow rate for a steam-water mixture at a temperature of 100 ^{o}C and atmospheric pressure.

The effect on the mass flow rate of varying the slip ratio is shown in Fig. 1.2 for constant liquid phase velocity. From equation (1.8) it is clear

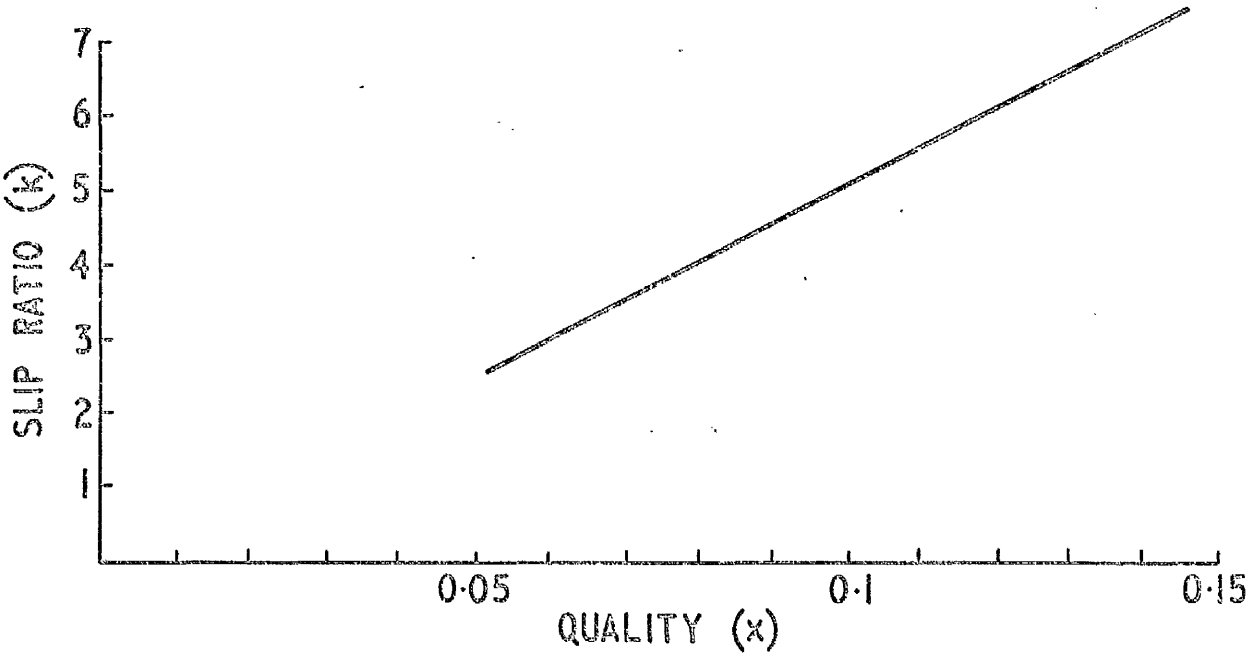

Fig. 1.1. Variation of slip ratio with quality for a fixed flow rate and fixed liquid velocity.

that under certain conditions the liquid phase velocity produced by some fixed pressure gradient will not vary greatly over a range of slip ratios. This is the case for low quality flows ($x < 0.1$) and Fig. 1.2 shows the variation of mass flow rate with slip ratio for the flow of a steam-water mixture at atmospheric pressure and 100 ^{o}C with a liquid phase velocity of 30 m/s, for a range of qualities.

Clearly from Fig. 1.2 variations of slip ratio will not greatly affect the value of mass flow rate for low quality flows, if the slip ratio always has values greater than 10.

An author proposing a model of two-phase flashing flow may use the interaction of slip ratio and quality shown in Fig. 1.1. together with the reduced effect of the slip ratio on mass flow rate shown in fig. 1.2 to overcome some of the difficultiesof predicting quality and slip ratio.

The authors of such models are normally attempting to produce theoretical predictions for the mass flow rates in some flow system and compare these with observed experimental values. If a value of quality is chosen which is higher than the experimental value in the real flow (for example by assuming thermodynamic equilibrium between phases) then the theoretical model should underpredict mass flow rates if the slip ratio is correctly predicted, but this underprediction can be overcome by choosing some increased value of the slip ratio. Further if the quality is correctly predicted an error in prediction of the slip ratio will not greatly affect the prediction of the mass flow rate.

Although this work is concerned with critical or mass limiting flows, discussion of mass limiting or choking mechanisms will be deferred until the presentation of theoretical models in section 1.4.

From the above discussion it is possible to identify a number of factors which require to be considered in any study of two-phase critical flashing flow, whether theoretical or experimental. These include:

(a) the variation of the quality of the flow and the effects of these variations on flow rates, especially cases of deviation from thermodynamic equilibrium between phases,

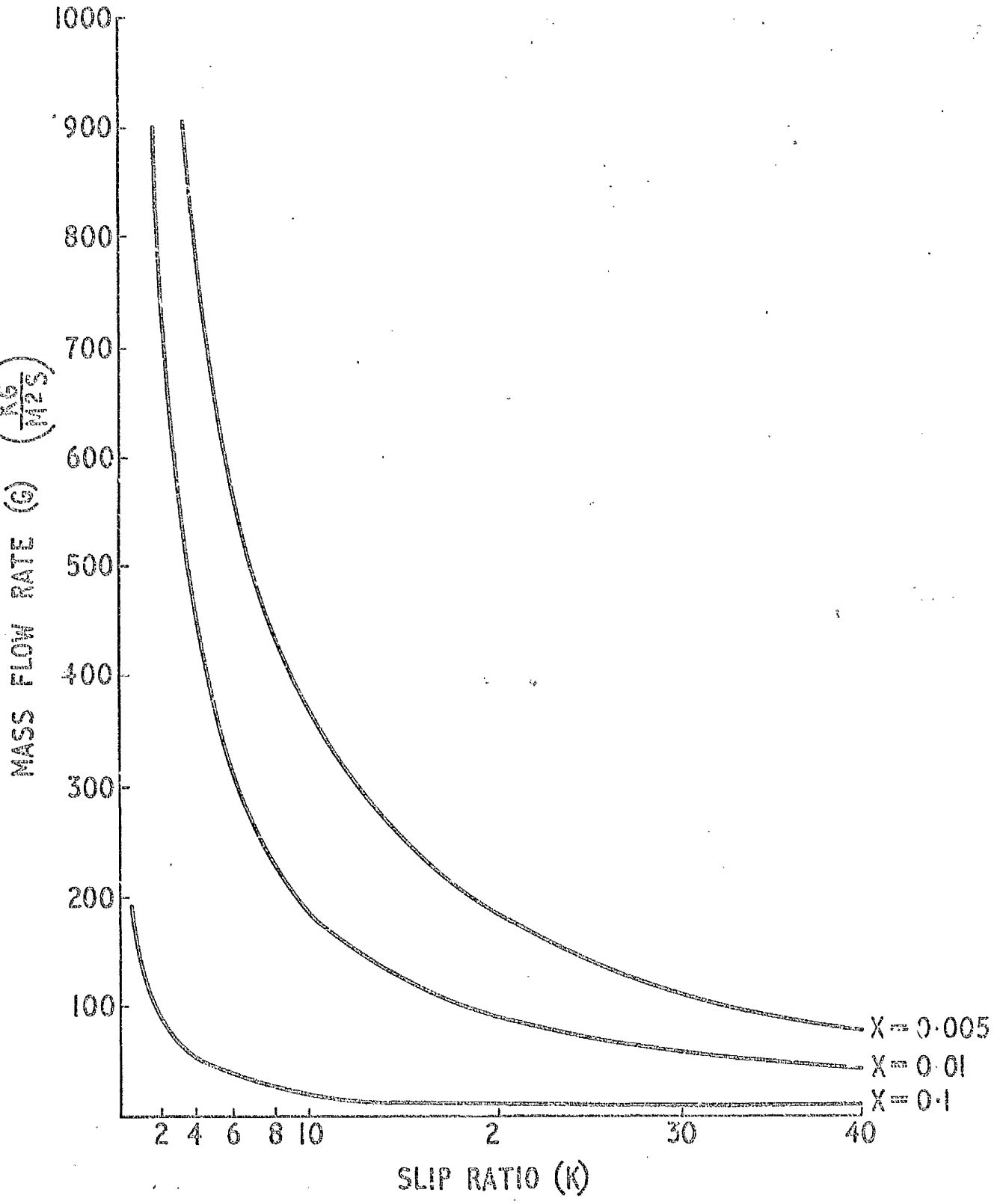

Fig. 1.2 Effect of slip ratio on mass flow rate. Water-steam at 100°c ($V_l = 30$ m/s)

(b) the velocities of the phases, and the slip ratio,

(c) the critical pressure and the mechanism for choking.

In the next sections various experimental and theoretical studies are discussed with particular emphasis on the three factors noted above.

1.3 Experimental Work

This section reviews various contributions to the volume of experimental data on two-phase critical flows in pipes and nozzles. Most of the studies reviewed used water as the experimental fluid but some studies have used other fluids e.g. various refrigerants, and even liquid sodium.

All experimental apparatus used for studies of this type may be generalised as consisting of two vessels interconnected by a test section.

One vessel is pressurised and used to heat the working fluid while the other is maintained at a pressure lower than the saturation pressure for the fluid temperature. When the working fluid is allowed to flow between the vessels the flow rate is found to increase with the pressure drop between the vessels up to a limiting or choking value, as shown in Fig. 1.3. However this pressure drop can be obtained in two ways: (a) by increasing the pressure in the upstream vessel, or (b) by decreasing the pressure in the downstream vessel. In investigations of single phase flows method (b) is normal, however studies of two-phase critical flow have been made using both methods, to obtain a choked condition, for example Silver and Mitchell (3) used method (a) while Zaloudek (4) used method (b).

One of the earliest studies of two-phase flashing flow was carried out by Bottomley (5) in 1936. Bottomley was concerned with the flow of water near boiling conditions through orifices, and as part of his research performed experiments of the maximum rate of flow of water from a short nozzle into a glass pipe. The water was held near to boiling at atmospheric pressure and discharged into a partial vacuum. These experiments showed that vapour bubbles did not form until a point some distance downstream from the nozzle although the pressure at the throat was reported as being approximately 0.6 bar.

This observation is consistent with a finite time for nucleation and

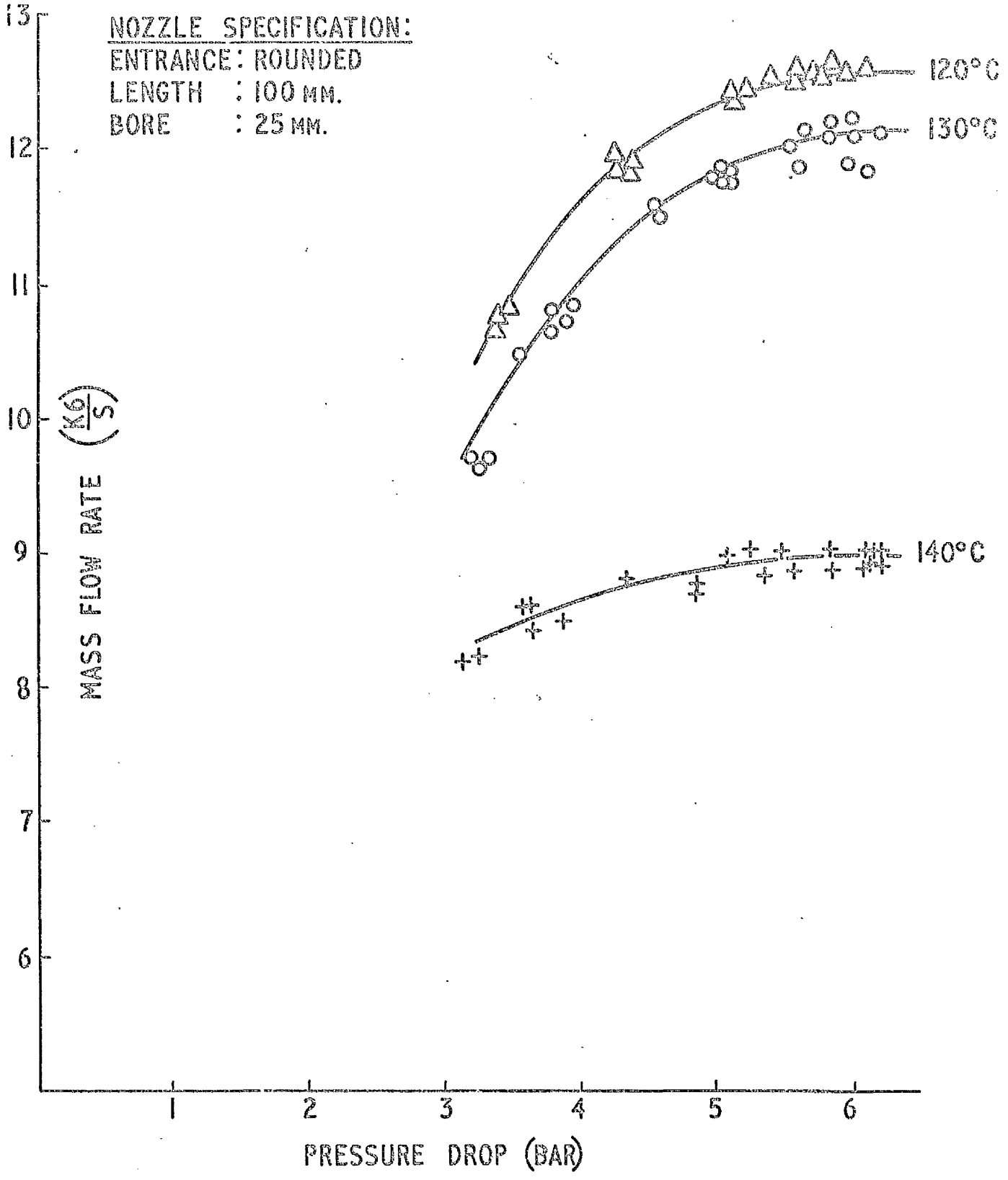

Fig. 1.3 Typical Variation of Mass Flow Rate with Pressure Drop.
[Exit Pressure – Atmospheric]

bubble formation but it does not necessarily imply, as Bottomley suggested, that no vapour formed in the nozzle.

Benjamin and Miller (6) & (7) continued the study of discharge of water through orifices obtaining results comparable to those of Bottomley. The authors also reported that if very small fractions of steam entered the orifice with the liquid then the maximum flow rates showed a considerable drop. Since from eqn. (1.8) the mass flow rate is inversely proportional to the quality of the flow this observation is consistent with there being a large voidage in the flowing mixture. Further this voidage is larger than the voidage upstream of the orifice implying that in this case at least some mass transfer took place between phases.

Stuart and Yarnall (8) examined the flow rates of water through two orifices in series discharging at atmospheric conditions. Once again bubble formation was observed to be delayed until some distance downstream of the orifices, the distance required for nucleation being observed to decrease with increased water temperature (indeed no nucleation was observed for water temperatures below 138 ^{o}C). Stuart and Yarnall also made measurements of the temperature of the liquid jet emerging from the second orifice. These temperatures were found to be considerably in excess of the saturation temperature corresponding to the pressure acting on the liquid surface. In one case this temperature difference was 50 ^{o}C for a saturation temperature of 100 ^{o}C.

Similar observations of high liquid jet temperatures were made by Cruver (9) in the critical flow of steam-water mixtures. Cruver made simultaneous measurements of temperature and pressure in such flows and observed both superheating of the liquid and subcooling of the vapour. In Cruver's work, however, some suspicion arises as to whether his measurements were always made in the phase stated, but in any event his results are worthy of comment.

The more general case of non-equilibrium in two-phase flows of water and steam has been examined by Christensen and Solberg (10). These authors compared experimental results for boiling water flows in an experimental nuclear system with a theoretical model and showed that the model gave good agreement with

experiment provided the model did not assume thermodynamic equilibrium at all points in the flow.

In these studies (5),(6),(7),(8),(9),(10) strong evidence can be found for the existence of metastability in two-phase flashing flows. These studies show that vapour evolution in such flashing flows could be retarded due to a delay in bubble formation. Studies of bubble formation in the static liquid case (11) show that bubble growth is delayed for a finite time after the liquid has become superheated. In the flashing flow case this implies that, provided no vapour bubbles already exist in the flow, vapour will not evolve in the form of bubbles until some distance downstream of the point at which the local pressure drops below the saturation value for the bulk liquid temperature. However this does not preclude the evolution of vapour as soon as the pressure drops below the saturation value, but vapour evolution will only take place at the free surface, if any, of the flowing liquid.

If, however, a small quantity of vapour is present initially, it will probably be dispersed in the form of small bubbles and bubble growth will begin without any delay for nucleation. Since a dispersed bubbly mixture has a much larger average surface area per unit mass than say a liquid jet then for similar flow situations the quality of the bubbly mixture will be greater at all points in the flow until both flows reach equilibrium. As the flow rate per unit area is affected by the quality, the presence of a very small quantity of vapour upstream of the flow passage will greatly affect the flow rate, giving a variation similar to that observed in (6).

Among early studies of the more specific problem of flashing flows in nozzles is the work of Silver and Mitchell (3).

Silver and Mitchell studied the discharge of water in short tubes ($\frac{L}{D} < 12$) with rounded entrances, (discharge coefficient 0.98). These authors reported limiting flow rates for water initially at a temperature of about 140 ^{o}C discharging to atmosphere through a vertical nozzle. They found that this maximum flow rate decreased for increasing nozzle length, for constant throat diameter. In these experiments the water temperature and downstream pressure

were fixed, for subcooled water at the nozzle entrance. If decreased flow rate implies increased quality of the flowing mixture, then these experimental observations are consistent with increased quality for increasing nozzle length, that is the phases approach thermodynamic equilibrium as the nozzle length increases.

Bailey (12) reported similar effects, and by assuming that the mean flow velocities of the phases were equal, calculated a rate of evaporation which predicted sufficient quality to produce the observed flow rate.

Further experiments of this type were performed by Zaloudek (4) for short nozzles with square entrances. In this study the pressure drop across the nozzles was varied by changing the downstream pressure. Zaloudek observed two flow limiting or choking processes, one apparently situated upstream near the entrance and the other situated near the nozzle exit. However upstream choking was observed only in cases when the pressure at the vena contracta was close to the saturation pressure while downstream choking was observed for larger pressure drops. In most cases of interest the pressure drops are much larger than those required for upstream choking and so this evidence would suggest that for such cases the choking phenomenon is located at the nozzle exit.

Zaloudek also commented on the effects of the presence of dissolved air in the water used in his experiments on the observed flow rates. By heating water in an open tank to 90 ^{o}C he claimed that he could reduce the content of dissolved air to give an increase of 5% to 8% in the resultant flow rates.

This study also included visual observations of the flow pattern, showing that the flow could be considered as a central core of liquid surrounded by an annulus of vapour. Similar flow patterns have also been observed in the studies of critical flow by Fauske (13) for water, Min, Fauske and Petrick (14) for Freon 11 and Hesson and Peck (15) for carbon dioxide. This annular flow pattern would seem to be characteristic for critical flows of initially subcooled liquid in short nozzles.

Fauske (14) carried out experiments on the blowdown of a large pressure

vessel for nozzles with square entrances and ratios of length to throat diameter of less than 40. ($\frac{L}{D} < 40$).

When considering the variation of both critical flow rates and of the ratio of the upstream stagnation pressure to the critical pressure over a range of length to diameter ratios, Fauske noted a difference in flow characteristics in nozzles with $\frac{L}{D} \leq 12$ when compared with flows in nozzles having $12 < \frac{L}{D} < 40$. He suggested that this might be due to a sudden bubble growth at a stage equivalent to a length diameter ratio of about 12 but presented no evidence tc support this hypothesis.

Comparison of the flow rates obtained in reference (3) with those of, say, reference (4) indicates a variation of critical flow rate with entrance profile. This variation was more fully examined and confirmed by Fauske and Min (14) using Freon 11 as working fluid.

Henry (16) made an investigation of the effects of exit shape on critical flow rates for steam-water mixtures and reported no observable variation. Henry also investigated the pressure distribution in the nozzle at critical flow by using an axial pressure probe, and detected a radial pressure gradient at the exit. His observations were generally confirmed by those of Klingebiel (17) for steam-water and by Edmonds and Smith (18) for Refrigerant 11, the latter study including some evidence for metastability in the flow, obtained from temperature measurements.

A number of attempts have been made to determine values of the slip ratio experimentally. Klingebiel (17) determined the average velocities of the phases in a steam-water critical flow by measuring the thrust of the expanding free jet on an impulse plate, obtaining values of about 3 for the slip ratio.

Measurements taken in the free jet, however, may be suspect when used to describe the slip ratio in an enclosed nozzle, since any expansion of the vapour in the free jet would give spurious low values.

Fauske (19) obtained values for the slip ratio in the critical flow of air-water mixtures. For qualities in the range 0.001 to 0.1 he found slip ratios of between 2 and 4. Fauske correlated the slip ratio with x by the relation,

$$K = 4.46\, x^{0.18} \left(\frac{V_g}{V_f}\right)^{\frac{1}{2}} \qquad .....(1.14).$$

However the flow pattern reported for these results consisted of air bubbles widely dispersed in the water instead of the separated phase flow patterns reported in references (4) (13) (14) (15). In a bubbly flow system of this type the vapour liquid interface is very large so that the shear stress due to different phase velocities acts over a large area. Therefore the velocity of the vapour phase will be lower than in the equivalent separated flow system with the same quality, giving a lower value of the slip ratio.

Measurements of the slip ratio in vertical flows of steam-water mixture by Cimorelli and Evangelisti (20), give values of the slip ratio in the range 5 to 6 for qualities from 0.005 to 0.001 for a bubbly flow pattern. Thus, because of the possible errors in the experimental values noted above, the slip ratio can be regarded as having a value not less than 3 for the low pressure flows discussed in this thesis.

In this section experimental evidence has been presented which suggests; that a number of noteworthy effects are present in critical flow phenomena. These effects can be summarised.

(1) A lack of equilibration is found in critical flashing flows in short nozzles. This is coupled with observations of vapour evolution taking place only at the surface of the liquid phase and not by bubble growth.

(2) The slip ratio departs from the value of unity and has values probably less than 10.

(3) Critical flashing flow rates are affected by the shape of the nozzle entrance but not the nozzle exit shape.

(4) Critical flow rates vary with the ratio of overall length to throat diameter for the nozzles considered.

In the next section various theoretical models, intended to describe these flow situations, will be discussed in the light of this experimental evidence.

1.4 Theoretical Models of Two-Phase Flashing Flow.

This section is concerned with various theoretical models of two-phase critical flows and their relation to the experimental evidence presented in section 1.3. Although this thesis lays special emphasis on flashing flows where the fluid upstream of the nozzle consists solely of the liquid phase certain of the models reviewed here are applicable to other two-phase critical flow situations.

All the models presented here make some assumptions to predict, quality at points in the flow, slip ratio, flow pattern and include a choking mechanism.

The simplest models assume that the phases are in thermodynamic equilibrium at all points in the flow and that the slip ratio is unity. With these assumptions the problem of defining flow pattern may be ignored since no shear stress acts on the surface between phases and the rate of mass transfer between phases is assumed to be independent of surface area. In these models the vapour phase is regarded as being uniformly dispersed throughout the mixture and consequently these are known as homogeneous equilibrium flow models.

In the case of a homogeneous mixture the specific volume of the mixture may be written in terms of the quality as

$$V = (1 - x)V_f + x\,V_g \qquad .....(1.15)$$

and the mean entropy as $S = (1 - x)S_f + x\,S_g$ .....(1.16).

For the homogeneous equilibrium model the critical flow rate is found by analogy with the single phase case. In the single phase case critical flow takes place in nozzles when the velocity of the fluid in the throat of the nozzle is equal to the sonic velocity. The critical flow rate is then given by

$$G_c^2 = -\left(\frac{dP}{dV}\right)_{s\,=\,0} \qquad .....(1.17)$$

by analogy a similar expression can be derived for the homogeneous mixture assuming adiabatic flow. Substituting for the specific volume in (1.17) from (1.15) the homogeneous equilibrium critical flow rate is found as,

$$G^2_{c_{HE}} = \left\{ -\frac{d}{dP}\left[(1 - x)V_f + x\,V_g\right]\right\}^{-1} \qquad .....(1.18)$$

The predictions of equation (1.18) have been shown to considerably underestimate the comparable experimental flow rates by several authors e.g. (21),(22),(23).

An obvious alternative to the assumption of complete equilibration is to assume that no mass transfer takes place between phases. This gives the frozen flow model. Chisholm (24) showed that this model would predict the critical flow rates of air-water mixtures provided the slip ratio was assumed to have the form of equation (1.14). Although Fauske (19) attempted to use a frozen flow model to predict the critical flow of steam-water mixtures his model assumed thermodynamic equilibrium between phases until the exit plane when he imposed the "frozen" condition. Fauske thus compensated for an assumed overestimation of quality by introducing a gross underestimation of rate of phase change at one point.

Both homogeneous and frozen flow models can show no variation of flow rate with nozzle length.

Various techniques have been used to improve the homogeneous equilibrium model. These improvements can be regarded as falling into two groups;

Firstly, models which assume some value of the quality less than the equilibrium value, usually by performing calculations of mass transfer rates between phases. Such models require estimation of the area of surface exposed between phases and frequently assume a value of unity for the slip ratio.

Secondly, models which assume thermodynamic equilibrium between phases but take the slip ratio as being greater than unity. In this case the values of the slip ratio will certainly be greater than the experimental values found in references (17), (19), (20), in order to compensate for an overestimation of the flow quality. Models of this type will not show any variation of critical flow rate with nozzle length.

Among models in the first category is that proposed by Silver (2). Silver assumed a flow pattern of liquid core and vapour assumption consistent with the observations of references (13), (14), (15), (16). The rate of mass transfer between phases was calculated from the rate of heat transfer to the liquid

surface in the liquid phase. In the calculation the nozzle was assumed to have a discharge coefficient of unity. Silver used the choking criteria of equation (1.17) and, assuming unit slip ratio defined the specific volume for equation (1.17) on the basis of a homogeneous mixture, i.e. equation (1.15) for his calculated quality. The inconsistency of using a choking mechanism applied to a homogeneous mixture in a model assuming separated flow was realised by Silver himself (25). However Silver's model did show very good agreement with the experimental results of Silver and Mitchell (3), for a nozzle with discharge coefficient 0.98. The model also predicted the variation of critical flow rate with nozzle length for a fixed throat diameter.

A similar model was derived by Bailey (12) also assuming unit slip ratio. Bailey calculated empirical evaporation rates from experimental results and assumed a flow pattern identical to that of Silver (2). Choking in this model takes place when the annulus surrounding the liquid core is entirely filled with vapour. Bailey was able to show agreement with data discharges of water from 98 ^{o}C and atmospheric pressure to sub-atmospheric conditions. Bailey's model predicts a decrease of critical flow rate with increasing length to diameter ratio.

More recently Henry and Fauske (26) have produced a non-equilibrium model for critical flashing flows in nozzles. The model is intended for use at high pressure and unit slip ratio is assumed. Non-equilibrium conditions are admitted by introducing a semi-empirical parameter N defined as

$$N = \frac{x_E}{0.14} \qquad x_E \leqslant 0.14 \qquad \text{.....(1.19)}$$

$$N = 1 \qquad x_E \geqslant 0.14 \qquad \text{.....(1.20)}$$

The parameter N is used to compensate for the departure of values of the quality from equilibrium values. Critical flow values are calculated from equilibrium values of common parameters by an iterative technique.

The authors found good agreement for nozzle flows including the general case with initially subcooled fluids but recognised that their model might be unsuitable for calculating critical flows in short nozzles where the unusual

separated flow pattern is found.

Simpson and Silver (27) proposed a model of flashing flow in which vapour evolves in widely dispersed bubbles. The authors assumed unit slip ratio. The equations for flashing flow in this model include two constants which are not defined analytically. These constants relate to the number of nucleation sites (A) and the activation energy required for nucleation (B). By choosing suitable dimensionless groups for comparison or by selecting suitable values for their constants the authors showed that their equations for mass flow rates could be made to show good agreement with the data of reference (3). The theory also predicts a limiting mass flow rate which decreases with increasing length of flow passage.

This theory is attractive but the authors produce no evidence for their assumption of vapour evolution in bubbles for flows of the type observed in (3) and in view of the evidence for delayed nucleation and flow pattern presented in section 1.3 of this work, this model of Simpson and Silver cannot be regarded as entirely satisfactory. However, the authors noted that the value for the density of nucleation sites required to fit their equations to the experimental data was too low, an observation consistent with the real flow having less surface area than would be the case for true bubbly flow and suggesting that the correct flow pattern would be the expected pattern of separated flow.

Although (27) is not satisfactory in the case of initially subcooled flows, it will apply to the case of a flow with initially a very small amount of dispersed vapour as in (6).

The second type of model assumes thermodynamic equilibrium between phases at all points, but uses some value of the slip ratio greater than unity to make the theoretical predictions conform with the experimental observations.

A model of this type due to Moody (28) assumes an annular flow pattern, with the liquid phase flowing on the nozzle wall, and thermodynamic equilibrium between phases. Moody obtained expressions for the mass flow rate in terms of the slip ratio and the stagnation properties of the fluid. The choking criterion is that both,

$$\left(\frac{\partial G}{\partial K}\right)_P = 0 \qquad \text{.....(1.21)}$$

and $$\left(\frac{\partial G}{\partial P}\right)_K = 0$$

hold at the choking condition. Moody obtained a value of the slip ratio at maximum flow rate as

$$K = K_M = \left(\frac{V_g}{V_f}\right)^{\frac{1}{3}} \qquad \text{.....(1.22).}$$

A similar value of slip ratio had been obtained by Zivi (29) by minimising the kinetic energy flow rate at the choked condition.

This model (28) overpredicts in the range of quality 0.01 to 0.5 and cannot predict the effects of increased nozzle length or of nozzle entrance shape.

An alternative derivation of the slip ratio appears in a critical flow model by Fauske (30) again assumes thermodynamic equilibrium between phases but uses as the criterion for choking

$$\left|\frac{dG}{dP}\right| = 0 \qquad \text{.....(1.23).}$$

By assuming a momentum balance condition with the additional assumption that the kinetic energy dissipation is the same in each phase, Fauske obtained a value for the slip ratio of

$$K = \left(\frac{V_g}{V_f}\right)^{\frac{1}{2}} \qquad \text{.....(1.24).}$$

The two values of slip ratio given in (1.18) and (1.20) will have similar values at high pressures for steam-water but at lower pressure the values predicted vary widely for most fluids (e.g. at atmospheric conditions for steam-water mixtures (1.22) predicts $K \doteq 11$ and (1.24) $K \doteq 40$).

Since the experimental data of references (17), (19), (20) suggest values of less than 6 for the slip ratio under atmospheric conditions. For steam-water and air-water mixtures, the form of slip ratio given in (1.22) is probably to be preferred. However, Moody (28) noted that the variation

in the predictions from his model, introduced by using the value of the slip ratio from Fauske [eqn (1.24)] were quite small, provided the choking criterion of eqn (1.20) was used.

The use of the choking criterion of eqn (1.21) for two-phase flows was originally proposed by considering the analogy with choking of single phase flows. In single phase critical flows, choking is held to take place when the flow velocities at the throat of the nozzle reach the sonic velocity of the fluid. The extension of this idea to two-phase flows has been noted previously but clearly this mechanism does not apply in the case of separated flows. Some authors, however, have suggested that choking takes place in separated flows, when the velocity of the vapour phase reaches the sonic velocity of the vapour for the relevant local conditions. One example of the use of this choking mechanism is found in the model of Stuart and Murphy (31).

This concept of vapour choking has been rejected by Fauske (30) and Zaloudek (32). Both authors have compared experimental critical flow rates with flow rates predicted by a vapour choking model which assumes thermodynamic equilibrium between phases. When a slip ratio of the form given in (1.24) is used in these models, such comparison with experimental results indicate that the velocity of the vapour phase is below the sonic velocity for all values of the quality less than one. However, the assumption of thermodynamic equilibrium and of the high value of slip ratio are both open to question, leaving the attractions of the vapour choking mechanism unaffected.

1.5 Chapter Closure

In the previous section a number of theoretical models of two-phase critical flow have been discussed and compared with experiment. Many of these models give impressive predictions of critical flashing flows, but for the particular case of critical flashing flows of initially subcooled liquid in short nozzles most of these models are inadequate. Among the inadequacies of the models reviewed are failures to predict the experimentally observed variation of flow rate with nozzle length or variation of flow rate with nozzle entrance profile.

The experimental work presented in section 1.3 covers a wide range of experimental situations and a large body of experimental data exists for two-phase critical flashing flows. For the case of two-phase critical flows at low pressures, however, the experimental data is not complete.

This thesis is, therefore, divided into two parts.

In the first part, a new model of two-phase flashing flow is presented. This model allows for all the experimentally observed variables, especially slip ratio and the existence of metastability. A new method of calculating evaporation rates, at short exposure times, is developed and applied to a separated flow model of two-phase flow.

In the second part, the results of experiments on two-phase flows are reported. These experiments were carried out for low pressure flows in a set of short nozzles.

Finally the experimental results and theoretical predictions are compared.

In the next chapter, the theoretical development begins with the presentation of a simple model for the prediction of heat transfer in turbulent flows.

Chapter 2 - The Reynolds Flux and Danckwerts' Surface Renewal Theory

2.1 Introduction

In Sections 1.4 and 1.5 the importance attached to the prediction of rates of mass transfer between phases in flashing flows was emphasised. One of the most important factors in determining these mass transfer rates is the rate of heat transfer in the phases. Since two-phase flashing flows are usually turbulent flows, some prediction mechanism for heat transfer in turbulent flows must be used if values for mass transfer rates between phases are to be included in a model of two-phase flashing flow.

The development of such a model for flashing flows will therefore depend on the model of the turbulent transfer process chosen and in this introductory section some simple theories for the prediction of turbulent transfer processes are reviewed, before the theoretical model used in this work is introduced.

Although in principle it might be possible to predict the properties of turbulent flows by analysis of the Navier-Stokes equations together with the relevant boundary conditions such a task is, at present, impractical for most worthwhile situations even with the development of modern methods of numerical analysis. Thus in the study of turbulent flows as in most other fields of theoretical analysis various models of differing complexity have been introduced.

Perhaps the earliest effective model of turbulent flow was due to Reynolds (33) Reynolds was able to relate convective heat and mass transfer by assuming that both processes were due to a lateral movement of fluid particles relative to the mean axial motion of the fluid. Thus Reynolds Theory describes turbulent transfer processes in terms of a single parameter, a lateral motion or flux. Reynolds also postulated that this flux could be described as consisting of "lumps" of fluid of greater than molecular size, or in Reynolds' words "non-molecular fluid particles". Unfortunately Reynolds' actual theoretical model was neglected for many years although the "Reynolds Analogy" was widely used.

After Reynolds' model had been largely abandoned, other theoretical models were proposed. The "mixing length" model of Prandtl (34) is perhaps the best

known of these. Prandtl attempted to describe turbulence phenomena in terms of a single parameter - a length scale. This length is the "mixing length" and depends on the geometry of the flow. However, this model is insensitive to variations of turbulence level inside the flow and by 1945 Prandtl had developed an analogous two-parameter model, (35), using as the second parameter the level of kinetic energy of the turbulent fluctuation. Development of this and similar models has continued and despite increasing complexity of the analysis useful predictions have been made particularly by Spalding and his associates (36), (37).

The increasing complexity of these analyses has assisted the revival of the basic Reynolds Theory. Silver (38), in 1950, reintroduced Reynolds' concepts and used them to calculate combustion rates (39) and also to predict condensation rates with the corresponding pressure drops (40). Wallis further developed the theory and extended its use to two-phase flows (41).

The basic model was also used by Spalding (42), who introduced the term "Reynolds Flux" to describe the lateral motion of the fluid particles.

Reynolds Theory has now been established as having great utility but despite success in theoretical predictions, the basic theory fails, because it cannot predict the turbulent Prandtl Number. Therefore the basic flux concept must be further developed if an adequate theory of turbulence is to be derived.

Such a development appears as the entity model of Tyldesley and Silver (43). In this model the turbulent flow field is idealised by assuming that it can be considered to be composed of a collection of fluid entities, analogous to Reynolds' "non-molecular fluid particles", of various shapes and sizes. This theory uses two parameters, an entity scale, and an entity velocity, once again an example of a simple one parameter model being improved by the introduction of a second parameter. The model has been used successfully to predict temperature profiles in channel flow (44) and the transport properties of suspension of solids (45).

The present work, however, uses an extension of the original Reynolds

Theory to produce a less sophisticated turbulence model. In all previous presentations of Reynolds Theory, the lateral flux was assumed instantaneously to reach equilibrium with the conditions at the boundary surface or wall, although Silver (46) did accept the possibility of the return flux not being in equilibrium with the wall.

By allowing for such deviation from equilibrium the Reynolds Theory may be further developed. This is achieved by a synthesis of the Reynolds Theory and the Danckwerts "Surface Renewal" Theory.

2.2 The Use of Surface Renewal in Reynolds Theory

In 1951 Danckwerts (47) discussed gas absorption in liquid films in terms of the renewal of the liquid surface by a lateral flux of lumps, or eddies of liquid, while Mickley and Fairbanks (48) later adapted this to heat transfer in fluidised beds. Danckwerts was able to include the possibility of incomplete equilibration of the eddies with the walls be defining a duration of contact of eddies with the surface and hence derive a statistical mean contact life in terms of the lateral flux. The diffusion equations for energy, mass, or momentum, transfer are applied for the mean duration times to give mean transfer rates.

The Danckwerts' model has been widely used, most recently by Thomas, Chung and Mahaldar (49) to evaluate temperature profiles in high Prandtl Number fluids but the relation between this theory and the Reynolds Flux had not been noted.

The ideas of the surface renewal theory can be used to develop an improved two parameter form of the Reynolds Theory.

In this variation of the conventional theory, the Reynolds Flux(Θ) is retained as one parameter but a second parameter ($\mathbb{S}$) is introduced which physically corresponds to a normal dimension of the eddies or entities in contact with the surface or wall. This situation is illustrated in Fig 2.1.

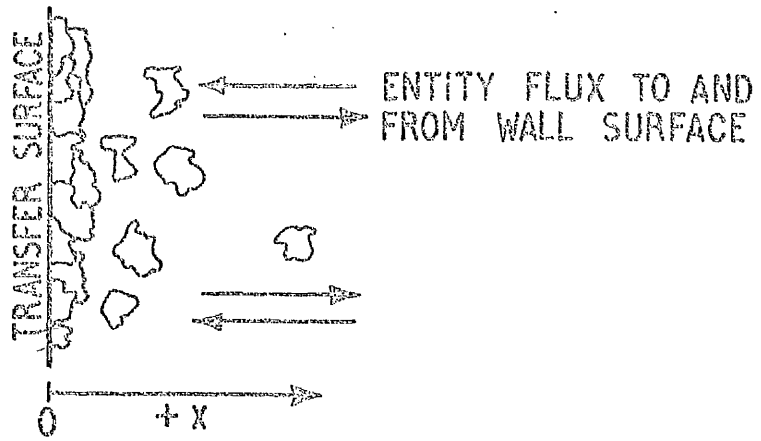

Fig 2.1

The boundary surface at x = 0 is supposed to consist of entities or "lumps" of fluid, these having been in direct contact with the wall for various times.

As in Danckwerts' original presentation we find a surface age distribution $\phi(t)$ but since different parameters are used the following presentation differs from that given in (47).

The mass of surface dA having an age between t and t + dt is simply $\rho\delta dA\phi(t)dt$.

The rate of decrease of surface of any age is equal to the rate at which that surface is replaced. The rate of replacement of surface of age t to t + dt is $\Theta\phi(t)dt.dA$

For mass equilibrium at the surface

$$-\frac{d\phi(t)}{dt}\rho\delta = \Theta\,\phi\,(t) \qquad .....(2.1)$$

Solving for $\phi(t)$

$$\phi(t) = +(\text{const})\,\exp(-\frac{\Theta}{\rho\delta}t) \qquad ..(2.2)$$

Now $\phi(t)$ must be such that

$$\int_0^\infty \phi(t)dt = 1 \qquad .....(2.3)$$

So using (2.3) to evaluate the constant in (2.2)

$$\phi(t) = \frac{\Theta}{\rho\delta}\,\exp(-\frac{\Theta}{\rho\delta}t) \qquad .....(2.4).$$

The surface age distribution is now used to evaluate mean values of heat, mass and momentum transfer coefficients.

These coefficients are derived by first solving the relevant diffusion equations for diffusion in the entities in contact with the wall.

If the transfer coefficients are to be evaluated for a plane surface with a coordinate system as shown in Fig 2.1, then the diffusion equations are, using the standard notation

$$\left.\begin{array}{lll} \alpha \quad \dfrac{\partial^2\theta}{\partial x^2} = \dfrac{\partial\theta}{\partial t} & - & \text{heat transfer} \\ \nu \quad \dfrac{\partial^2\bar{U}}{\partial x^2} = \dfrac{\partial\bar{U}}{\partial t} & - & \text{momentum transfer} \\ D_D \quad \dfrac{\partial^2 C_D}{\partial x^2} = \dfrac{\partial C_D}{\partial t} & - & \text{mass transfer} \end{array}\right\} \quad (2.5)$$

The elements are treated as extending from $x = 0$ to $x = \infty$ i.e. they are semi-infinite. The boundary conditions imposed are;

$t = 0 \quad x \geq 0 \quad \theta = \theta_\infty \quad \bar{U} = \bar{U}_\infty \quad C = C_\infty$

$t > 0 \quad x = 0 \quad \theta = 0 \quad \bar{U} = 0 \quad C = C_o$

$x = \infty \quad \theta = \theta_\infty \quad \bar{U} = \bar{U}_\infty \quad C = C_\infty$

Equations (2.5) may be solved using an error function solution to give instantaneous transfer coefficients at the solid surface. This solution is standard and can be found in many texts e.g. Carslaw and Jaeger (50).

These instantaneous transfer coefficients are

$$\left.\begin{array}{lll} h_i = \left[\dfrac{k\rho C_p}{\pi t}\right]^{\frac{1}{2}} & - & \text{heat transfer} \\ \tau_i = \left[\dfrac{\mu^2\bar{U}^2}{\pi \nu t}\right]^{\frac{1}{2}} & - & \text{momentum transfer} \\ h_{D_i} = \dfrac{D}{\left[\pi D t\right]^{\frac{1}{2}}} & - & \text{mass transfer} \end{array}\right\} \quad \ldots\ldots(2.6)$$

The mean transfer coefficients will be the instantaneous values weighted by the surface age distribution. Combining (2.4) with (2.6), for heat transfer.

$$\bar{h}_\infty = \left[\frac{k\rho C_p}{\pi}\right]^{\frac{1}{2}} \frac{\int_0^\infty t^{-\frac{1}{2}}\phi(t)dt.}{\int_0^\infty \phi(t)dt.} \quad \ldots\ldots(2.7)$$

$$= \left[\frac{k\rho C_p}{\pi}\right]^{\frac{1}{2}} \frac{\theta}{\rho\delta} \int_0^\infty t^{-\frac{1}{2}} \exp\left(-\frac{\theta}{\rho\delta}t\right)dt$$

$$\overline{h}_\infty = \left[\frac{kC_p\epsilon}{\delta}\right]^{\frac{1}{2}} \qquad \text{.....(2.8a)}$$

Similarly $$\overline{\tau} = \overline{U}_\infty\left[\frac{\mu\epsilon}{\delta}\right]^{\frac{1}{2}} = \frac{f}{2}\rho U_\infty^2 \qquad \text{.....(2.8b)}$$

and $$\overline{h}_D = \left[\frac{D\epsilon}{\rho\delta}\right]^{\frac{1}{2}} \qquad \text{.....(2.8c)}$$

The mean age of the entities at the surface is

$$\overline{t} = \int_0^t t\,\phi(t)\,dt = \frac{\rho\delta}{\epsilon} \qquad \text{.....(2.9)}$$

2.3 Comparison with the Reynolds Theory

It is customary to write the various transfer coefficients in terms of the Reynolds Flux (ϵ_o) as

$$\left.\begin{aligned} h &= \epsilon_o C_p \\ \frac{f}{2} &= \frac{\epsilon_o}{\rho U_\infty} \\ h_D &= \frac{\epsilon_o}{\rho} \end{aligned}\right\} \qquad \text{.....(2.10)}$$

and to express the Reynolds Analogy as

$$\frac{h}{C_p} = \frac{f}{2}\rho\overline{U}_\infty = h_{D\rho} \qquad \text{.....(2.11)}$$

(2.9) and (2.10) have been widely used e.g. by Silver (40) and by Wallis (41).

The forms given in (2.10) and (2.11) must be reconciled with the similar expressions given in (2.8) together with the corresponding "analogy equation".

$$\frac{h}{C_p} = [Pr]^{-\frac{1}{2}}\frac{f}{2}\rho\overline{U}_\infty = h_{D\rho}[Le]^{-\frac{1}{2}} \qquad \text{.....(2.12).}$$

Two approaches may be used to reconcile this apparent contradiction.

The first is an approach due to Spalding (42). Spalding sees the Reynolds Flux as a device to assist calculation of transfer coefficients and uses known transfer coefficients to define the flux (ϵ_o). The different forms

of equations (2.8) and (2.10) would not be regarded as having any importance using this approach. Taking the same position Morsy and Silver (51) have shown that using the forms of equations (2.10) it is possible to define a value of the Reynolds Flux for all flow situations.

Alternatively, the Reynolds Flux, can be regarded as "real" in the sense that it is, in some way, related to the structure of the turbulent flow. Thus ϵ_o, the Reynolds Flux, defines the transfer coefficients and could, possibly, be derived from other parameters using some statistical theory of turbulence. This is an approach advocated by Silver (46). If this approach is used then the apparent difference between equations (2.8) and (2.10) must be resolved.

This difference in form can be shown to be due to the introduction of the possibility of incomplete equilibration at the wall in the formulation of the surface renewal form.

If the mass flux is regarded as "real" then consider the case of heat transfer. Assume that the entities enter the layer at the wall at temperature T_∞ and leave at temperature T'. The wall temperature is T_o and constant.

In the steady state $h = \frac{\dot{q}}{(T_\infty - T_o)}$

and $\dot{q} = \epsilon_o C_p (T_\infty - T')$

So $$h = \epsilon_o C_p \frac{(T_\infty - T')}{(T_\infty - T_o)} \qquad .....(2.13)$$

If the entities reach thermal equilibrium with the wall, $T' = T_o$, and $h = \epsilon_o C_p$, the form given in (2.10).

For the case where equilibrium is not reached

$$T' > T_o$$

and from (2.13) $h < \epsilon_o C_p$.

Clearly the conventional form given in equation (2.10) represents the maximum possible heat transfer coefficient for a given flux. Similar analysis shows that the conventional values for mass and momentum transfer in equation (2.10) are also maxima.

The relation between the forms of (2.8) and (2.10) is best examined by

considering the entity size parameter (δ). The entities considered here are regarded as having a finite size denoted by δ but the diffusion equations (2.5) were solved for semi-infinite boundary conditions. It would seem that some restriction must therefore be imposed on the depth to which the molecular diffusion processes penetrate, so that this depth is less than the entity size. The depth of penetration of diffusion effects is given in (50) for this solution, so that this condition is;

$$\left.\begin{aligned} \delta^2 &> \alpha t \\ \delta^2 &> V_t \\ \delta^2 &> Dt \end{aligned}\right\} \quad \ldots\ldots(2.14)$$

If the mean age of the entities is substituted from (2.9) into (2.14)

$$\left.\begin{aligned} & \delta > \frac{k}{C_p \theta} \\ \underline{\text{or}} \quad & \delta > \frac{\mu}{\theta} \\ \underline{\text{or}} \quad & \delta > \frac{D_\rho}{\theta} \end{aligned}\right\} \quad \ldots\ldots(2.15)$$

Using these minimum values of δ to evaluate maximum values of the corresponding transport coefficients

$$\left.\begin{aligned} \bar{h} &= \left|\frac{kC_p\theta}{\delta}\right|^{\frac{1}{2}} < \theta.C_p \\ \tau &= \bar{U}_\infty \left|\frac{\mu\theta}{\delta}\right|^{\frac{1}{2}} < \theta\, \bar{U}_\infty \\ h_D &= \left|\frac{D\theta}{\rho\delta}\right|^{\frac{1}{2}} < \frac{\theta}{\rho} \end{aligned}\right\} \quad \ldots\ldots(2.15)$$

Thus the restriction on the depth of penetration of diffusion effects imposed by the choice of solution of the diffusion equation can be seen to be consistent with the requirement that the conventional Reynolds Theory coefficients of (2.10) represent maxima.

The relation between the forms of the analogy equations (2.11) and (2.12) is resolved by noting that the forms are the same when the Prandtl, Schmidt, and Lewis numbers are all unity. The equations (2.11) are generally

considered to hold under this condition, but when the condition is not satisfied Spalding (42) has suggested that equations of the form of (2.12) may still be used, although Spalding states that the power to which the Prandtl or Lewis number is raised should be between 0.5 and 0.66.

"Analogy equations" of the form of (2.12) can be devised directly from Danckwerts' original theory (47) and were used successfully by Thomas and Fan (52) for heat and momentum transfer.

2.4 Adaption of the Theory for Curved Boundary Surfaces

In section 2.2 the surface renewal transfer coefficients were evaluated for solutions of equations (2.5). Equations (2.5) describe diffusion processes at a plane surface and hence the transfer coefficients of equations (2.8) will only apply strictly to plane boundaries. In this section modifications are introduced to allow for cylindrical boundary surfaces.

In cylindrical coordinates the diffusion equations take the form,

$$\left.\begin{aligned} \frac{\partial\theta}{\partial t} &= \frac{1}{r}\frac{\partial}{\partial r}\left(r\alpha\frac{\partial\theta}{\partial r}\right) \\ \frac{\partial\bar{U}}{\partial t} &= \frac{1}{r}\frac{\partial}{\partial r}\left(r\nu\frac{\partial\bar{U}}{\partial r}\right) \\ \frac{\partial C}{\partial t} &= \frac{1}{r}\frac{\partial}{\partial r}\left(rD\frac{\partial C}{\partial r}\right) \end{aligned}\right\} \qquad \text{.....(2.17)}$$

where r is the radial distance from the axis.

If these equations are solved for a cylinder surface of radius a, with boundary conditions

$$t = 0 \quad 0 < r < a \quad \theta = \theta_\infty \quad \bar{U} = \bar{U}_\infty \quad C = C_\infty$$

$$t > 0 \quad r = a \quad \theta = 0 \quad \bar{U} = 0 \quad C = C_o$$

Then it has been shown by Crank (53) for the case of diffusion that the solutions of eqn.(2.17) have the form

$$\frac{C - C_\infty}{C_o - C_\infty} = 1 - \frac{2}{a}\sum_{n=1}^{\infty} \exp(-D^2\alpha_n t)\,\frac{J_o(r\alpha_n)}{\alpha_n J_1(a\alpha_n)} \qquad \text{.....(2.18)}$$

while the solutions for heat and momentum diffusion have analogous forms.

The solution given by (2.18) is unwieldy and difficult to evaluate except by using numerical methods. However in this case it is only necessary to evaluate the concentration gradient at the cylindrical surface and the restriction of eqn. (2.14) must still be imposed.

For these restrictions, the form of solution for short times given by Crank may be used. Crank imposes the condition that $\frac{Dt}{a^2} << 1$; this condition is consistent with the restrictions of equation 2.14 if $\delta^2 << a^2$. Since δ is the entity size parameter, on physical grounds it is probable that $\delta << a$. Hence Crank's solution is

$$\frac{C - C_\infty}{C_o - C_\infty} = \left(\frac{a}{r}\right)^{\frac{1}{2}} \text{erfc}\ \frac{a - r}{2\sqrt{Dt}} + \frac{(a - r)(Dta)^{\frac{1}{2}}}{4ar^{3/2}}\ i\ \text{erfc}\frac{a - r}{2\sqrt{Dt}} + \frac{(Qa^2 - 7r - 2ar)Dt}{32a^{3/2}\ r^{3/2}}\ i^2\ \text{erfc}\ \frac{a - r}{2\sqrt{Dt}} \quad .....(2.19)$$

At the surface $a = r$ and all the coefficients of terms other than the first are zero. Hence the mass transfer coefficient derived from (2.19) is identical to that for diffusion at a plane surface

$$\text{i.e. } h_D = \left[\frac{D}{\pi Dt}\right]^{\frac{1}{2}} \quad .....(2.6)$$

Similar results can be derived for heat and momentum transfer.

The identity of the transfer coefficients at plane and cylindrical surface for short times is a result of the condition that the penetration depth $Dt < \delta^2 << a^2$. Physically this implies that the depth of penetration is so much smaller than the radius of the cylindrical surface that the radius of curvature could be regarded as infinite and the diffusion effects were identical with those at a plane surface.

2.5 Chapter Closure and Discussion of Model

The value of the surface renewal form of Reynolds Theory derived in this chapter depends solely on its utility in predicting some real situation. This model, however, uses two parameters, a mass flux and an entity scale, whereas the conventional Reynolds Theory requires only one parameter, a mass flux. Consequently, the surface renewal form would not seem to offer any advantages over the more conventional form of Reynolds Theory.

This difficulty can be overcome by either

(a) introducing experimental data to evaluate either the entity scale or the mass flux or both, or alternatively

(b) by confining the application of the model to situations which will allow one or other of the parameters to be approximated or neglected.

The most obvious choice is to proceed using course (a). If this is done then, since experimental evaluation of the Reynolds Flux has proved difficult, except for the trivial case in the use of the analogy equations, progress can be made only by relating the entity size (δ) to some property. If the approach of Tyldesley and Silver (43) to the length parameter in their turbulence model is used, then the entity size should be taken as of the same order as the turbulent microscale. Experimental data for turbulent microscales has been published by Laufer (54) for the flow of water in pipes, and by Wells, Harkness, and Meyer (55) for water flows in closed ducts. From this data it would seem that typical values of the microscale near the boundaries of the flow would be of order 0.05 d, where d is the hydraulic diameter of the duct. Further, turbulent microscales for air flows are of the same order as those for water flows in the same passage and turbulent microscales would seem to be largely unaffected by changing Reynolds Numbers.

An alternative view would be that the laminar sublayer which appears in the case of turbulent flows over a surface could be considered as representing a layer of entities in contact with the surface. Laufer (54) gives experimental values of the sublayer thickness as being of order 0.01 d.

Since the experimental values of microscale and laminar sublayer thickness are of the same order either value could probably be used. The value for sublayer thickness should be preferred for work concerning fixed, solid surfaces.

Although the choice of alternative (b) might seem to severely restrict the use of the model, it is this approach which must be used unless some value for the mass flux can be found. In this work use of the surface renewal model is confined to cases where the need for values of both the mass flux and the entity size can be avoided.

The next chapter will present an application of the surface renewal model

to the calculation of evaporation rates of liquids and will show that by considering only initial evaporation rates for short time intervals, such evaporation rates may be calculated from simple physical properties of the liquid, without reference to either entity size or mass flux.

Note: The bulk of the work in Chapter 2 has been published in a short paper: THOMSON, G.M. and SILVER, R.S. "Reynolds Flux and Danckwerts Surface Renewal Theory", Int. J. Heat Mass Transfer, Vol.15 (1972) p.1284.

A copy of this paper forms Annexe A1 to this thesis.

Chapter 3 - Evaporation and Condensation Rates for Short Time Intervals

3.1 Introduction

The discussion of two-phase flashing flows in Chapter 1 indicated that the mass flow rates for flashing flows are, at least in part, controlled by the quality of the flow mixture.

Thus any model of two-phase flashing flow must incorporate some assumptions, not only of quality, but also of rates of vapour evolution.

In the case of critical flashing flow processes, the flashing liquid is exposed to large pressure drops during a very short exposure time. For the low pressure critical flows discussed in this work, residence times in flow passages are less than 10 milliseconds for superheats up to 40 ^{o}C.

This chapter demonstrates the use of the surface renewal model to predict rates of evaporation (and condensation) of liquids. This application of the surface renewal model is restricted to situations where the surface of the liquid is exposed to pressures, less than the saturation pressure corresponding to the bulk liquid temperature, for very short exposure times.

3.2 Prediction of Evaporation Rates using the Surface Renewal Model

Consider a plane liquid-vapour interface with the phases in equilibrium. Let the liquid bulk temperature be T_o and let the pressure acting on the surface be P_b.

Suppose now that the pressure acting on the liquid surface is now suddenly reduced at time $t = 0$ to a value P_2 with corresponding saturation temperature T_{sat} such that $T_{sat} < T_b$. The liquid is therefore taken suddenly into a metastable state.

This situation can be pictured in the form of Fig 3.1.

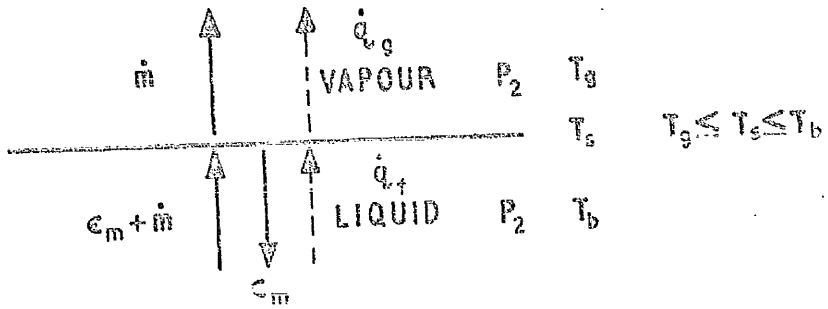

FIG. 3·1. EVAPORATION.

The system will return to an equilibrium state by evaporation of liquid at some mass rate $\dot{m}_t$ per unit area, at time t.

Heat transfer takes place at a rate $\dot{q}_f$ from the bulk liquid to the interface surface and then into the bulk vapour. The heat transfer process to the surface is assumed to be due to a lateral flux motion of entities at a constant rate G_m.

For energy balance at the surface

$$\dot{q}_g + \dot{m}_t h_{fg} = \dot{q}_f \qquad \ldots\ldots(3.1)$$

and $\dot{q}_f = U(T_b - T_v)$

where U is the total heat transfer coefficient.

If the vapour is well mixed and the heat losses from the vapour are small then temperature gradients in the vapour phase may be neglected i.e. $q_g \doteq 0$. $T_v \doteq T_{sat}$.

The total heat transfer coefficient U may be written as

$$\frac{1}{U} = \frac{1}{h_t} + \frac{1}{h_s}$$

where h_t = heat transfer coefficient for liquid phase,

h_s = heat transfer coefficient for liquid vapour interface.

Whence (3.1) may be written as

$$\dot{m}_t = \frac{U(T_b - T_{sat})}{h_{fg}}$$

$$= \frac{x_E}{C_{pf}} U = \frac{x_E}{C_p} \frac{h_t}{\left[1 + \frac{h_t}{h_s}\right]} \qquad \ldots\ldots(3.2)$$

where $x_E = \frac{C_{pf}(T_b - T_{sat})}{h_{fg}}$

The function x_E is constant if the liquid bulk temperature does not vary. In this presentation it will be assumed that the mass of vapour evolved is much less than the mass of liquid and so x_E may be considered constant.

The heat transfer coefficient h_t and h_s must now be evaluated. When the surface renewal form is used for h_t, the expression for the heat transfer coefficient is found by calculating instantaneous heat transfer coefficients for individual entities and weighing these by a surface-age distribution $\phi(t)$ to give:

$$\bar{h} = h_\infty = \left[\frac{k\rho\ C_p}{\pi}\right]^{\frac{1}{2}} \frac{\int_0^\infty t^{-\frac{1}{2}}\ \phi(t)dt}{\int_0^\infty \phi(t)dt} \qquad .....(2.7)$$

Because the distribution is averaged over an infinite time span and the system is supposed to be in a steady state, equation (2.7) gives a steady state value equation (2.8a).

If, however, heat transfer takes place only over a short exposure time interval, say from $t = 0$ to $t = \tau$, then clearly the integrals in equation cannot have infinite upper limits.

Further, if the exposure time is less than the mean entity life at the surface, equation (2.9), then the integral will give not a steady state value but an instantaneous value of the heat transfer coefficient at age .

Rewriting (2.7) for finite limits

$$h_\tau = \left[\frac{k\rho\ C_p}{\pi}\right]^{\frac{1}{2}} \frac{\int_0^\tau t^{-\frac{1}{2}}\ \phi(t)dt}{\int_0^\tau \phi(t)dt} \qquad .....(3.3)$$

with $h_\tau = \bar{h}$ for $\tau < \frac{\rho\delta}{\epsilon_m}$

however $h_\tau \to \bar{h}$ as $\tau \to \infty$

From equation (2.4)

$$\phi(t) = \frac{\epsilon_m}{\rho\delta} \exp(-\frac{\epsilon_m}{\rho\delta} t) \qquad .....(2.4)$$

and substituting for $\phi(t)$ in equation (3.3)

$$h_\tau = \left[\frac{k\rho C_p}{\pi}\right]^{\frac{1}{2}} \frac{\int_0^\tau t^{-\frac{1}{2}} \exp(-\frac{\epsilon_m}{\rho\delta} t)dt}{\int_0^\tau \exp(-\frac{\epsilon_m}{\rho t})\ dt} \qquad .....(3.4)$$

terms of the form $\int_0^\tau t^{-\frac{1}{2}} \exp(-\frac{\epsilon_m}{\rho\delta} t)dt$ are difficult to evaluate analytically. If however values of τ are constrained such that $\tau << \frac{\rho\delta}{\epsilon}$ (exposure time less than mean time at surface for entities) then (3 4) can be approximated as

$$h_\tau = 2\left[\frac{k\rho\ C_p}{\pi t}\right]^{\frac{1}{2}} \qquad .....(3.5)$$

For h_s the form of heat transfer coefficient for liquid-vapour interfaces used is

$$h_s = \frac{1}{\sqrt{2\pi RT}} \left(\frac{\partial P}{\partial T}\right)_{sat} h_{fg} \qquad .....(3.6)$$

This form has been used by many authors e.g. Silver (58) and Jamieson (57).

Now $\left(\frac{\partial P}{\partial T}\right)_{sat} \doteq \frac{h_{fg}}{T.\nu_{fg}}$ from Clausius-Clapeyron.

Substituting for h_t and h_s in (3.2)

$$\dot{m}_t = \frac{2x_E}{C_p}\left[\frac{k\rho C_p}{\pi t}\right]^{\frac{1}{2}} \Bigg/ \left[1 + \frac{2\left[2k\rho C_p RT\right]^{\frac{1}{2}} T\,\nu_{fg}}{h_{fg}^2\, t^{\frac{1}{2}}}\right] \qquad .....(3.7)$$

The mean value of $\dot{m}$ over the period $t = 0$ to $t = \tau$ is given by

$$\bar{\dot{m}} = \frac{1}{\tau}\int_0^{\tau} \dot{m}_t\, dt. \qquad .....(3.8)$$

$$\text{So}\quad \bar{\dot{m}} = \frac{2\,x_E}{C_p\,\tau}\left[\frac{k\rho C_p}{\pi}\right]^{\frac{1}{2}} \int_0^{\tau} t^{-\frac{1}{2}} dt \Bigg/ \left[1 + \frac{2\left[2k\rho C_p RT\right]^{\frac{1}{2}} T\nu_{fg}}{h_{fg}\, t^{\frac{1}{2}}}\right] \qquad .....(3.9)$$

Equation (3.8) is rather unwieldy but fortunately the term

$\frac{2\left[k\rho C_p RT\right]^{\frac{1}{2}} T.\nu_{fg}}{h_{fg}^2\, t^{\frac{1}{2}}} = \frac{h_t}{h_s}$ can be shown to be small for water substance even at short exposure times. The properties defining the term with the exception of T and ν_{fg} are not greatly affected by pressure or temperature.

For example at 1 bar pressure and 100 °C $\quad \frac{h_t}{h_s} \doteq \frac{10^{-4}}{t^{+\frac{1}{2}}}$

while for 10 bar pressure and 170 °C $\quad \frac{h_t}{h_s} = \frac{6 \times 10^{-4}}{t^{+\frac{1}{2}}}$

Hence for evaporation with exposure times greater than 10^{-4} sec $\frac{h_t}{h_s} < 0.01$.

Therefore equation (3.9) can be simplified for water substance to give

$$\bar{\dot{m}} = \frac{2x_E}{\tau C_p}\left[\frac{k\rho C_p}{\pi}\right]^{\frac{1}{2}} \int_0^{\tau} t^{-\frac{1}{2}}\, dt$$

$$= \frac{4x_E}{C_p}\left[\frac{k\rho C_p}{\pi\tau}\right]^{\frac{1}{2}} \qquad .....(3.10)$$

Equations (3.9) and (3.10) are derived using the surface renewal heat transfer coefficient appropriate to a plane interface. If the evaporation

rate is to be calculated for a cylindrical surface then the discussion of section 2.4 shows that the use of equations (3.9) and (3.10) is fully justified.

3.3 Application to the Calculation of Condensation Rates

The theoretical model presented in section 3.2 can be readily adapted to the prediction of condensation rates.

Once again a plane liquid-vapour interface is considered with the phases in equilibrium. The liquid and vapour are at temperature T_b and the pressure acting on the surface is P_b. If the saturation temperature of the vapour phase is T_b then if the pressure on the surface increases to P_2 some vapour will condense.

This situation can be idealised as Fig. 3.2, using the same notation as in Section 3.2.

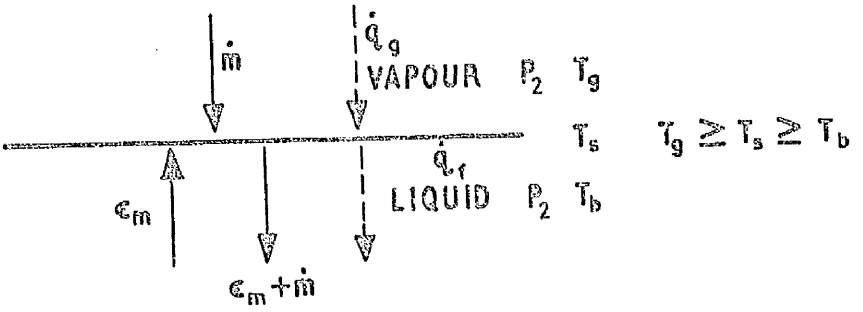

FIG. 3.2. CONDENSATION.

Once more a flux ϵ_m in the liquid phase produces the heat transfer effects from the surface.

On this idealisation the energy balance at the surface is given as

$$\dot{q}_g + \dot{m} h_{fg} = \dot{q}_f \qquad \text{.....(3.1)}$$

and

$$\dot{q}_f = U_t(T_s - T_b)$$

If the temperature gradient in the vapour phase is neglected then the derivation using the surface renewal form of heat transfer coefficient proceeds exactly the same way as the derivation in section 3.2 and the condensation rate is given by eqn. (3.9) or (3.10).

For exposure times greater than about 10^{-4} secs. for water the condensation rate is given by (3.10) as

$$\bar{\dot{m}} = \frac{4x_E}{C_p}\left|\frac{k\rho C_p}{\pi t}\right|^{\frac{1}{2}} \qquad \text{.....(3.10)}$$

with

$$x_E = \frac{C_p(T_{sat} - T_b)}{h_{fg}}$$

3.4 Discussion of the Model

Although the predictions of the model presented in sections 3.2 and 3.3 will be compared with experimental data in section 3.5, certain features and assumptions of the model should be discussed before the predictions are subjected to such comparisons.

Firstly, the form given for the average mass transfer rate by equation (3.9) tends to a large constant value as the exposure time decreases. If the simplified form of the predictive equation, equation (3.10), is to be used then this simplified form will only give accurate predictions for exposure times greater than a limiting exposure time. If (3.10) is to be used then the assumption that the interface heat transfer coefficient is large must be carefully examined.

Secondly, the approximations introduced in evaluating the integrals in equation (3.4) can be shown, by expanding terms, to introduce a tendency for equations (3.9) and (3.10) to overpredict at long exposure times, This error could be reduced by introducing some numerical solution for the evaluation of the integrals in (3.4).

Thirdly, the derivations in sections 3.2 and 3.3 ignore the effect of temperature gradients and consequently,heat transfer in the vapour phase will certainly occur in the case of evaporation it would seem that the model should overpredict evaporation rates.

Critical flashing flow rates at low qualities are typically in the region of 10^4 kg/m^{2}s to 2.5 x 10^4 kg/m^{2}s so that the residence time of the liquid phase in passage of length 10 cm is of order 10^{-3} seconds. Hence if the model set out in sections 3.2 and 3.3 is to be used to predict qualities in a model of two-phase flashing flow, it must be shown to be applicable for exposure times in the range 5 x 10^{-4} seconds to 5 x 10^{-3} seconds.

In the next section this model is compared with experimental data for evaporation and condensation rates at exposure times in the required range.

3.5 Comparison of Theoretical Predictions with Experimental Data

In sections 3.2 and 3.3, equations (3.9) and (3.10) were derived, using the surface renewal model, to predict evaporation and condensation rates. These predictive equations can have no value unless the predicted mass transfer rates can be shown to be in agreement with experimental data. Since this thesis is concerned principally with critical flashing flows of water only experimental data for the evaporation or condensation of water at short time intervals will be examined.

Hickman et al (56) examined the evaporation and condensation of water from the surface of jets, at low temperatures and pressures. Fig. 3.3 shows Hickman's data plotted against equation (3.10).

Hickman gives values for both evaporation and condensation rates at pressures of order 0.001 bar and temperature differences of the order of 10 ^{o}C, for exposure times in the range 5 x 10^{-4} sec. to 2 x 10^{-3} sec. From Fig. 3.3 it appears that equation (3.8) gives good agreement with experiment in the case of evaporation for exposure times of about 10^{-3} sec. but underpredicts condensation rates by about 10%.

Hickman attempted to produce theoretical predictions for evaporation and condensation rates. In this case the instantaneous mass transfer rate was defined by an equation similar to equation (3.2) viz.

$$\dot{m}_t = \frac{x_E}{C_{pf}} h_t \qquad .....(3.2)$$

However, h_t, the instantaneous heat transfer coefficient, was defined as

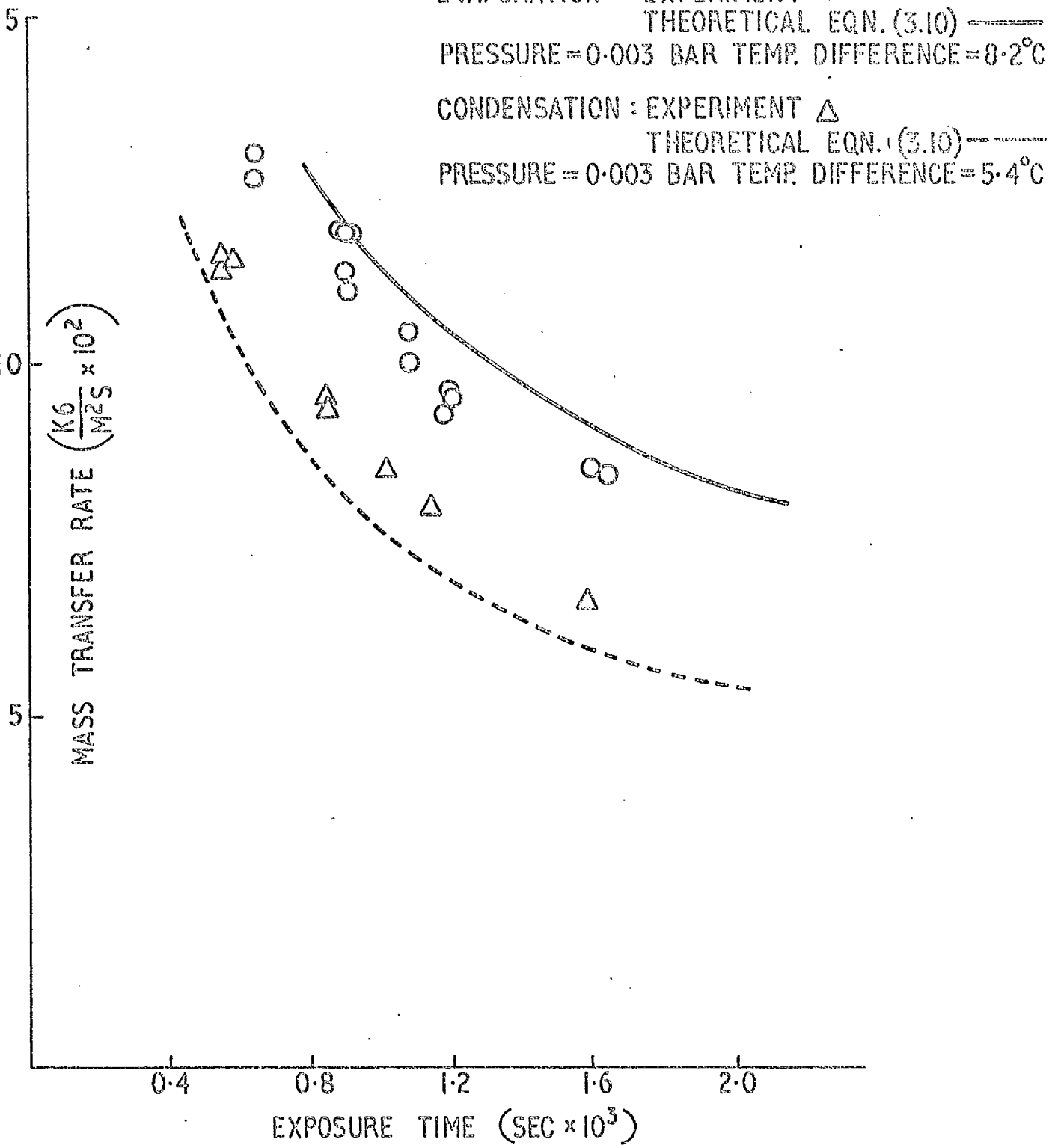

Fig. 3.3. Comparison of predictions of eqn. (3.10) Hickmans data.

the time average of an instantaneous heat transfer coefficient of the equation (2.6),

i.e. $$h_t = \frac{1}{\tau}\int_0^{\tau}\left[\frac{k\rho C_p}{\pi t}\right]^{\frac{1}{2}} dt \qquad .....(3.11)$$

with τ = exposure time,

and Hickman does not justify the use of this form.

Whence for Hickman's form,

$$\bar{\dot{m}} = \int_0^{\tau}\frac{x}{C_p}\,dt\,\frac{1}{\tau}\int_0^{\tau}\left[\frac{k\rho C_p}{\pi t}\right]^{\frac{1}{2}} dt \qquad .....(3.12)$$

this will give an analytical prediction for the average mass transfer rate over exposure time τ of the form of (3.8).

$$\bar{\dot{m}} = \frac{4x_E}{C_p}\left[\frac{k\rho C_p}{\pi t}\right]^{\frac{1}{2}} \qquad .....(3.10)$$

Of course an equation identical to (3.10) will give reasonable agreement with experiment but Hickman's derivation cannot be regarded as satisfactory without some explanation of the use of (3.11) as an instantaneous value.

Jamieson (57) also examined the rates of condensation of an atmosphere of steam labelled with tritium onto the surface of a water jet. The condensation rate was evaluated by measuring the radioactivity in water collected from the water jet. Experiments were carried out over a range of steam pressures from 0.185 bar to 0.98 bar with temperature differences from 30 ^{o}C to 100 ^{o}C. Exposure times ranged from 2×10^{-5} seconds to 3×10^{-4} seconds.

By careful visual observation of the operation of his apparatus Jamieson was able to reject the possibility of any large scale entrainment of steam bubbles in the exposed jet. However these observations would be least reliable for the shortest exposure times.

In Fig. 3.4 Jamieson's results are compared with values calculated from equation (3.10) and it appears that while equation (3.10) underpredicts by about 10% for exposure times above 2×10^{-4} seconds, this underprediction is much worse at shorter exposure times. If any entrainment took place then it is these results at short times which would be expected to be too high, however entrainment effects could not account for the massive underprediction apparent in Fig. 3.4.

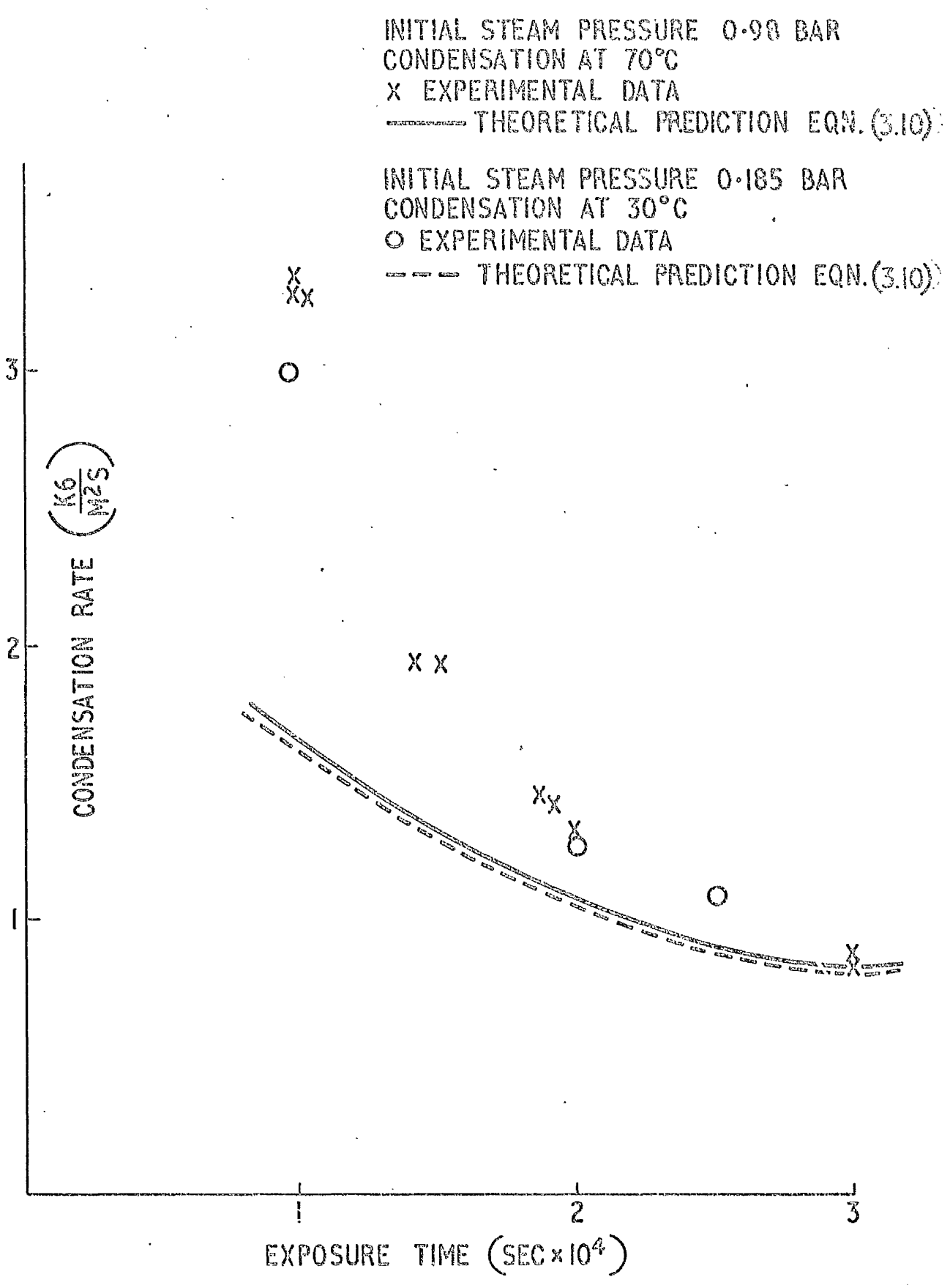

Fig. 3.4. Comparison of predictions of eqn.(3.10) with data of Jamieson (57)

From this comparison of the predictions obtained from equation (3.10) with experimental data it seems that equation (3.10) provides an accurate prediction method for evaporation rates on the surface of liquid jets for exposure times in the range 2×10^{-4} seconds to 2×10^{-3} seconds.

In conclusion it would seem that the simplified predictive equation (3.10) from the model of condensation and evaporation at short exposure times derived from the surface renewal theory in this chapter can be used with some confidence provided that

(i) exposure times are above 2×10^{-4} seconds;

(ii) the slight overprediction of evaporation rates is accepted.

3.6 Chapter Closure

In this chapter the surface renewal model has been successfully applied to the prediction of evaporation and condensation rates of water exposed to changes of pressure or temperature for short times.

From the discussion of two-phase flashing flows in Chapter 1 it is clear that a mechanism for the prediction of changes in quality is necessary before any model for critical flashing flows can be formulated.

In this chapter a suitable method of prediction has been derived and in the next chapter this model will be used in a theoretical model of two-phase flashing flow in short passages. However the predictive procedure outlined in this chapter gives evaporation (and condensation) rates in terms of a mass transfer rate per unit area. Thus if equation (3.10) is to be incorporated into a model of flashing flow it will be necessary to define the area of the liquid vapour interface before equation (3.10) can be used to predict changes in quality for flashing flows.

Note: The work in Chapter 3 has been submitted, in condensed and simplified form, as a paper to be read at the N.E.L. Meeting on Two-phase Flow Through Orifices and Nozzles, 29 November 1972.

The paper is, THOMSON, G.M. "An approach to the Calculation of Equilibration Rates in Flashing Flow".

This paper forms Annexe A2 to this thesis.

Chapter 4 - A Theory of Critical Flashing Flow

4.1 The two previous chapters have demonstrated the application of surface renewal theory to the prediction of rates of evaporation from the surfaces of water jets. The model developed in Chapter 3 was shown to give adequate predictions for exposure times in the range 2×10^{-4} secs. to 2×10^{-3} secs.

In this chapter the theoretical expression for evaporation rates developed in Chapter 3 (equation 3.10) will be used in a model for the prediction of flow rates in two-phase critical flashing flows in short nozzles, (i.e. with $\frac{L}{D} < 12$).

The model developed here will predict the variations in critical mass flow rate for

(i) various nozzle entrance profiles on a fixed nozzle length at fixed liquid temperatures;

(ii) variation of length/diameter ratios for given entrance profiles at fixed liquid temperature;

(iii) variation of liquid superheat at nozzle entrance for fixed $\frac{L}{D}$ ratio and entrance profile.

In order to produce this model, it is necessary to make certain assumptions. These assumptions are reviewed in the next section.

4.2 Assumptions used in Model

The assumptions used in formulating the model developed in section 4.3 are set out in this section.

Most of these assumptions are based on experimental evidence reviewed in section 1.3 of Chapter 1 and many of them have been previously used in theoretical studies by other authors discussed in section 1.4.

The assumptions made are briefly discussed below.

1. Annular Flow Pattern

The phases are assumed to flow in a separated annular pattern with a liquid core surrounded by an annulus of vapour. Both phases are assumed to behave as single-phase fluids. Visual observations in references (4),(13),(14) support this assumption for short nozzles. The upper limit for the use of the assumption being set at $\frac{L}{D} = 12$ as suggested by Fauske (13).

This assumption was used in the models of Silver (2), Bailey (12), and Rushton and Leslie (59).

2. Mass Transfer takes place only at the surface of the liquid core.

This assumption implies that no mass transfer takes place as a result of bubble growth. The evidence for lack of bubble growth due to the necessity for a finite nucleation time was reviewed in the discussion of references (5), (6) and (8).

This assumption of no bubble growth sets an upper limit on the residence time of the liquid phase in the flow passage. For water at an ultraheat of $5^{o}C$ the time for nucleation suggested by reference (11) is about 5×10^{-3} seconds. This assumption further restricts the model to cases where the flow upstream of the nozzles consists solely of subcooled liquid.

References (2) and (12) both used this assumption of vapour evolution only at the surface of the liquid core.

3. Rates of vapour evolution at short residence times are described by eqn.(3.10).

The justification for this assumption is given in the comparison with experimental data of section 3.4 in Chapter 3.

As discussed in Chapter 3 the use of equation (3.10) seems permissible if the residence time of the liquid phase is between 2×10^{-4} and 2×10^{-3} seconds. This restriction on residence time imposes a limit on the maximum length of nozzles to which the theory developed in this chapter may be applied. The application of this restriction is consistent with the restriction introduced by assumption 2. However the use of equation (3.10) even under these conditions has only been justified, by experimental data, for water substance.

4. The slip ratio is greater than unity.

Considerable experimental evidence exists to indicate that the slip ratio, defined as the ratio of vapour phase velocity to liquid phase velocity, has a value greater than one for critical two-phase flow situations of the type discussed here. Evidence from references (17),(19) and (20) would suggest that the value is of order 10.

An analytical form of the slip ratio first proposed by Zivi (29) viz $\sqrt[3]{\frac{\rho_f}{\rho_g}}$

will be introduced into the model of critical flashing flow. This form was derived by Zivi by minimising the kinetic energy flow rate per unit area for the two-phase mixture and assuming that the wall friction is negligible. Neither postulate conflicts with the assumptions made in this chapter and the slip ratio is assumed to apply at least at the nozzle exit and the densities used are those for exit conditions.

The derivation of this form for slip ratio is given in Appendix A to this chapter.

5. Choking Mechanism

The choked or critical flow condition is assumed to occur when the velocity of the vapour phase is at the local sonic velocity for the vapour. In this case choking is held to take place at the exit and the sonic velocity is defined at exit conditions.

This assumption was demonstrated to be inadmissible by both Fauske (30) and Zaloudek (32) for models which assume thermodynamic equilibrium between phases, but may still be suitable for non-equilibrium models.

Experimental evidence for this assumption is lacking.

6. Velocity of the liquid phase and residence time for liquid phase

The liquid phase velocity (U_f) is defined at the exit for choking conditions, by assumptions 4 and 5. From continuity arguments it can be shown that the variation in liquid velocity in the nozzle is small. This variation will be neglected and the residence time (τ) for the liquid phase will be taken as $\tau = \frac{L}{U_f}$ where U_f is the value defined at the exit.

The argument for disregarding variations in liquid velocity is given in Appendix B.

7. Vapour completely occupies the region about the core

The assumption that the liquid core behaves as in single-phase flows implies that the annular flow pattern could be observed without any vapour being evolved, since vena-contracta effects are seen in single phase flows. However, if the model is restricted to cases such that the ratio of liquid density to vapour density is high, then provided the quality is above some lower limit, the region round the liquid core can be regarded as being entirely filled with vapour.

For water substance this is the case when the quality is above $x = 0.006$.

8. The Change in Diameter of the Liquid Core due to evaporation effects is small.

The use of equation (3.8) to predict rates of vapour evolution, requires some assumption of liquid-vapour interfacial surface. In the case of the flow pattern used here, by introducing assumption 1, the area of the interfacial surface will change as the diameter of the liquid core changes. Clearly, then, any evaporation of the liquid will reduce the area of the interfacial surface.

However the change in core diameter due to evaporation can be shown to be small. This argument is given in Appendix B to this chapter.

The assumptions enumerated in this section impose certain restrictions on the utility of the model constructed from them. These restrictions may be summarised as;

(a) The model will apply only where the flow upstream of the entrance consists solely of subcooled liquid, i.e. the entrance quality is zero. This restriction is introduced with assumptions 1 and 2.

(b) The model only applies to short nozzles where the residence time is less than 2×10^{-3} seconds. This restriction is introduced in assumptions 2 and 3. Assumption 1 introduced a requirement that the $^{\text{Length}}/_{\text{Diameter}}$ ratio does not exceed a value of 12.

(c) Use of the model is only possible where the pressures in the nozzle systems are low, say below 10 bar for water substance, since assumption 1 may not apply at the higher pressures. Similarly for assumption 2 to hold it may be necessary to restrict the liquid superheat at the nozzle exit to 50 ^{o}C at least for longer nozzles.

4.3 A model of Critical Two-phase Flashing Flow in Short Nozzles

The assumption set out in section 4.2 can now be applied to the development of a model of critical two-phase flashing flow. The restrictions imposed by assumptions 1 and 3 will limit the application of this model to short nozzles with $\frac{L}{D}$ less than 12, and overall length such that the liquid phase residence time is less than 2×10^{-3} seconds.

Consider some nozzle or passage of circular cross-section. The overall length is L and the diameter of the throat is D. The entrance profile is such that the contraction coefficient for single phase liquid flows is C. The form of the flow passage must be such as to permit the use of the various assumptions made in section 4.2.

The liquid and vapour phases are separated with the liquid phase flowing as a central core. This liquid core has approximately circular cross-section with axis coinciding with the axis of the nozzle. The liquid velocity is U_f and the vapour velocity is U_g.

From assumption 1, the flow of the liquid phase can be treated as a single phase flow and so the liquid core diameter just after the entrance is $(C)^{\frac{1}{2}}D$. Values of C can be calculated from streamline theory, e.g. Batchelor (60).

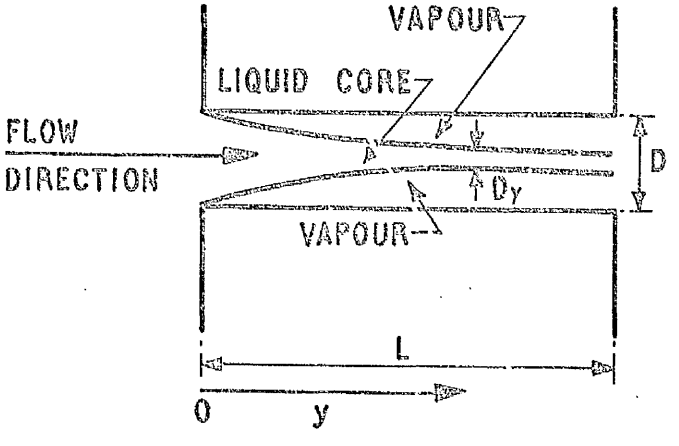

FIG. 4.1.

The notional flow rate of the liquid phase in the absence of any evaporation from the liquid core is W_{f_o} where

$$W_{f_o} = \rho_f U_f \left[\frac{\pi C D^2}{4}\right] \qquad \ldots\ldots(4.1)$$

The actual flow rate W in the nozzle will differ from W_{fo} by some amount ΔW

i.e. $W = W_{fo} = \Delta W.$ .....(4.2)

ΔW may be related to the mass flow rate of vapour in the nozzle.

For steady flow, the mass flow rate of vapour at the exit is equal to the total mass of vapour evaporated per unit time from the liquid surface (M).

$$M = \pi C^{\frac{1}{2}} D L \bar{\dot{m}}$$

where $\bar{\dot{m}}$ = mean evaporation rate/unit area over the entire nozzle length.

In calculating M the effective diameter of the liquid core is assumed to be constant down the length of the nozzle. In fact the core diameter varies. Appendix B includes arguments to show that this variation is small and may be disregarded, but this variation in core diameter is calculated using equation (4.3). Examination of the magnitudes of the quantities involved show that this procedure is acceptable.

M is, of course, the total change in the vapour flow rate, i.e. $\Delta W_g = M$.

At the exit the vapour phase velocity is fixed at U_g and the density is ρ_g. Hence mass flux M occupies a cross-section of

$$\Delta A = \frac{M}{\rho_g U_g} \qquad .....(4.4)$$

The increase in cross-section occupied by vapour reduces the cross-section occupied by the liquid core by an equal amount for a nozzle of constant cross-sectic

Hence the liquid flow rate is reduced by

$$-\Delta W_f = -\rho_f U_f \Delta A = -\frac{\rho_f U_f}{\rho_g U_g} M. \qquad .....(4.5)$$

Now $\Delta W = \Delta W_f + \Delta W_g$

$$= -\left(\frac{\rho_f U_f}{\rho_g U_g} - 1\right) M. \qquad .....(4.6)$$

Substituting for ΔW in (4.2)

$$W = W_{fo} - \left(\frac{\rho_f U_f}{\rho_g U_g} - 1\right) M. \qquad .....(4.7)$$

Substitute for W_{fo} and M in (4.7) from (4.1) and (4.3)

$$W = \frac{\pi C D^2}{4}\left[\rho_f U_f - \left(\frac{\rho_f U_f}{\rho_g U_g} - 1\right)\frac{L}{D C^{\frac{1}{2}}}\bar{\dot{m}}\right] \qquad .....(4.8)$$

Using equation (3.10) for $\bar{m}$ and taking $\tau = \frac{L}{U_f}$ with the variation in U_f disregarded.

$$G = \frac{4W}{\pi D^2}$$

$$= C\rho_f U_f \left\{ 1 - \frac{16x_E}{\rho_g U_g} \left[\left(\frac{L}{D^2}\right)\left(\frac{k\rho}{\pi C_p}\right)\left(\frac{U_f}{C}\right) \right]^{\frac{1}{2}} \right\} \qquad .....(4.9)$$

For the critical flow rate only values for liquid and vapour velocities need be defined.

Using assumption 4.

$$U_f = U_g \left(\frac{\rho_g}{\rho_f}\right)^{1/3}$$

and $U_g = U_{gc}$.

Substituting in (4.9)

$$G_c = C\rho_f U_{gc} \left(\frac{\rho_g}{\rho_f}\right)^{1/3} \left\{ 1 - \frac{16x_E}{\rho_g} \left[\left(\frac{L}{D^2}\right)\left(\frac{k\rho}{\pi C_p}\right)\left(\frac{1}{U_{gc} C}\right)\left(\frac{\rho_g}{\rho_f}\right)^{1/3} \right]^{\frac{1}{2}} \right\} \qquad .....(4.10)$$

4.4 Discussion of Model

Equation (4.16) predicts the mass flow rate at the choking condition in terms of (i) the length and throat diameter of the nozzle and the "cold-water" discharge coefficient;

(ii) the thermodynamic properties of the liquid phase;

(iii) the sonic velocity in the vapour phase;

(iv) the difference between the liquid bulk temperature at the nozzle entrance and the saturation temperature corresponding to the exit pressure.

With the exception of the sonic velocity all these parameters can be easily determined.

The sonic velocity could be found using an analytical expression for the velocity of sound in a gas.

For example the use of the form for the sonic velocity in a perfect gas would give acceptable predictions of pressures of the order of one atmosphere viz,

$$U_{g_c} = \sqrt{\gamma RT} = \sqrt{\frac{\gamma P_o}{\rho}} \qquad \text{.....(4.17)}$$

with $\gamma = 1.4$,

P_o = local pressure.

Other more sophisticated forms could be used to give improved accuracy or values of sonic velocities at the relevant conditions could be extracted from tables of physical properties.

The velocity of sound in a vapour increases with increased pressure. Thus if the vapour velocity is regarded as being equal to the sonic velocity at choking and if no pressure recovery is to take place in the vapour flow down the nozzle, then clearly the appropriate value of the sonic velocity to equate to the vapour velocity is the value for exit conditions.

Further for water and many other substances the ratio of the density of the liquid phase to the saturated vapour density decreases for increased pressure. If equation (4.14) is used to define the liquid velocity, then this velocity will have a minimum value if the slip ratio is evaluated at the nozzle exit conditions.

To summarise; if the value of the critical mass flow rate is evaluated by using equation (4.16), then equation (4.16) will predict the lowest value of mass flow rate if the values substituted for the various parameters are taken, at the nozzle exit conditions of pressure and temperature.

In the next section the mass flow rates predicted by equation (4.14) are compared with experimental values for short nozzles and with predictions from other models of two-phase critical flashing flow.

4.5 Comparison with experimental Data and Previous Theoretical Models

The model of two-phase critical flashing flow developed in section 4.3 must now be compared with experimental data before any further useful discussion of the model can take place. The assumptions made in section 4.2 and certain of the simplifications introduced in section 4.3 restrict the application of this model to certain types of two-phase critical flashing flow. These restrictions are that; (a) the $^{\text{length}}/_{\text{diameter}}$ ratio of the nozzle is less than 12;

(b) upstream of the nozzle entrance the flow consists solely of subcooled liquid;

(c) the model is restricted to low-pressure flows, say with a maximum upstream pressure of 10 bar, and with a maximum liquid superheat of 50 $^{\circ}$C.

Critical flashing flows have been studied in systems which permit the application of the model presented in this chapter. Such studies include these of Silver and Mitchell (3) and Burnell (61) for nozzles with rounded entrances (discharge coefficient 0.98) and of Zaloudek (4), Fauske (13) for nozzles with square entrances (discharge coefficients about 0.6). These

references were previously reviewed in section 1.3 of Chapter 1. Critical flow rates extracted from these experimental studies have been plotted against $^{\text{length}}/_{\text{diameter}}$ ratios in figures 4.2 and 4.3, for nozzles with square or rounded entrances respectively.

Equation (4.16) has been used to calculate rates of critical flashing flow for the appropriate experimental conditions and the resultant values are plotted as curves on the relevant figures. The flow rate values were calculated using properties of water substance given in steam tables (62), a sonic velocity value of 405 m/s.

From figure 4.3, the curve drawn from equation (4.16) shows good agreement with the experimental points of Silver and Mitchell, however, in fig 4.2, although the model certainly predicts the correct order of magnitude for the critical flow rate, it does not appear to successfully predict the variation of flow rate with $^{\text{length}}/_{\text{diameter}}$ ratio.

One possible reason for this failure may be deduced by noting that the experimental results in (4) and (13) are taken at higher pressures and temperatures than references (3) and (61). The overprediction of equation (4.16) at larger $^{L}/_{D}$ ratios may thus be due to the onset of bubble formation at lower $^{L}/_{D}$ ratios than expected. The experimental results from references (4) and (13) also show a considerable spread so the expected errors associated with these results could be rather larger than the error limits claimed by the authors in the original references.

Since many other theoretical studies of two-phase critical flashing flow use at least some of the assumptions listed in section 4.2, theoretical predictions from these models under the appropriate conditions have also been drawn on figures 4.2 and 4.3 for the purposes of comparison with the predictions of equation (4.16).

The models examined are those of Silver (2), Bailey (12), Henry and Fauske (26) and Moody (28). All these models were discussed in section 1.4 of chapter 1 but for the purposes of this chapter the main assumptions of these models are tabulated overleaf.

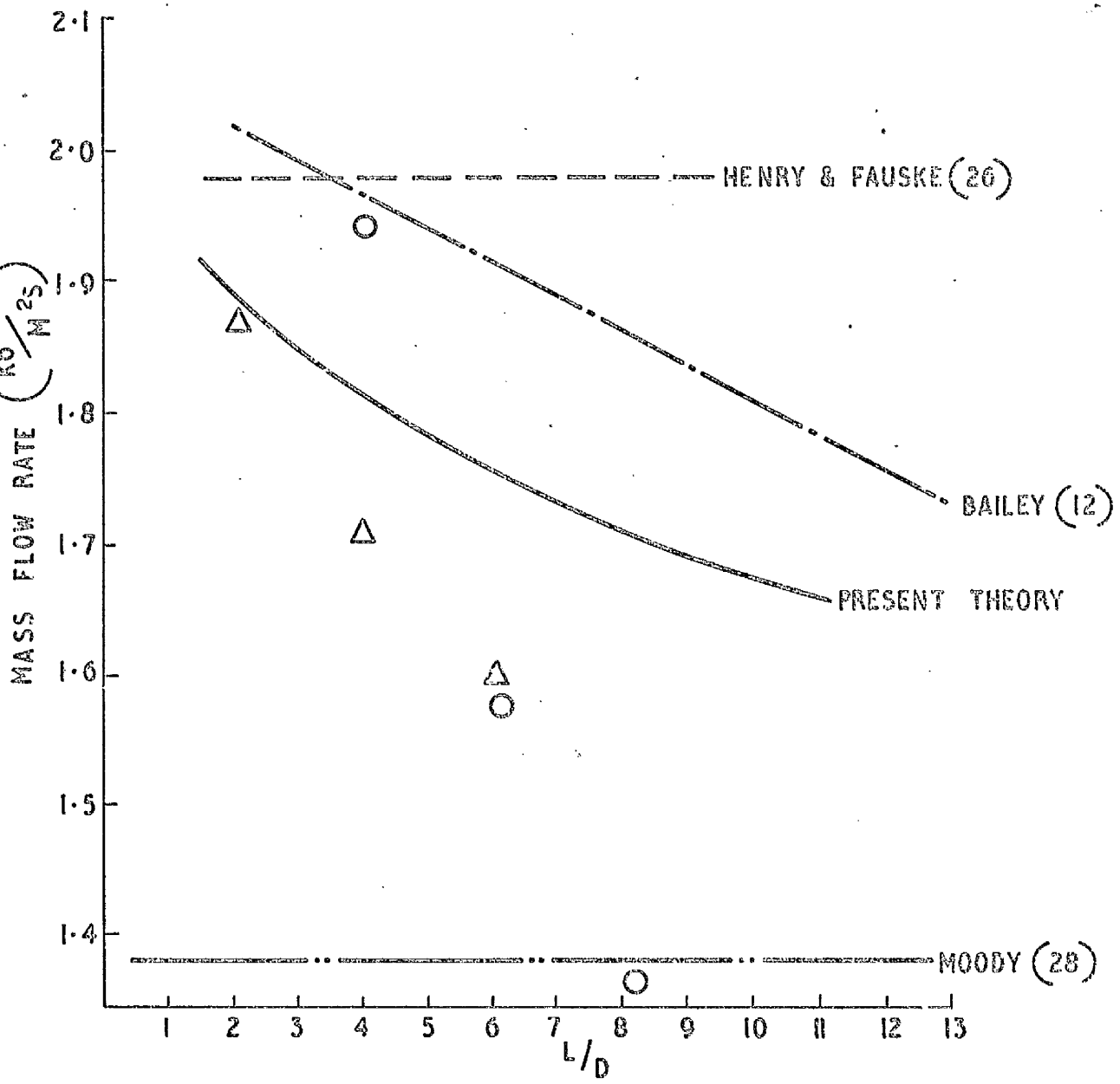

FIG. 4.2. COMPARISON OF PREDICTIONS FOR NOZZLES WITH SQUARE ENTRANCES. [DISCHARGE COEFFICIENT = 0·63]

△ DATA OF ZALOUDEK (4)
MAX. UPSTREAM PRESSURE 7 BAR
TEMPERATURE 160 °C

○ DATA OF FAUSKE (13)
MAX. UPSTREAM PRESSURE 7 BAR
TEMPERATURE 160 °C

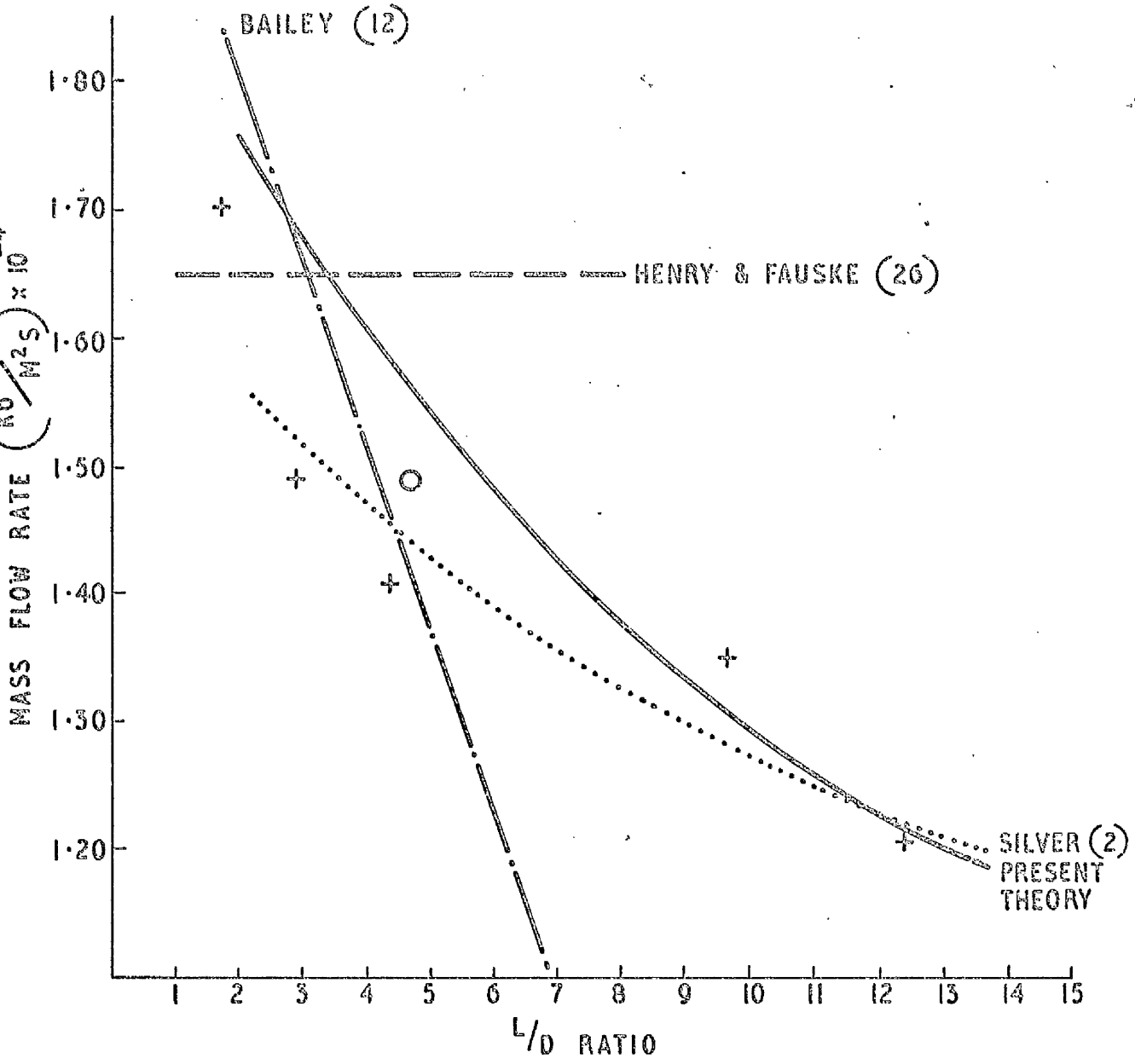

FIG. 4.3. COMPARISON OF PREDICTIONS FOR NOZZLES WITH ROUNDED ENTRANCES.
[DISCHARGE COEFFICIENT = 0·98]

+ DATA OF SILVER & MITCHELL (3)
MAX. UPSTREAM PRESSURE 3·6 BAR
TEMPERATURE 140 °C

O DATA OF BURNELL (61)
MAX. UPSTREAM PRESSURE 4 BAR
TEMPERATURE 140 °C

	Model	Flow Pattern	Slip-Ratio	Calculation of Quality
(a)	Silver (2)	Annular	Unity	Calculation of heat transfer from liquid core. (Non-equilibrium)
(b)	Bailey (12)	Annular	Unity	Semi-empirical calculation. (Non-equilibrium)
(c)	Moody (28)	Annular	$\sqrt[3]{\frac{\rho_f}{\rho_g}}$	Assumes thermodynamic equilibrium between phases.
(d)	Fauske and Henry (26)	Dispersed Mixture (but surface area undefined).	Unity	Uses semi-emprical constant to adjust value derived assuming thermo-dynamic equilibrium.

The model presented in this chapter is similar in many respects to those of Silver (2) and of Bailey (12); differing most markedly in the choice of slip ratio value. These models give predictions of the variation of mass flow rate with $^{L}/D$ ratio which compare favourably with the data of reference (3) as plotted in Fig 4.3. Reference (12) shows a linear variation which does not fit the data for values of $^{L}/D$ above 6, but reference (2) gives an excellent fit for all the data plotted in Fig 4.3.

The form of Silver's model (2) confines its use to nozzles with discharge coefficients close to unity and so this model cannot be used to predict critical flow rates for nozzles with square entrances, however reference (12) can be used to give such predictions. This model seems to overpredict critical mass flow rates and fails to predict the variation of critical flow rate with length/diameter ratio.

The models of Henry and Fauske (26) and Moody (28) give predictions

which show poor agreement with experimental data. Reference (26) does predict the magnitude of the critical flow rate at small values of $^{L}/_{D}$ but shows no variation of critical flow rate with $^{L}/_{D}$ ratio. The authors of reference (26), however, did have reservations concerning the application of their model to the critical flow situations examined here.

Predictions from reference (28) are extremely poor. The model does not allow for variation of flow rate with $^{L}/_{D}$ ratio or for variation with differing nozzle entrance. The predicted critical flow rates for square entrances are some 30% too low.

To summarise this comparison of the predicted critical flow rates obtained from the models of references (2),(12),(26) and (28) with the predictions of equation (4.16), and experimental data, it seems that neither reference (26) nor (28) offer even comparable accuracy of prediction while both reference (2) and reference (12) can offer worthwhile prediction of critical flow rates. However (12) certainly does not show the correct form of variation of critical flow rate with $^{L}/_{D}$ ratio. Reference (2) is restricted to nozzles with rounded entrances, but could, presumably, be easily adapted to provide predictions for other entrance shapes. Predictions from this model show very good agreement with experimental values of the critical flow rates. Thus while the predictions of equation (4.16) are certainly better than those of reference (12), or (26) and (28), equation (4.16) produces no better predictions than Silver's model (2). However, Silver's model requires an iterative process for the calculation of critical flow rates and so equation (4.16) may be preferred.

In general equation (4.16) would seem to offer an accurate method of predicting rates of two-phase critical flashing flow, within the limitations imposed by the assumptions used in developing the theoretical model.

Using equation (4.16) it is possible to produce values of critical flashing flow rate of water which, when compared with experimental data, correctly predict the variation of flow rate with,

(i) varying $^{L}/_{D}$ ratio for fixed entrance profile and temperature;

(ii) changes of nozzle entrance profile;

(iii) variation of liquid temperature.

By comparing the predictions for these variations of other theoretical models, it is clear that equation (4.16) gives the best prediction mechanism over the range of experimental values examined.

4.6 Review of Theoretical Work in Chapters 2, 3 and 4.

The theoretical model developed in this chapter has been shown to provide a useful prediction method for rates of critical flashing flow within the limitations of the assumptions used in constructing the model.

Many of the assumptions used in constructing this model have been previously used in other theoretical treatments of this problem, but this particular combination is original.

This theoretical part of the present work can therefore be seen to follow a definite course through chapters 2, 3, 4.

In chapter 1, the particular problem of possible non-equilibration between phases was identical as an important factor in the prediction of rates of two-phase critical flashing flows. In order to pursue this problem further a simple model for the prediction of heat transfer in turbulent flows was developed from the Reynolds Flux, in chapter 2, while in chapter 3, this model was successfully adapted to the prediction of rates of evaporation (and condensation) of water at short time intervals.

Finally by introducing features of other theoretical models of flashing flow and adding the predictive equation for evaporation rate developed in the earlier chapters, it was possible to produce a simple model for the prediction

of rates of critical flashing flow of water at low pressures. Since this simple model appears more successful in predicting critical flows than others which use many of the same assumptions, the use of the predictive method for evaporation rates set out in chapter 3 is further vindicated.

In the development of the theoretical work of chapters 3 and 4, lack of suitable experimental data was noted. This lack is especially marked in the case of critical flashing flows at low pressures. It appears that although much work has been carried out to produce data for critical flashing flows of water at high pressures and temperatures no comprehensive study exists which compares the effects of, altering the $^{\text{length}}/_{\text{diameter}}$ ratio, the entrance profile, for simple nozzles over a range of temperatures and pressures (up to 7 bar and 140 $^{\circ}$C). To remedy this apparent lack, and so provide further data of low pressure critical flashing flows, the work, described in the second part of this thesis, was carried out.

Appendix A to Chapter 4

The Derivation of the Slip Ratio

The slip ratio value used in chapter 4 is defined by

$$\frac{U_g}{U_f} = \sqrt[3]{\frac{\rho_f}{\rho_g}} \qquad (A.4.1)$$

The derivation of this value reproduced here is taken from Zivi, (29) and follows the derivation in (29) almost exactly, but with altered notation. This derivation assumes,

(a) negligible wall friction in the duct;

(b) the void-fraction is such as to minimise the kinetic energy flux through the flow passage.

The justification for these assumptions is fully discussed in (29).

If the mass flow rate in the duct is G, then

$$U_g = \frac{Gx}{\rho_g \alpha} \qquad (A.4.2)$$

$$U_f = \frac{G(1 - x)}{\rho_f (1 - \alpha)} \qquad (A.4.3)$$

α = void fraction.

The kinetic energy flux in the duct is

$$E = \frac{G}{2}\left[U_g^2 x + U_f^2 (1 - x)\right] \qquad (A.4.4)$$

the void fraction is assumed such that E is minimised

$$\text{i.e. } \frac{dE}{d\alpha} = \frac{G}{2}\left\{2U_g \frac{dU_g}{d\alpha} x + 2U_f \frac{dU_f}{d\alpha}(1 - x)\right\} = 0 \qquad (A.4.5)$$

Evaluating $\frac{dU_g}{d\alpha}$ and $\frac{dU_f}{d\alpha}$ from equations (A.4.2) and (A.4.3)

$$\left.\begin{aligned} \frac{dU_g}{d\alpha} &= -\frac{Gx}{\rho_g \alpha^2} \\ \frac{dU_f}{d\alpha} &= +\frac{G(1 - x)}{\rho_f (1 - \alpha)^2} \end{aligned}\right\} \qquad (A.4.6)$$

Substituting (A.4.2), (A.4.3) and (A.4.6) into (A.4.5) the solution for void fraction is

$$\alpha = \left| 1 + \frac{(1 - x)}{x} \left(\frac{\rho_g}{\rho_f}\right)^{\frac{2}{3}} \right|^{-1} \qquad (A.4.7)$$

However for two-phase flows the void-fraction is fixed while the slip ratio is variable, whence from (A.4.2), (A.4.3) and (A.4.7) the slip ratio is found as

$$\frac{U_g}{U_f} = \left(\frac{\rho_f}{\rho_g}\right)^{\frac{1}{3}} . \qquad (A.4.1)$$

Appendix B to Chapter 4

Change of Core Diameter and Liquid Velocity with Evaporation Effects

The flow rate of the liquid phase at any point in the flow is

$$W_f = \rho_f U_f A_f \qquad (B.4.1)$$

where A_f = cross section occupied by liquid = πr^2

r = liquid core radius

$$\therefore \quad \frac{dW_f}{dy} = \frac{d}{dy}(\rho_f U_f A_f) \qquad (B.4.2)$$

$$\frac{dW_f}{dy} = \rho_f \left[U_f \frac{dA_f}{dy} + A_f \frac{dU_f}{dy}\right]$$

$$= \rho_f \left[\frac{\pi U_f^2}{} \frac{dC}{dy} + \pi r_o^2 \frac{dU_f}{dy}\right] \qquad (B.4.3)$$

Integrating from y = 0 to y = L.

$$\Delta W_f = 2\pi\rho_f U_f r_o \int_o^L \frac{dr}{dy} + \pi\rho_f r_o^2 \int_o^L \frac{dU_f}{dy}\, dy.$$

$$= \pi\rho_f r \left[2U_f \Delta r + r \Delta U_f\right] \qquad (B4.4)$$

From equation (4.3) and (4.5) with $r = C^{\frac{1}{2}}D$.

$$\Delta W_f = \frac{\rho_f U_f}{\rho_g U_g} 8\pi r \, Lx_E \left[\frac{k\rho}{\pi C_p} \frac{U_f}{L}\right]^{\frac{1}{2}} \qquad (B.4.5)$$

whence $$\frac{2\Delta r}{r} + \frac{\Delta U_f}{U_f} = \frac{8Lx_E}{\rho_g U_g r} \left[\frac{k\rho}{\pi C_p} \frac{U_f}{L}\right]^{\frac{1}{2}} \qquad (B.4.6)$$

$r = C^{\frac{1}{2}}D.$

The expression $\frac{16Lx_E}{\rho_g U_g} \left[\frac{k\rho\ U_f}{\pi C_p LCD^2}\right]^{\frac{1}{2}}$ can be evaluated numerically for the values of the parameters used in the critical flow rate in Chapter 4.

For a nozzle with length 10 cm, throat diameter 2.54 cm, and an ultraheat of 40 ^{o}C.

$$\left[\frac{2\Delta r}{r} + \frac{\Delta U_f}{U_f}\right] \doteq 0.1.$$

Hence the effects of regarding liquid-phase velocity and core diameter as constant, together introduce an error of less than 10%

Since this error arises in ΔW_f, which is only about 0.1 W_{fo}, it may be safely disregarded in the evaluation of critical flow rates.

Chapter 5 - Introduction to Experimental Work

5.1 The first part of this thesis is concerned with the development of a theoretical model of two-phase flashing flow. During the construction of this model certain assumptions were made which restricted the application of the model to critical flashing flows of water at pressures less than 10 bar and liquid superheats less than 50 ^{o}C. The model introduced in chapter 4 gave predictions of variation in critical flow rate with changing nozzle entrance shape, length to diameter ratio, and liquid temperature. Little experimental data is available on the effects of these parameters on critical flow rates, for low pressure flows, as was shown when a comparison of the model with experimental data was made.

The experimental study was intended to give further data on critical flashing flow rates for water at low pressures in simple nozzles. This chapter sets out the areas of experimental study and discusses the criteria applied in designing the experimental apparatus.

5.2 Description of Experimental Study

The lack of experimental data, on critical flashing flow rates at low pressures, suggested that a comprehensive experimental study of the variation of critical flow rates in nozzles with certain parameters would be of value.

At the outset it was decided that the maximum pressure in the flow system would be limited to 10 bar, that the pressure downstream of the nozzle would be atmospheric and that the liquid superheat would not exceed 50 ^{o}C. These limits were established for two reasons; firstly the theoretical work described in chapters 2 to 4 was effectively limited to flows in systems having these limits. Secondly the introduction of these low pressures and temperature limits greatly simplified the design of the experimental system.

By examining the work of previous experimenters certain important parameters were chosen for study. In the final form, the programme would involve the determination of:

(1) the variation of critical flow rates with liquid superheat;

(2) the variation of critical flow rates with the shape of the entrance to the flow passage;

(3) the variation of critical flow rate with length/diameter ratio of test nozzle;

(4) pressure gradients in the nozzle and near exits and entrances;

(5) the quantity of dissolved gases in the water used. In practice this analysis was confined to dissolved oxygen.

Having defined the aims of the study some preliminary design work could be carried out.

Before further discussing the design of the rig it is necessary to digress, and discuss the use of the term "critical flow".

5.3 Note on the use of the term Critical Flow

The phenomenon of mass limiting or critical flow of fluids, whether single or multi-phase, is well established for certain conditions.

Critical flows are defined in terms of the variation of the mass flow rate (G) of the fluid in some test section or nozzle with changes in the difference between the entrance pressure (P_1) and the exit pressure (P_2) of the nozzle, with other parameters held constant. The critical flow is defined as the mass flow rate for which;

$$\left(\frac{\partial G}{\partial (P_1 - P_2)}\right)_{\substack{\text{constant} \\ \text{parameters}}} = 0 \qquad \ldots\ldots(5.1)$$

For a real nozzle the variation of $(P_1 - P_2)$ can be obtained in two ways.

(A) By changing P_2 and holding P_1 and other parameters constant.

(B) By changing P_1 and holding P_2 and other parameters constant.

For single phase flows it is well established that critical flows in nozzles occur when the velocity of flow at the nozzle throat is equal to the local sonic velocity. If friction effects are negligible this critical flow rate is a function of P_1 and T only. Hence variation of P_2 has no effect on the flow rate.

If an experiment is performed, to determine critical flow rates, by increasing the upstream pressure, (method B), the flow rate is still a function of P_1 and T, and the flow velocity will vary with P_1. Thus in this case the critical flow rate established by varying P_1 will vary with P_1.

For flow rates obtained by varying P_2 at constant P_1 and T the critical flow is independent of P_2 and will remain constant as P_2 varies.

Typical plots of the variation of flow rate with pressure drop obtained by varying P_1 and by varying P_2 are shown on Fig. 5.1.

Method A gives a well defined flat profile when the flow velocity is equal to the sonic velocity and

$$\left(\frac{\partial G}{\partial(P_1-P_2)}\right)_T = 0 \qquad .....(5.2(a))$$

However for method B the plot shows that values of G increase even after the flow velocity reaches the local sonic velocity at the throat,

and $$\left(\frac{\partial G}{\partial(P_1-P_2)}\right)_T \neq 0 \qquad .....(5.2(b))$$

If equation (5.1) is used as a criterion for defining a critical flow rate then for single phase flows only method A could be used to determine experimental critical flow rates.

For two-phase flows equation (5.1) is frequently used to define experimental critical flow rates. Clearly the experimental method chosen would be that for which there existed some range of values of $(P_1 - P_2)$, such that;

$$\left(\frac{\partial G}{\partial(P_1-P_2)}\right) = 0$$

Unfortunately the choking process for two-phase flows is not well understood. If, however, the two-phase choking mechanism is in some way related to the attainment of a sonic velocity in the flow then an argument analogous to that for single phase flows would suggest that for method A for some $(P_1 - P_2)$

$$\left(\frac{\partial G}{\partial(P_1-P_2)}\right) = K_A = 0 \qquad .....(5.2(a))$$

while for method B,

$$\left(\frac{\partial G}{\partial(P_1-P_2)}\right) = K_B \neq 0 \qquad .....(5.2(b))$$

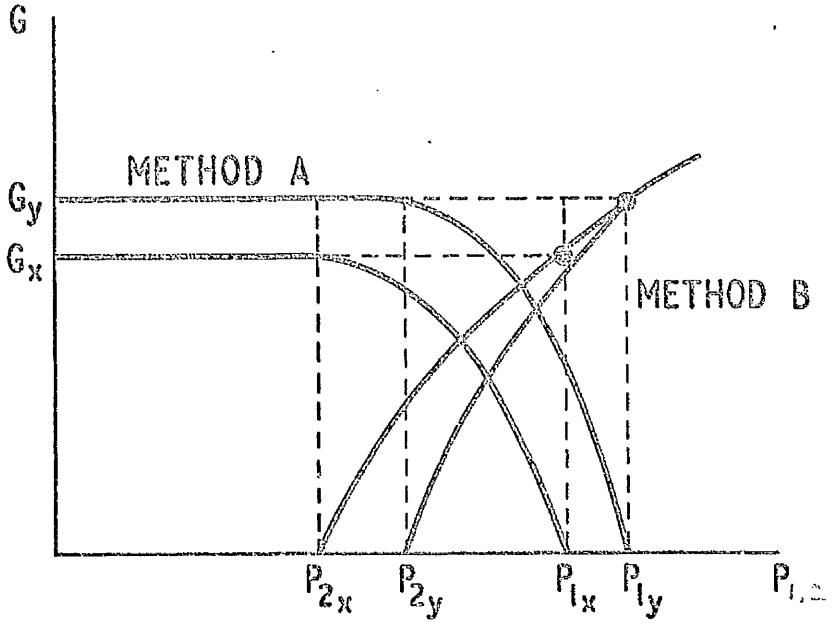

Fig. 5.1. Variation of G with pressure drop, critical ratio is P1/P2 in each case.

However although theoretical models have been constructed by making assumption of choked flow rates varying with a sonic velocity including the models with pseudo-sonic choking discussed in section 1.4 and the model discussed in Chapter 4 of this thesis; the experimental evidence does not uniquely establish sonic velocity as the choking velocity for two-phase flows of the type discussed in this thesis. Hence for such flows great care is necessary in using arguments based on evaluation of either K_A or K_B by analogy with the single phase case.

Nevertheless, in previous experimental work, experimenters have found critical two-phase flow rates by examining the variation of G with $(P_1 - P_2)$ using method B. The critical flow rate has been defined as the mass flow rate for which K_B is less than some minimum gradient.

Examples of the use of this experimental technique are references (3),(9),(12), (13),(17). It is interesting to note that the critical flow rates evaluated in an experiment where the pressure drop was altered using method A (reference (4)) are of similar magnitude to those found in reference (13) for similar flows.

In this present work the use of method B arises from the design of the experimental apparatus. The criteria for selecting the values of critical flow rate are given in the discussion in Chapter 7.

This choice was reinforced by the observation that for many design applications requiring a knowledge of critical two-phase flow rates the exit pressure is defined for the flow while the upstream conditions are variable. One example of this situation is the emergency blowdown of reactor pressure vessels.

5.4 Summary of Design Specification

After consideration of the various requirements and restrictions discussed in this chapter, an experimental rig was constructed. The rig was intended to provide facilities for experimental investigation of the areas tested in section 5.2, using water as the working fluid.

After reviewing the problems of definition of the term "critical flow" with regard to two-phase flashing flow, a design was evolved which would obtain limiting flow values in the test sections by increasing upstream pressures while holding downstream pressures constant.

Since pressure gradients were to be examined in the flow, the throat diameter of the nozzle had to be considerably larger than the probe cross-section dimensions in order to reduce the disturbance introduced by the probes. Nozzle bores, or throat diameters were chosen as 12.7 mm(0.5") and 25.4 mm(1"). Simple nozzle shapes were chosen to ease identification of the effects of variation in entrance shape and nozzle length. The nozzles are described in section 6.2 of Chapter 6.

The combination of nozzle throat diameters of order 10 mm with flow rates of the order of 10^4 kg/m^{2}s gave a large circulation rate, with attendant vapour condensation and liquid reheating problems thus indicating an intermittent ("single shot") mode of operation. This scale requirement, coupled with a rather tight project time scale, produced a design which utilised standard equipment as much as possible. The resultant experimental rig was therefore of simple, if massive, design but proved extremely reliable.

In chapter 6 the experimental rig is described in detail, with additional notes on instrumentation and operating problems.

Chapter 6 The Experimental Rig - Construction and Operation

6.1 Chapter 5 set out the design criteria for the experimental system used to study critical flashing flow rates of water in short nozzles. In this chapter the experimental rig is described and the operational and instrumentation problems associated with the system are discussed.

In general the rig was designed to utilise as many standard components and techniques as possible. Experimental values with uncertainties of less than 3% were normally considered acceptable.

Because the change from Imperial to S.I. units and standards had not then taken place in the workshops producing components for the rig, the drawings for the various components were made in Imperial units and the standards used were those expressed in Imperial units. In certain cases e.g. calibrations, calculations were then converted to S.I. Results are expressed in S.I. Many of the figures in this chapter are revised copies of the original engineering drawings and sketches and hence are in Imperial units. Further, in this chapter, where Imperial dimensions etc are quoted with S.I. equivalents, the measurement in Imperial units is the defining measurement and the S.I. expression is merely for convenience.

6.2 Construction and Layout

General views of the experimental system are given in Figs 6.1 and Plates 6.1. Examination of these figures and plates indicates the large size of the rig.

The system consists of two large tanks interconnected by a piping system. In the main pressure tank water can be heated by steam injection to a temperature of 150 ^{o}C. The pressure in this tank is adjusted by a compressed air system up to a maximum value of 7 bar (100 lbf/in^2).

Water is led from the main pressure tank through a 4 inch (101 mm) line, past thermometers and orifice plates to the nozzle test sections. From the horizontal test sections the steam-water mixtures pass into a deflector box mounted on the receiving tank and are deflected downwards into the receiving

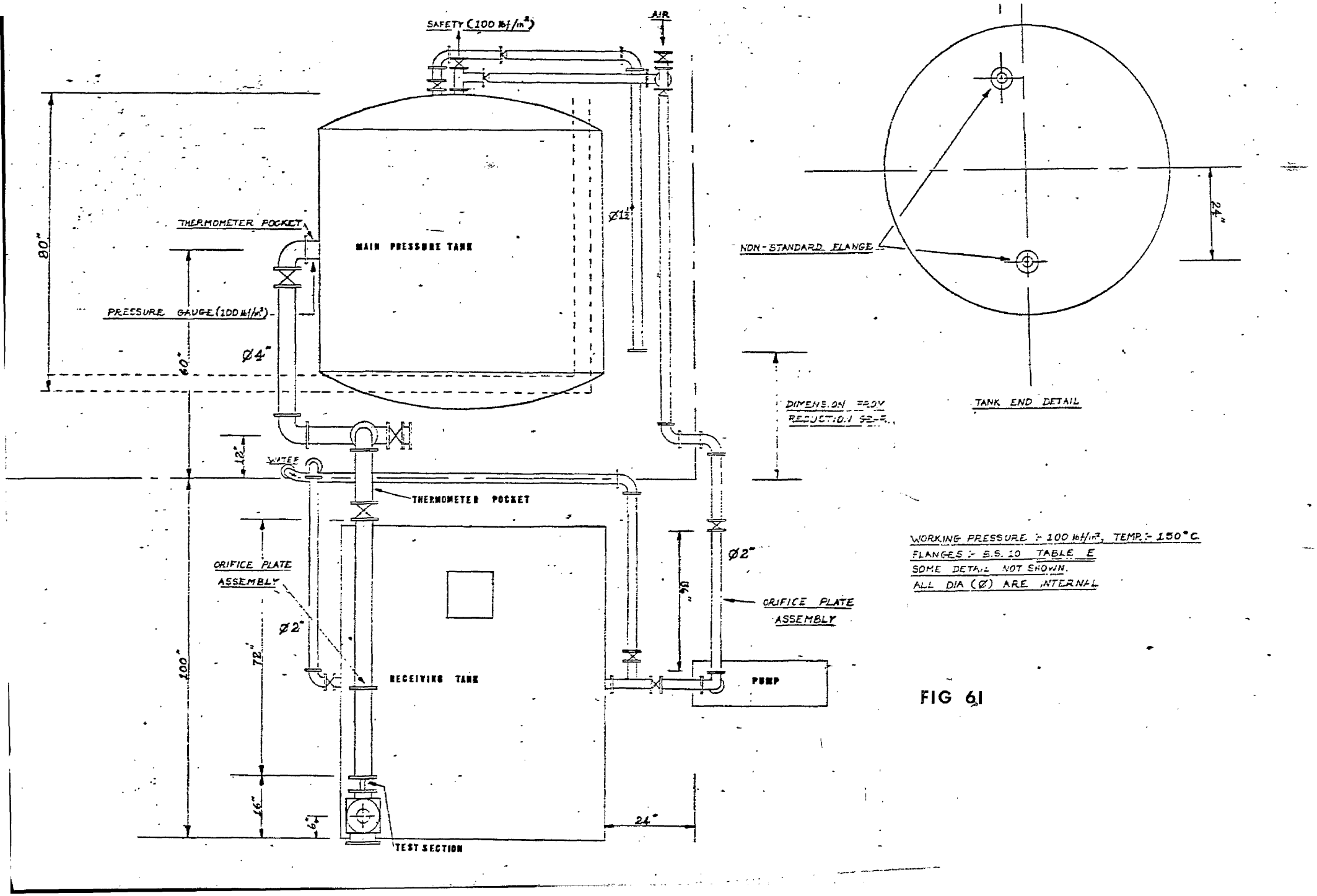

WORKING PRESSURE :- 100 lbf/in², TEMP.:- 150°C.
FLANGES :- B.S. 10 TABLE E
SOME DETAIL NOT SHOWN.
ALL DIA (Ø) ARE INTERNAL

FIG 61

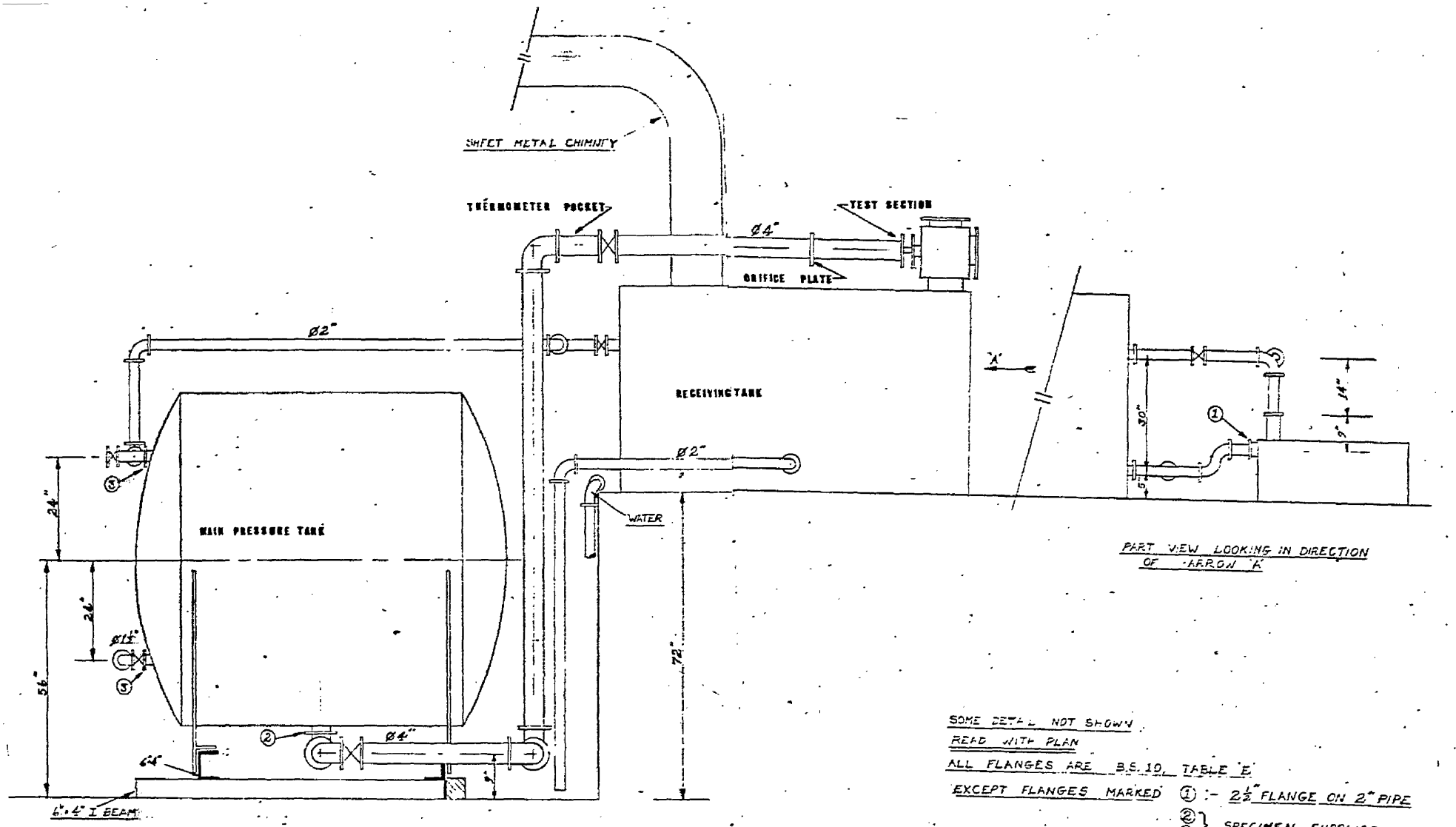
SHEET METAL CHIMNEY
THERMOMETER POCKET
TEST SECTION
Ø4"
ORIFICE PLATE
Ø2"
RECEIVING TANK
'A'
30"
14"
9"
5"
Ø2"
WATER
MAIN PRESSURE TANK
24"
24"
56"
72"
Ø1½"
Ø4"
6"
6"x4" I BEAM
PART VIEW LOOKING IN DIRECTION OF ARROW 'A'
SOME DETAIL NOT SHOWN
READ WITH PLAN
ALL FLANGES ARE B.S. 10, TABLE 'E'
EXCEPT FLANGES MARKED ① :- 2½" FLANGE ON 2" PIPE
②③ } SPECIMEN SUPPLIED

FIG 6.1

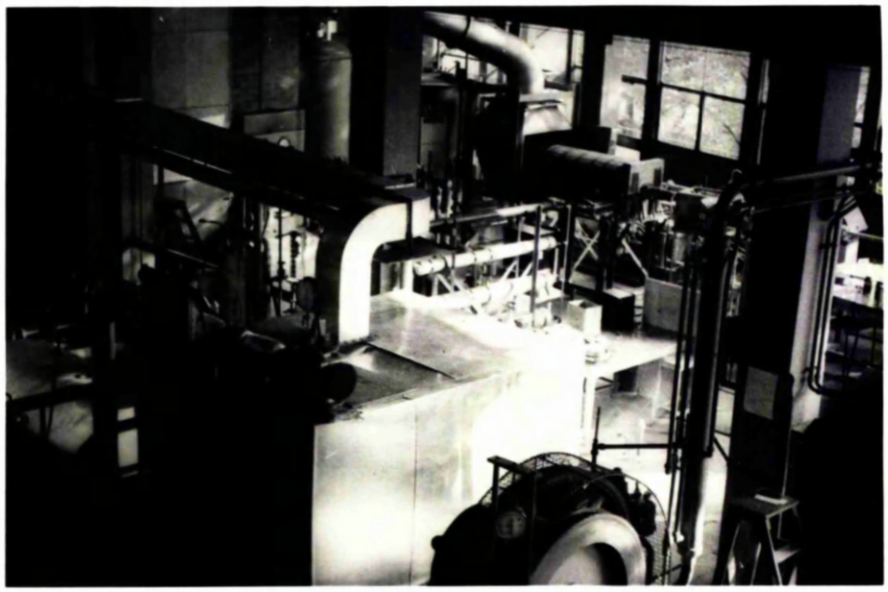

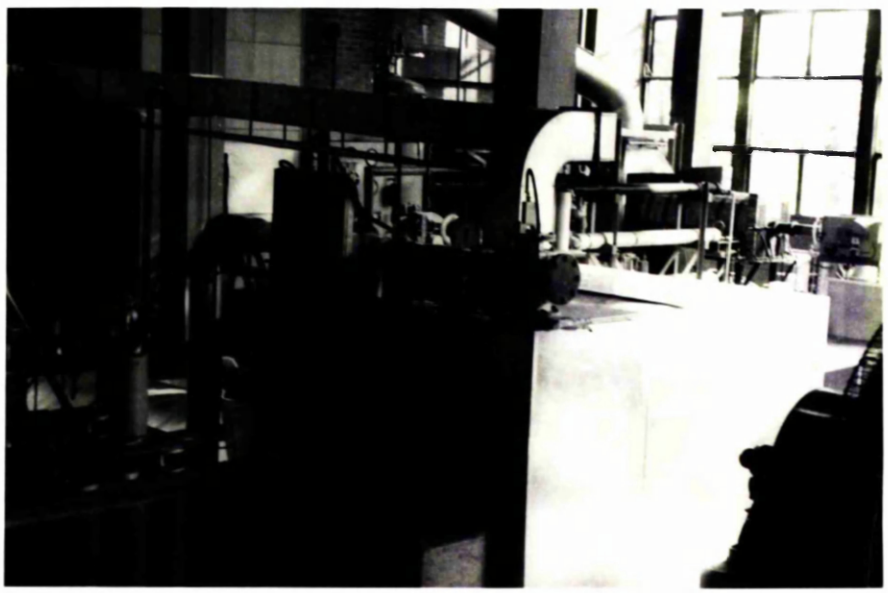

Pl. 6.1 GENERAL VIEWS of EXPERIMENTAL RIG

tank through an 8 inch (203 mm) diameter opening. In the receiving tank the water and steam components of the flow separate. No condensing system is fitted and the steam is blown off to atmosphere down a large duct. Receiving tank pressures are always within 0.1 bar (2 lb/in^2) of atmospheric pressure.

Water from the receiving tank is returned to the main pressure tank by a pump system.

The main components of the system are now described in detail, using the designation of Figs 6.1.

(1) Main Pressure Tank. A cylindrical tank of approximate dimensions length 7 ft (2.1 m) diameter 6 ft 8" (1.7 m). This tank is of foreign manufacture and does not conform to BS1500. The operating conditions are defined by insurance inspection requirements and are; maximum pressure 100 lb/in^2 (7 bar) at a maximum temperature of 150 ^{o}C.

The tank is fitted with a steam injector heater. Steam is supplied in a saturated condition through a reduction system at a normal operating rate of 900 lb/hr (400 kg/hr). A time of about 4 hrs. is required to heat a full tank of cold water.

Other connections to the main pressure tank are for an air supply line from a compressor system and for a safety valve blowing off at 100 lb/in^2 (7 bar) pressure. Water is discharged to the test section through a 4" (101 mm) diameter opening beneath the tank. The main pressure tank is mounted on a grillage system.

Thermometers and pressure gauges are fitted at various points.

(2) Receiving Tank. A rectangular tank with approximate dimensions 6 ft (1.8 m) x 8 ft (2.4 m) x 3 ft (1.2 m), constructed of $\frac{1}{2}$ inch (12 mm) steel plate. The nominal operating pressure for this tank is atmospheric pressure at temperatures up to 110 ^{o}C.

This tank has connections for drain lines, for cold water feed lines and a return line to the main pressure tank. A sight gauge for water levels and a pressure gauge are fitted to the tank.

A 12 inch (300 mm) opening onto top surface of the tank is connected to a square duct. The duct carries off steam from the receiving tank. On the top of the tank the deflector box is also fitted. The deflector box is 10 inches (250 mm) square and constructed of $\frac{1}{2}$ inch (12 mm) steel plate. This box also provides mountings for pressure probes.

(3) The Piping System. The sizes and approximate form of the piping layout is shown in Fig 6.1. All piping and flanges conform to British Standards for a system operating at a design maximum pressure of 120 lb/in^2 (8 bar). Certain sections of the smaller pipes are fitted with screwed fittings. These also conform to British Standards. No attempt has been made to protect the system against rusting or other forms of corrosion.

(4) The nozzle test sections. The nozzles used in the experimental programme are of two types, (a) metal, (b) glass. The dimensions and forms of these nozzles are shown in Figs 6.2(a) and 6.2(b), and Plates 6.

Metal nozzles were constructed from stock steel plate and piping with an internal finish to 0.002 inch. For these nozzles dimension L was 5" (127 mm), 4" (101 mm), 3" (76 mm) and 2" (51 mm) for each entrance profile. The corresponding dimension D was 1" (25 mm) and 0.5" (12mm) but two sets were made with D of 1.5" (38 mm) and 0.75" (19 mm) with a length L of 4" (101 mm). This gives a total of 30 nozzles.

Glass nozzles were constructed only for D of 1" (25 mm) with L values of 4" (101 mm), 5" (127 mm) and 3" (76 mm) in each of three entrance profiles. For these nozzles the entrance and exit flanges were made from the same stock steel as the metal nozzles.

Some problems were found in sealing the glass tube section to the entrance and exit flanges. The glass being held in place by a compression force due to the expansion of the steel pipe system.

Both types of nozzle were set into the 4" pipe system just before the deflector box. A 5" (127 mm) gap was made to accept the nozzles. For nozzles shorter than 5" (127 mm) spacer pieces were inserted just upstream of the nozzle entrance. A typical nozzle assembly is shown in Fig 6.3.

Attempts to protect the internal metal surfaces of the nozzles from

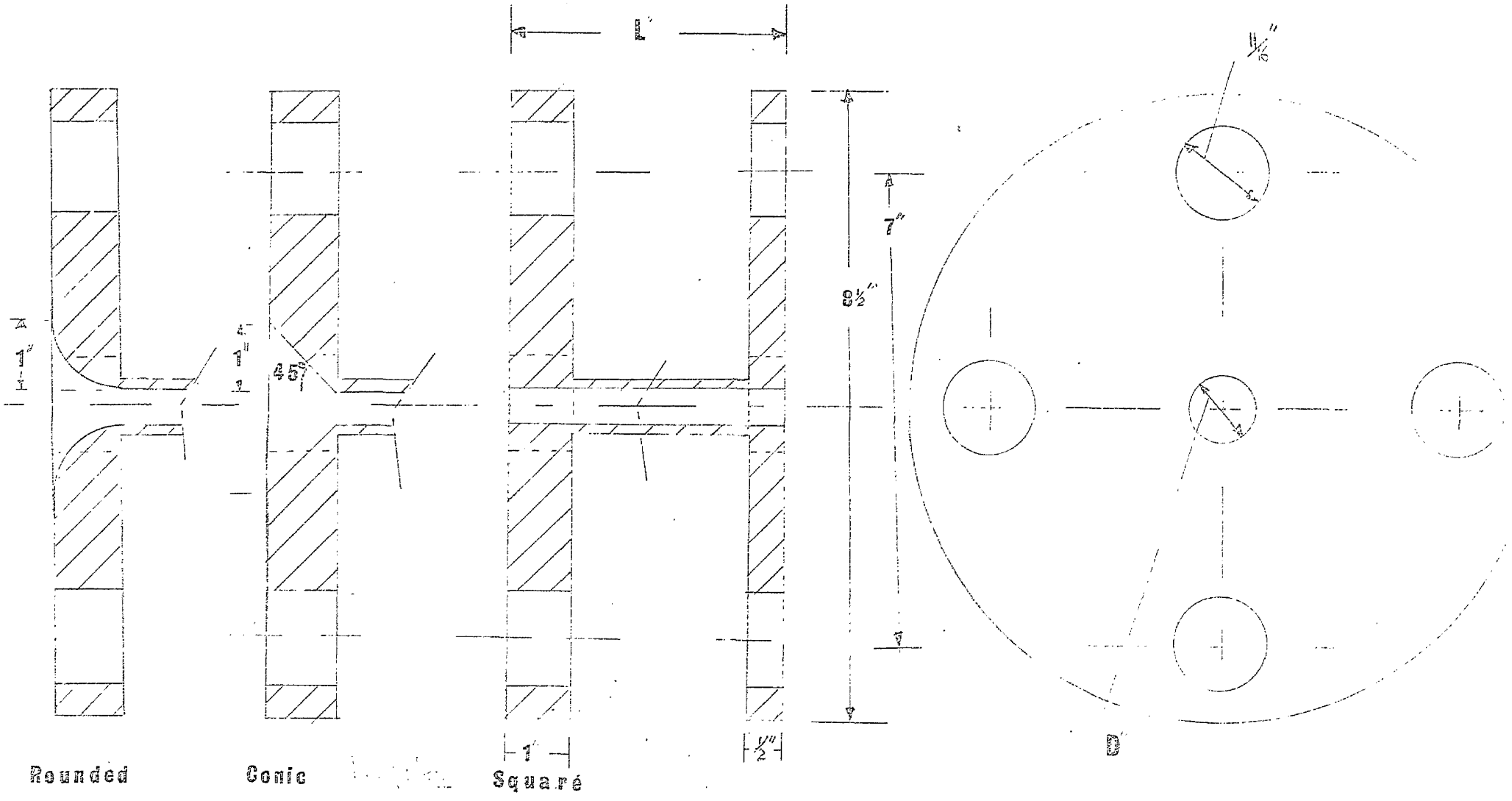

Alternate Entrance Profiles

FIG 6.2(a) NOZZLE TEST SECTIONS (Metal)

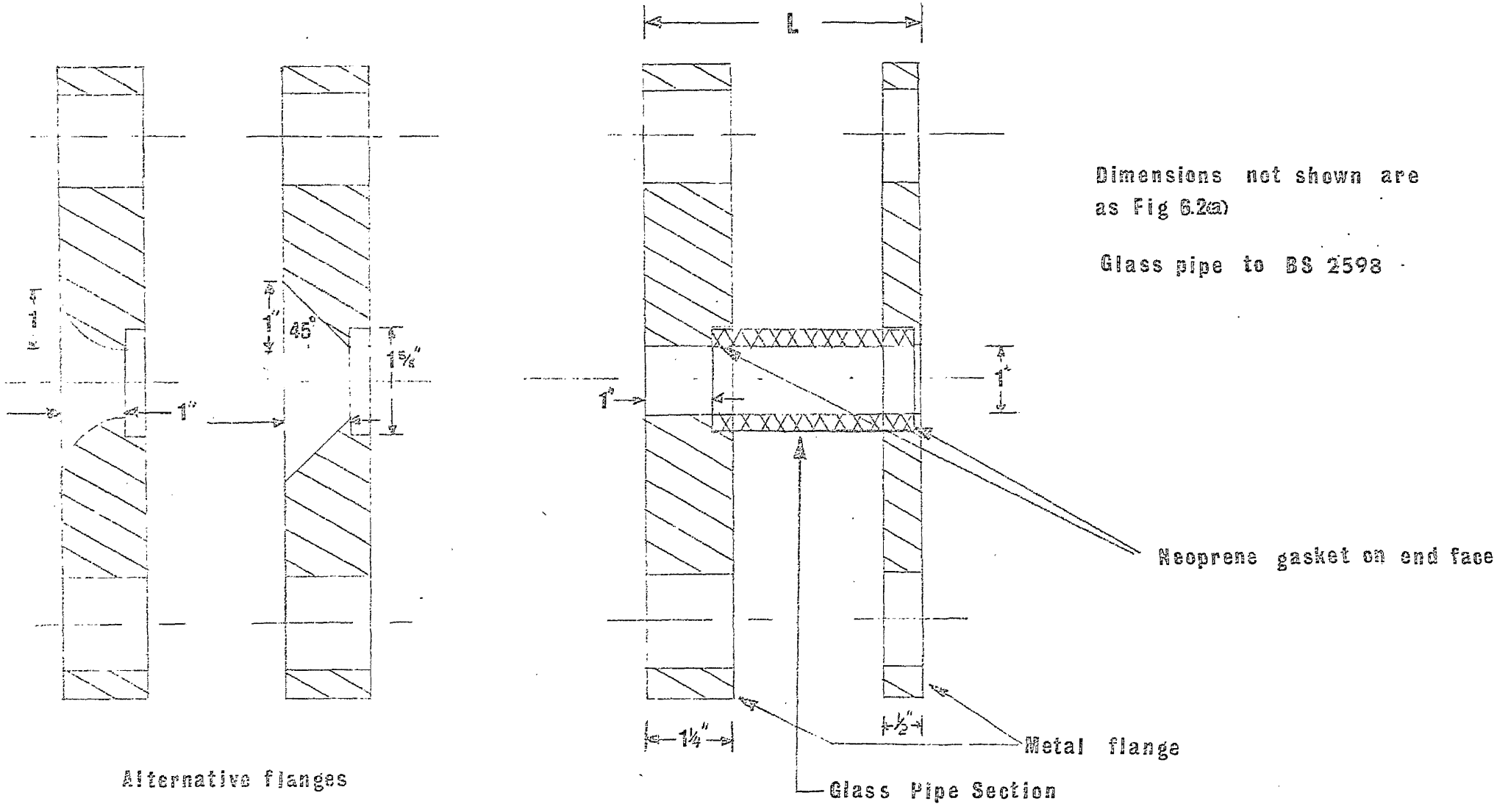

Dimensions not shown are as Fig 6.2(a)

Glass pipe to BS 2598

FIG 6.2(b) NOZZLE TEST SECTIONS (Glass)

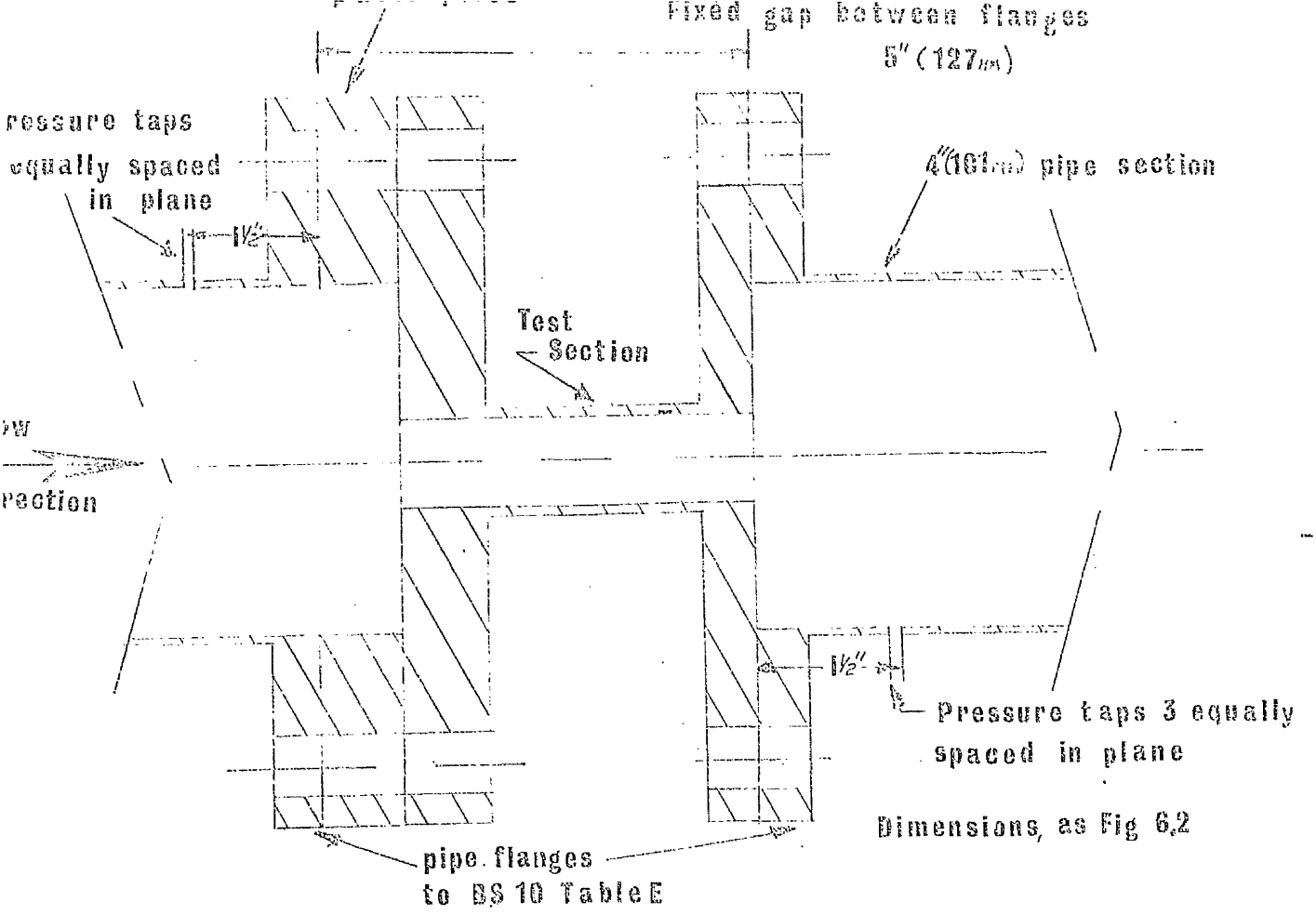

FIG. 6.3 TEST SECTION ASSEMBLY

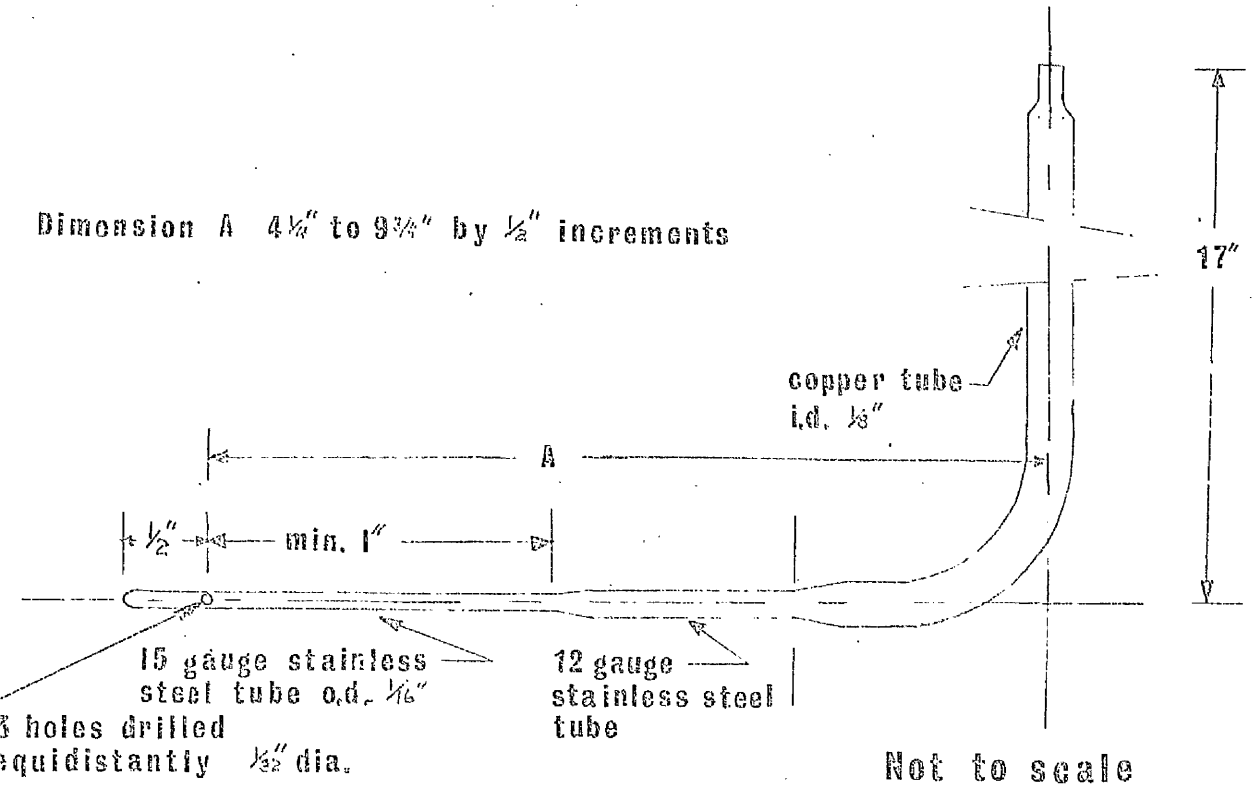

FIG 6.4 AXIAL PRESSURE PROBES

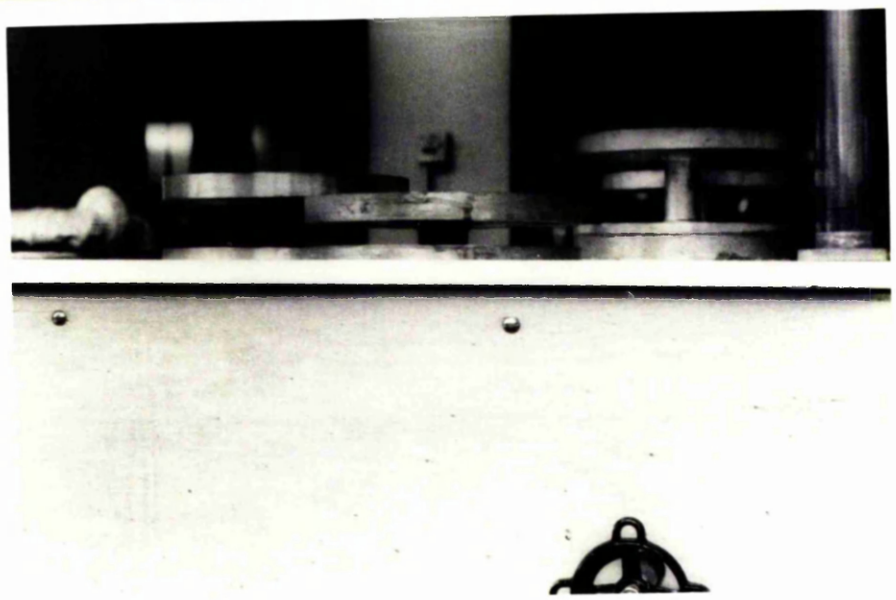

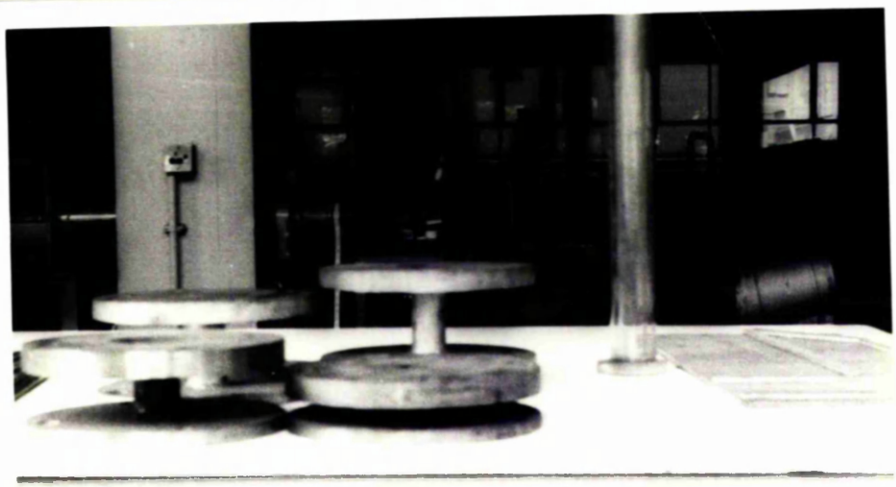

Pl. 6.2 (a) COMPARITIVE VIEWS of NOZZLES

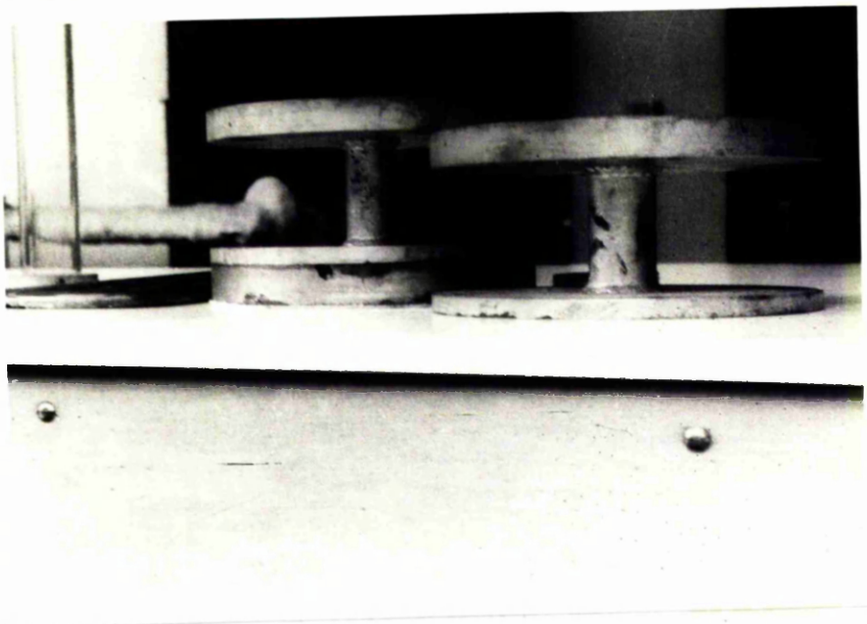

Pl. 6.2 (a) COMPARITIVE VIEWS of NOZZLES

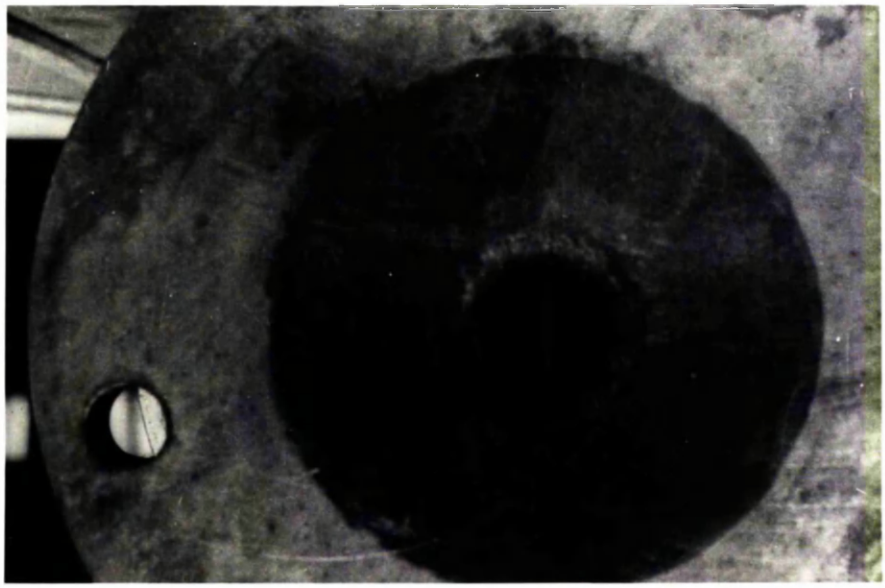

ROUNDED

CONIC

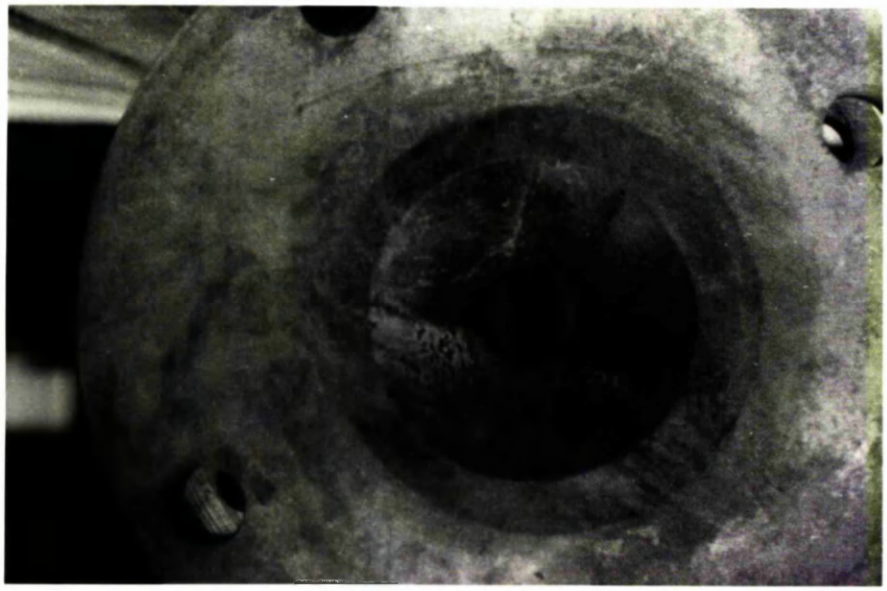

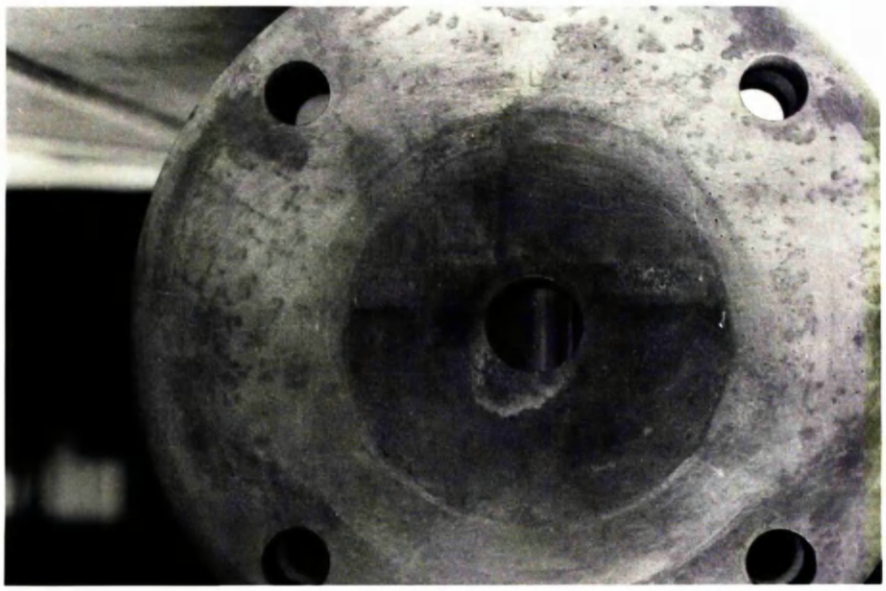

SQUARE

NOTE CORROSION

PL 62(b) NOZZLE ENTRANCES

corrosion damage by using various coatings proved unsuccessful.

The main components of the system being described, the instrumentation used to provide the experimental results will be discussed in section 6.3.

6.3 Instrumentation

To achieve the aims set out in chapter 5, measurements were required of certain parameters in two phase flashing flows.

These measurements were (a) flow rate;

(b) liquid bulk temperature;

(c) pressure drop across test section - i.e. upstream and downstream pressures;

(d) pressure distributions within the nozzle;

(e) dissolved gases in the liquid.

To obtain these measurements instruments had to be installed in the experimental system. As a matter of policy the type of measuring instruments chosen were simple standard types capable of giving accuracies within 3% and preferably of robust construction.

The methods of obtaining the required measurements will now be reviewed. Details of calibration procedures and calibration curves are given in Annexe A to this chapter.

(a) Flow rate. Flow rate measurements were made by using an orifice plate. The orifice plate was used with pressure tappings of the "D and $\frac{D}{2}$" type and conformed in all respects to B.S.1042. An orifice plate system was chosen to permit the plates to be changed quickly and easily in the event of damage by cavitation. In fact no such damage was observed.

The use of an orifice plate for flow measurements of this type requires that the flow shall be single-phase at the orifice plate. The conditions of pressure and temperature in the region of the orifice plate during operation of the system were such that the water was in a subcooled state. From this observation, coupled with the results of the calibration tests, it would seem that the use of an orifice plate designed to B.S.1042 is justified in this case.

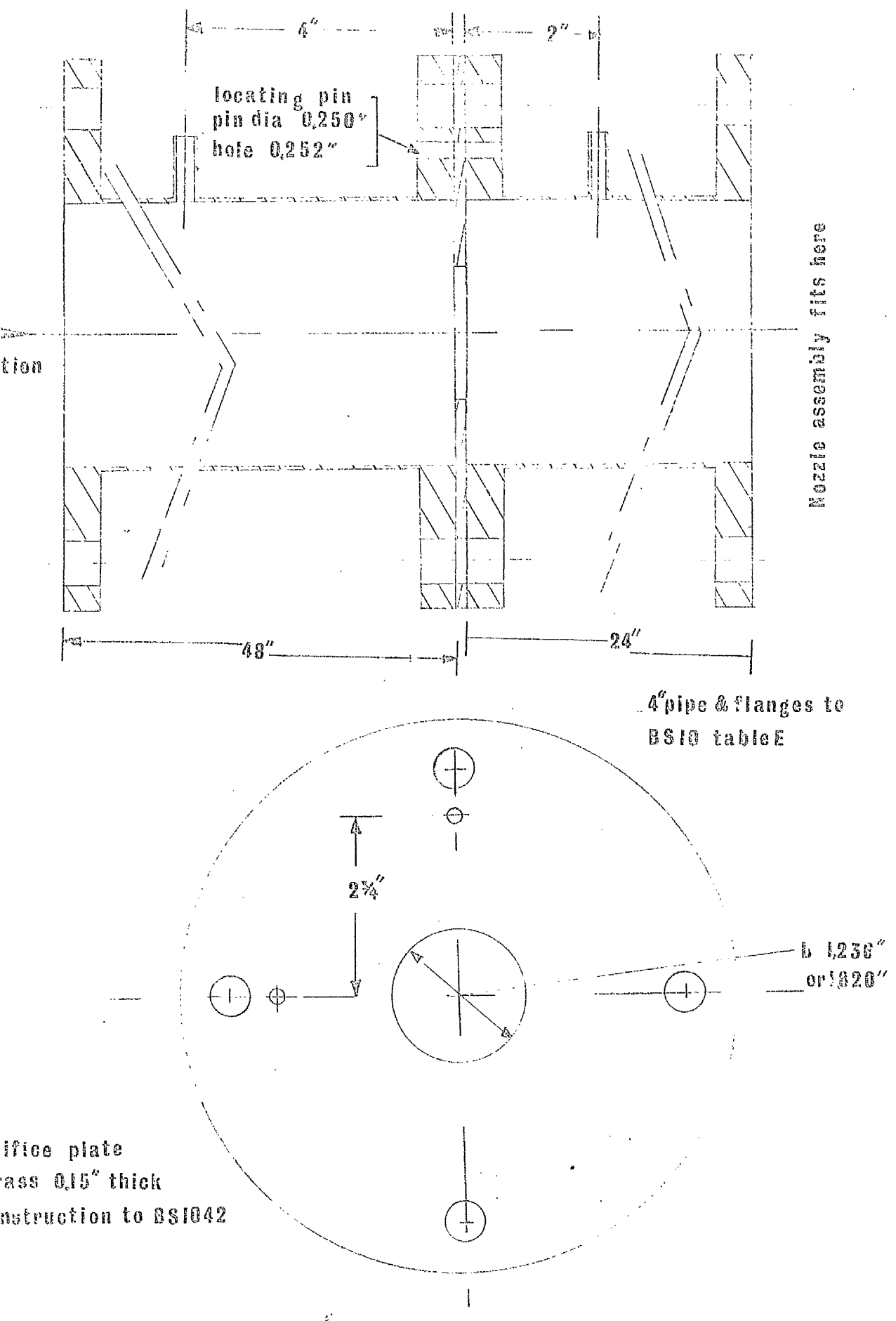

FIG 6.5 ORIFICE PLATE ASSEMBLY

This observation does not of course preclude the evolution of vapour at some point in the flow between the orifice plate and the nozzle entrance.

Two sizes of orifice plate were used with a water over mercury manometer system and calibration curves for these are included at Annexe A. The 1.236" orifice plate was used with 0.5" (1.27 mm) bore nozzles and the 1.826" with all other nozzles. Measurements of flow rates under the same conditions gave the same values with either orifice plate.

(b) Liquid Bulk Temperature. Liquid temperatures were measured using a good quality mercury in glass thermometer installed in the position shown in Fig 6.1 to meet the requirements of B.S.1041. Although the use of a thermometer introduces a considerable lag in temperature readings, the thermometer system was found to be as accurate as thermocouple systems of comparable cost. The thermometer has the advantage of being direct reading without the additional complication of electronic systems operating in a damp atmosphere. Calibrations and correction factors are again given in Annexe A.

(c) Pressure Drop across Test Sections. The definition of critical flashing flow as a mass limiting flow implies that experimental determination of such critical flow rates will also require measurements of the pressure drop across the nozzles.

From Fig 6.3, pressure taps are provided 1.5" (37 mm) upstream and downstream of the test section. Each set of tappings consists of 3 taps spaced equally in the same plane. These sets of tappings were each connected to a Bourdon tube pressure gauge reading from 0 to 7.0 bar (0 to 100 lb/in^2). The gauges were of a high quality test type with a manufacturer's accuracy of $\pm$ 0.05 bar.

Copies of the manufacturer's calibration are at Annexe A.

(d) Pressure Distribution. Pressure distributions were determined by an axial probe system. The probe design is shown in Fig 6.4 and Plates 6.3. The probes form a set of various lengths and could be traversed in the vertical plane by a traversing mechanism (plate 6.4). The various lengths of probe gave positions of the tappings from 0.25 inch (6.5 mm) behind the nozzle exit

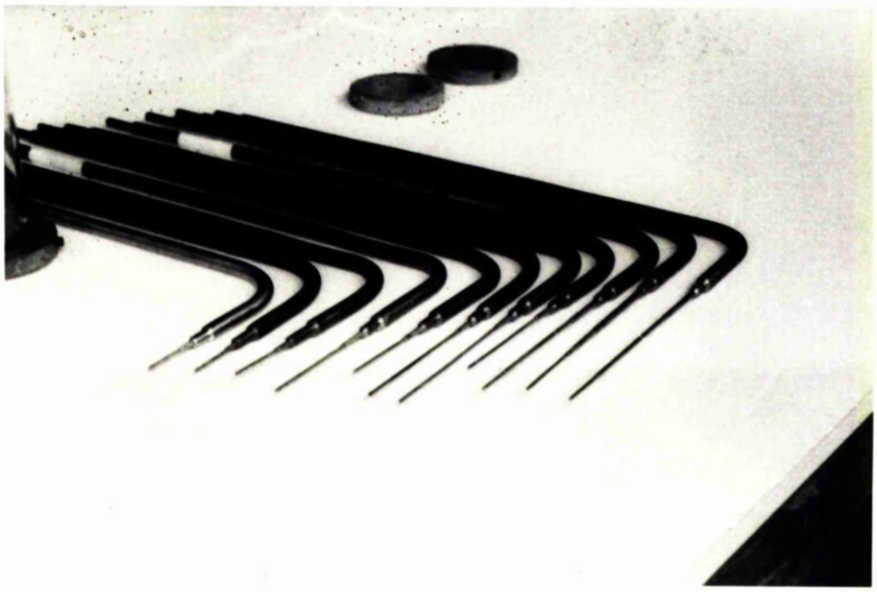

COMPLETE SET of 11 PROBES

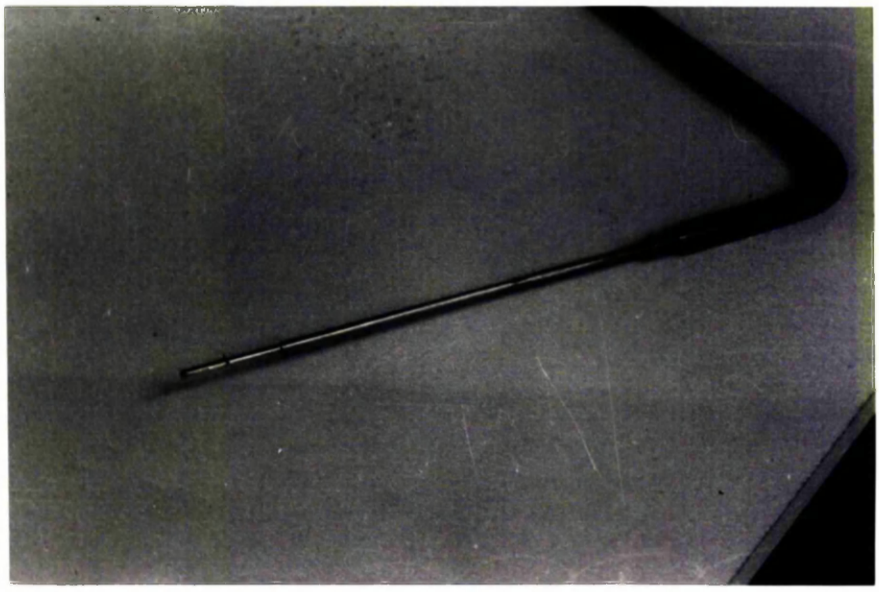

DETAIL of PROBE TIP

PI. 6.3 PRESSURE PROBES

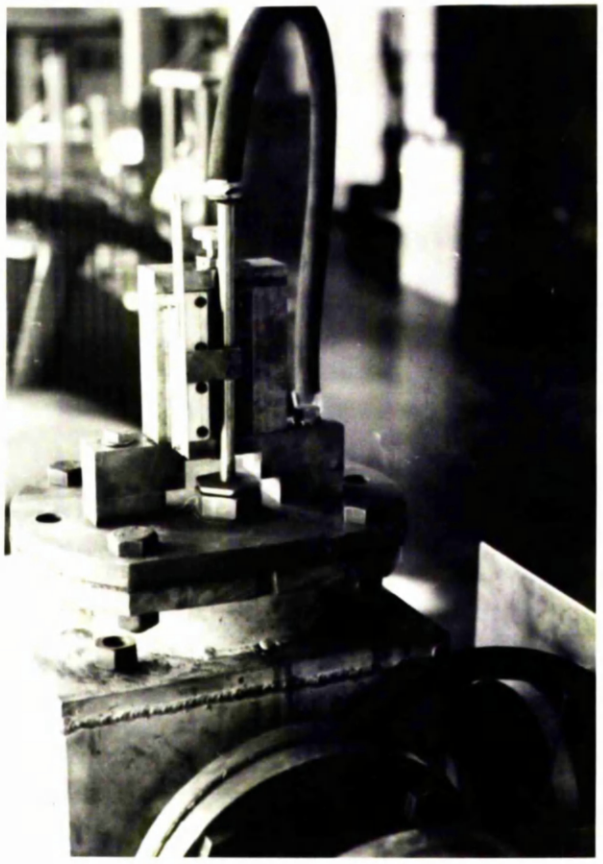

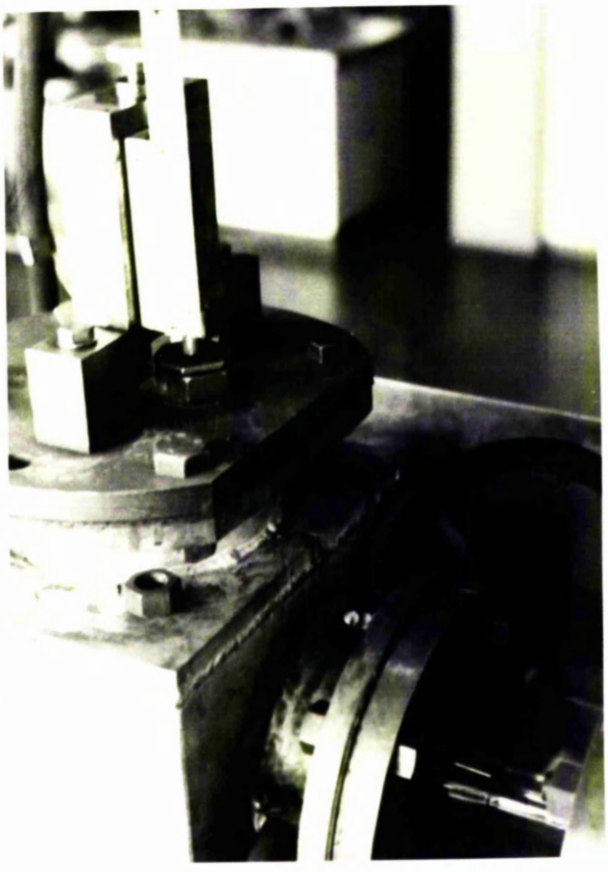

Pl.64 PROBE TRAVERSING MECHANISM

to 0.5 inch (12 mm) upstream of the nozzle exit. The design of the probes follows the form of the N.P.L. pitot tubes (though, of course, with no static pressure tap). The ends of the probes were connected to a Bourdon tube type pressure test gauge. Response time for the system was judged to be about 10 seconds.

The traversing mechanism permitted accurate positioning of the probes within 1 mm (0.04 inch), although some vibration of probe tips in the flow was noted.

Although no actual calibration tests were run, special probes were constructed to give a traverse in the plane of the upstream and downstream pressure taps. Traverses with this probe gave pressure readings identical to those from the wall tap, after allowance was made for gauge reading errors. These were regarded as supporting the use of these pressure probes to obtain local pressures in the flows.

(e) Dissolved Gases. The rate of bubble formation in a flashing liquid is known to be affected by the presence of dissolved gases. For this reason an analysis for the presence of dissolved oxygen was carried out using the "Winkler test".

Samples of water at pressures up to 4 bar (60 lb/in^2) and temperatures of up to 140 ^{o}C were drawn from a tapping situated near the thermometer pocket and analysed for the presence of dissolved oxygen. The sampling apparatus is shown in Fig 6.6 and plate 6.5. The lines are heavy duty flexible steam tubing and the system has copper fittings.

Details of the Winkler test theory are given in Annexe A.

In operation the sampling system was set up as shown in Fig 6.6(a). The two glass ampoules for the test were placed in the sampling vessel as shown in Fig 6.6(b). The sampling vessel was evacuated and filled with nitrogen, the evacuation and filling cycle being repeated 4 times to purge the air from the system. The system was pressurised with nitrogen and the pressure difference between the sampling vessel and the 4" line reduced to 0.5bar. By opening the

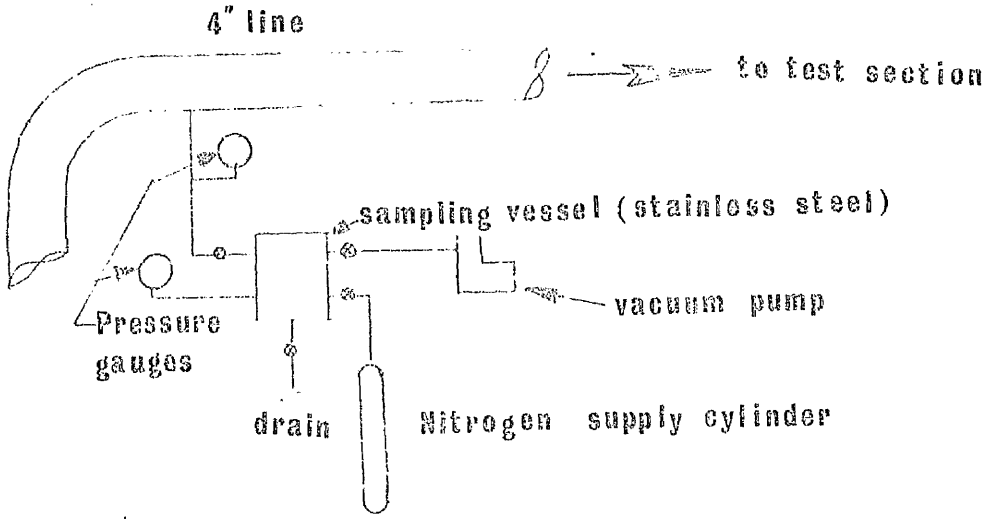

FIG 6.6a) WATER SAMPLING SYSTEM (NOT TO SCALE)

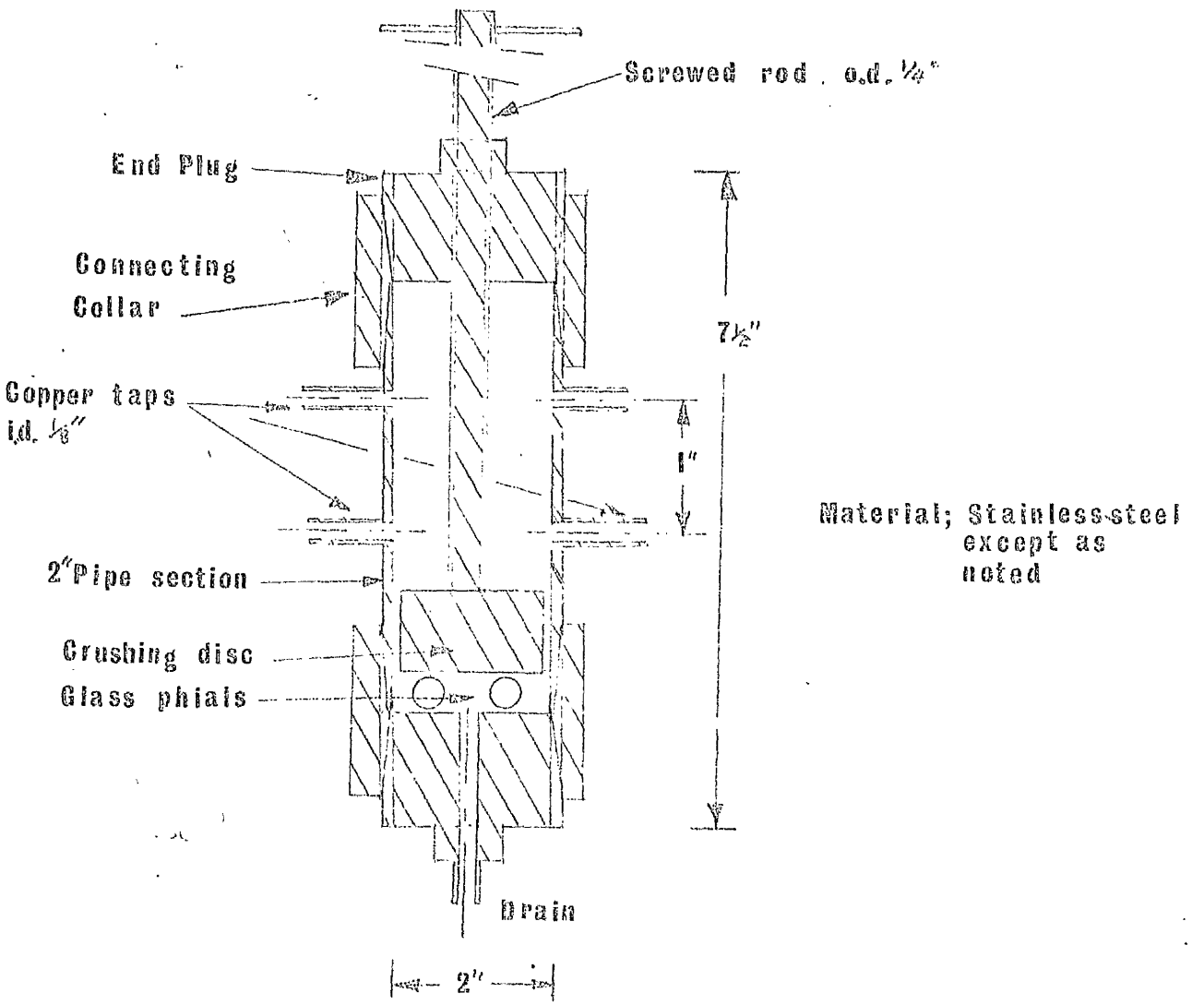

FIG 6.6b) DETAIL OF SAMPLING VESSEL

Pl 64(b) LAYOUT of PRESSURE GAUGES

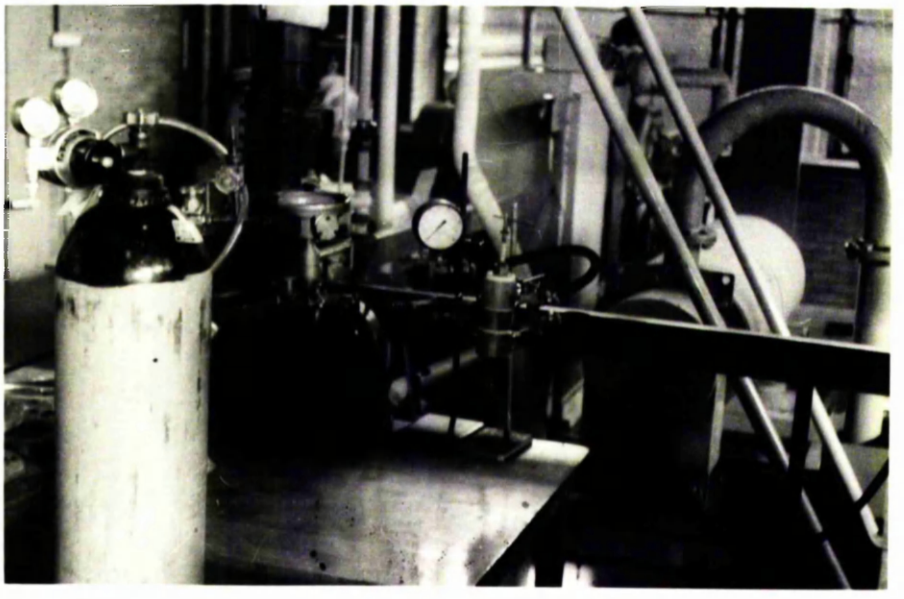

Pl 65 WATER SAMPLING SYSTEM.

various valves, the water sample flowed from the line to the sampling vessel. When the pressures in vessel and line had equalised the sampling vessel was isolated. The crushing disc was then screwed down onto the glass phials until they broke. Some 100 s were then allowed for mixing and the water sample was removed through the drain tap, 5 ml Analar sulphuric acid added to the sample, and a starch solution indicator is then added. If the solution does not turn blue, a known quantity of iodine may be added until the solution does have a blue colour.

The sample is then titrated with 0.001 ml Sodium Thiosulphate solution and the quantity of dissolved oxygen calculated using the formulae given in Annexe A.

In the case of the blank, used to eliminate the effects of oxidants in the sample, only the ampoule containing reagent A (see Annexe) is crushed under pressure. The ampoule containing reagent B is crushed and the contents added after the Analar sulphuric acid.

6.4 Operation

In this section the general operating procedure for the rig is described. Detailed information on the particular procedures used for each set of experiments is given at the appropriate point in Chapter 7.

Assume that the experimental apparatus starts dry at ambient temperature.

The system is filled with water by filling the receiving tank with 3.5 m^3 of water from the feed pipe. The sight gauge on the tank permits the amount of water in the tank to be adjusted. This water is then pumped through the return system to the main pressure tank. With the main pressure isolated by the various valves fitted, the cold water is heated by steam injection. Typically a flow rate of 300-400 kg/hr heated a full tank of water (about 3.5 m^3) from 20 ^{o}C to 140 ^{o}C in 3 to 4 hours.

The temperature of the water in the tank may be determined by use of the various thermometers fitted to the tank. No temperature control system is fitted to the tank and the adjustment of temperature to the desired value

depends entirely on the skill of the operator. In practice the temperature could be set to $\pm$ 1 ^{o}C.

When the water temperature has reached the desired value the steam supply is shut off and the tank pressurised by the air compressor system. The compressor system is fitted with an automatic control mechanism and the pressure in the system may be set to $\pm$ 2 lb/in^2 (0.1 bar).

With the main pressure tank at the desired temperature and pressure the valves in the 4" line connecting the tank to the test section and receiving tank are opened. The main pressure drop in this line is across the test section. The pressure at the pressure taps just upstream of the nozzle is normally about 0.5 bar (8 lb/in^2) below the pressure in the main pressure tank. In normal operation, before recorded runs, the line valves were opened with the main pressure tank at a lower pressure of about 3.5-4 bar, and the system run for about 60 s. This removed cold, stagnant water from the lines, heated the system and, hopefully, identified any poor sealing or defects in the line.

At normal rates of flow used for the experiments a full tank of heated water would require 300 to 400 secs. for complete discharge, however the compressor system cannot supply sufficient air at pressures above 6 bar to maintain flow for several minutes and so each experimental run is divided into 3 or 4 shorter runs each of 60 - 100 s.

Between each short run the upper valve in the 4" line is closed and the system allowed to settle for at least 60 s.

When the main pressure tank is empty, the safety valve is opened to depressurise the tank. The water in the receiving tank is then pumped back to the main pressure tank and reheated for the next run. Typically, reheating takes about 1 hr for a full tank.

During the operation of the rig it was found that 4 or 5 complete runs, each producing 4 experimental points, could be achieved in one working day.

6.5 Chapter Closure

This chapter, together with its Annexe, has described the experimental rig and its operation. The rig and its attendant instrumentation could be used to

obtain experimental data on certain aspects of two-phase critical flashing flow.

Chapter 7 will describe the methods used in obtaining particular data and will present the data thus obtained.

ORIFICE PLATE CALIBRATION

Theoretical Calibration

Theoretical Orifice Plate Calibrations were calculated from Formula 3 of B.S. 1042 for an orifice plate with "D and D/2" tappings, in a single phase flow. Allowance was made for a water over mercury manometer.

The calibration may be expressed as

$$G = A \sqrt{\frac{h}{100}}$$

where G = mass flow (kg/s)

h = head of mercury (cm).

A is a temperature dependant constant tabulated below.

Experimental Calibration

The theoretical calibrations for the two orifice plates were checked by experiment for "cold" water flows, i.e. at 60°C. Due to the design of the rig the calibrations for flows where flashing took place, i.e. at temperatures above 100°C, could be checked only with less accuracy.

In all cases the calibration was checked by setting the flow past the orifice plate to some steady value and noting

(i) the orifice plate manometer reading

(ii) the change in levels in the receiving tank over a known period (usually 60 or 100s).

Hence the true flow rate G_T is given by

$$G_T = \frac{1}{(1 - x)} \times \frac{A \times \ell \times s}{t}$$

where A = area of base of receiving tank = $4.35 = 0.01\ m^3$

ℓ = difference in levels in tank after time t

s = density of water

t = length of run

x = mass fraction of the flow flashed into vapour assuming complete equilibrium.

The mass fraction x is calculated as

$$x = \frac{C_p\ (T - 100)}{h_{fg}}$$

where C_p = specific heat of water

T = temperature of run

h_{fg} = specific enthalpy for phase change.

The mass fraction can be tabulated as:

Temperature	x
60°C	0
120°C	0.06
130°C	0.10
140°C	0.14

The true and calculated flow rates for a number of orifice plate readings are tabulated below in Tables III and IV for both orifice plates.

Comparison of Calibrations

Both experimental and theoretical calibrations have been graphed. That for the 1.82 in. diameter orifice plate on Graph I and for the 1.21 in. diameter orifice plate nn Graph II.

From the curves it is clear that the experimental values of flow rate are consistently higher than the theoretical values calculated from the orifice plate pressure drop.

However since the estimated error on the theoretical calibration is 2% and on the experimental values at least 5%: the two calibrations were held to be consistent and the theoretical calibrations used throughout the experimental work.

TABLE I

Orifice Plate Diameter = 1.820"

Water Temperature	A
60°C	15.76
100°C	15.55
105°C	15.52
110°C	15.49
115°C	15.46
120°C	15.44
125°C	15.40
130°C	15.36
135°C	15.33
140°C	15.30
145°C	15.26

Tolerance on Calibration = 2%

TABLE II

ORIFICE PLATE DIAMETER = 1.236"

Temperature	A
60°C	7.08
100°C	6.99
105°C	6.98
110°C	6.96
115°C	6.95
120°C	6.94
125°C	6.92
130°C	6.90
135°C	6.89
140°C	6.87
145°C	6.86

Tolerance on Calibration = 2%

TABLE III

Comparison of Calculated and Experimental Calibrations for 1.820 in. diameter Orifice Plate

Water Temperature 60°C: Length of Runs = 60s

Orifice Plate Reading (cm)	Calculated Mass Flow Rate (kg/s)	Mean Difference in Receiving Tank Levels (cm)	True Mass Flow Rate (kg/s)
25	7.88	11.4	8.1
32	8.91	12.6	9.0
37	9.59	13.6	9.7
41	10.09	14.2	10.1
47	10.80	15.2	10.9
49	11.03	15.6	11.1

Water Temperature 120°C Length of Run = 60s

Orifice Plate Reading (cm)	Calculates Mass Flow Rate (kg/s)	Mean Difference in Receiving Tank Levels (cm)	True Mass Flow Rate (kg/s)
30	8.46	11.8	8.5
35	9.13	12.6	9.2
42	10.00	13.8	10.0
47	10.58	14.8	10.7
59	11.86	16.6	12.0
65	12.45	17.2	12.5

Water Temperature = 130°C Length of Run = 60s

Orifice Plate Reading (cm)	Calculated Mass Flow Rate (kg/s)	Mean Difference in Receiving Tank Levels. (cm)	True Mass Flow Rate (kg/s)
25	7.68	10.4	7.9
29	8.27	11.0	8.3
30	8.41	11.4	8.5
35	9.09	12.2	9.2
41	9.83	13.2	10.0
48	10.64	14.0	10.5

Water Temperature = 140°C Length of Run = 60 s

Orifice Plate Reading (cm)	Calculated Mass Flow Rate (kg/s)	Mean Difference in Receiving Tank Levels. (cm)	True Mass Flow Rate (kg/s)
23	7.34	9.6	7.5
29	8.24	10.8	8.4
32	8.65	10.8	8.4
36	9.18	11.8	9.3
40	9.68	12.4	9.7
45	10.26	13.2	10.3

TABLE IV

Comparison of Calculated and Experimental Calibrations for 1.236 in. diameter Orifice Plate.

Water Temperature 60°C Length of Run = 100s

Orifice Plate Reading (cm)	Calculated Mass Flow Rate (kg/s)	Mean Difference in Receiving Tank Levels (cm)	True Mass Flow Rate (kg/s)
8	2.00	4.7	2.0
11	2.35	5.8	2.5
14	2.65	6.3	2.7
18	3.00	7.2	3.1
21	3.25	7.7	3.3
32	4.00	9.6	4.1

Water Temperature = 120°C Length of Run = 100s

Orifice Plate Reading (cm)	Calculated Mass Flow Rate kg/s)	Mean Difference in Receiving Tank Levels. (cm)	True Mass Flow Rate (kg/s)
12	2.40	5.5	2.4
25	3.47	8.0	3.5
33	3.99	9.2	4.0
37	4.22	9.8	4.3
42	4.50	10.6	4.6
51	4.96	11.5	5.0

Water Temperature = 130°C Length of Run = 100s

Orifice Plate Reading (cm)	Calculated Mass Flow Rate (kg/s)	Mean Difference in Receiving Tank Levels (cm)	True Mass Flow Rate (kg/s)
14	2.58	5.8	2.6
27	3.58	8.2	3.7
36	4.14	9.6	4.3
41	4.42	9.8	4.4
53	5.02	11.3	5.1
59	5.30	11.8	5.3

Water Temperature = 140°C Length of Run = 100s

Orifice Plate Reading (cm)	Calculated Mass Flow Rate (kg/s)	Mean Difference in Receiving Tank Levels. (cm)	True Mass Flow Rate (kg/s)
15	2.66	5.8	2.7
21	3.15	6.6	3.1
29	3.70	8.0	3.7
35	4.06	9.0	4.2
41	4.40	9.6	4.5
49	4.81	10.2	4.8

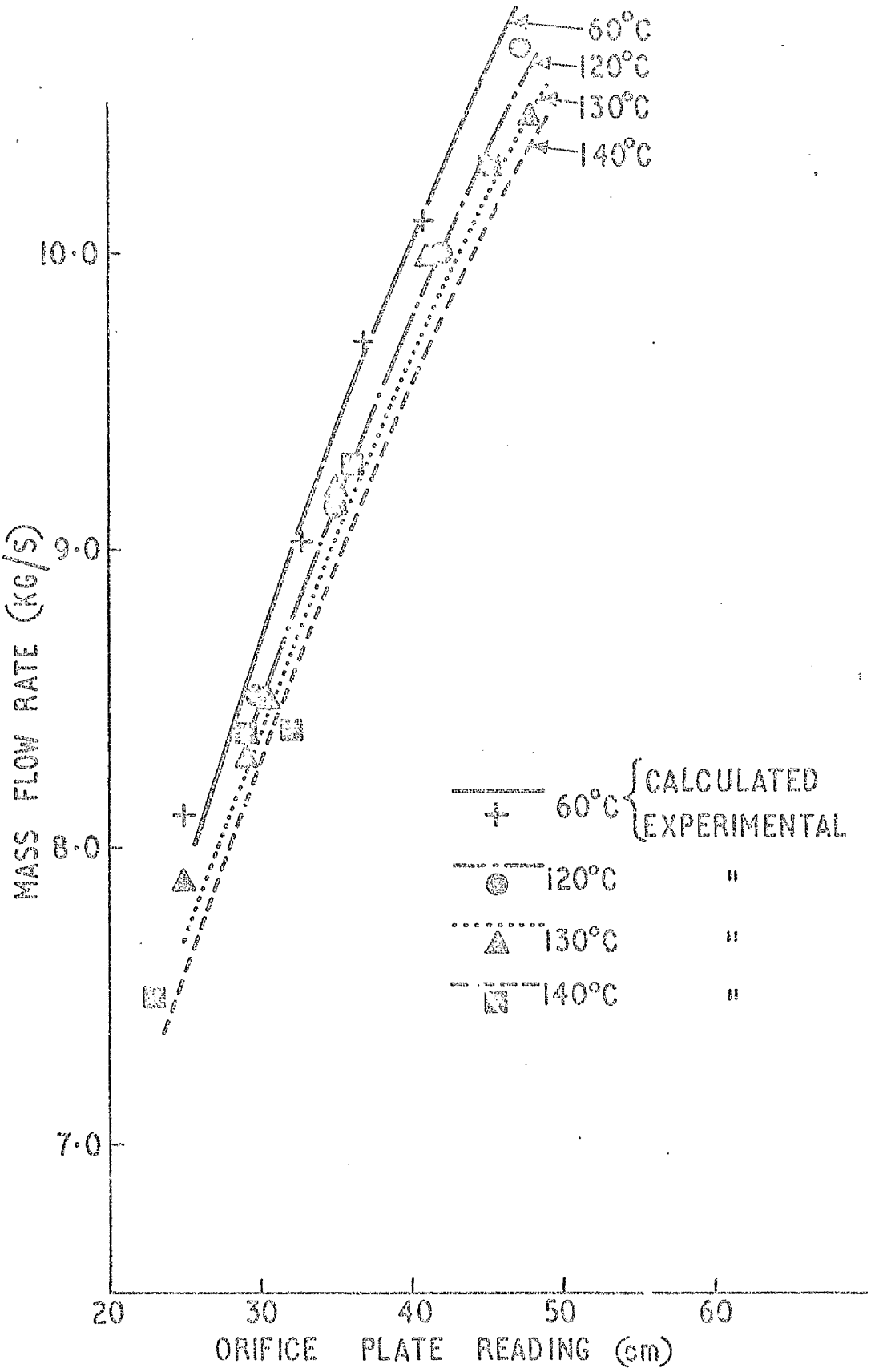

Calibration for 1·820 In Orifice Plate

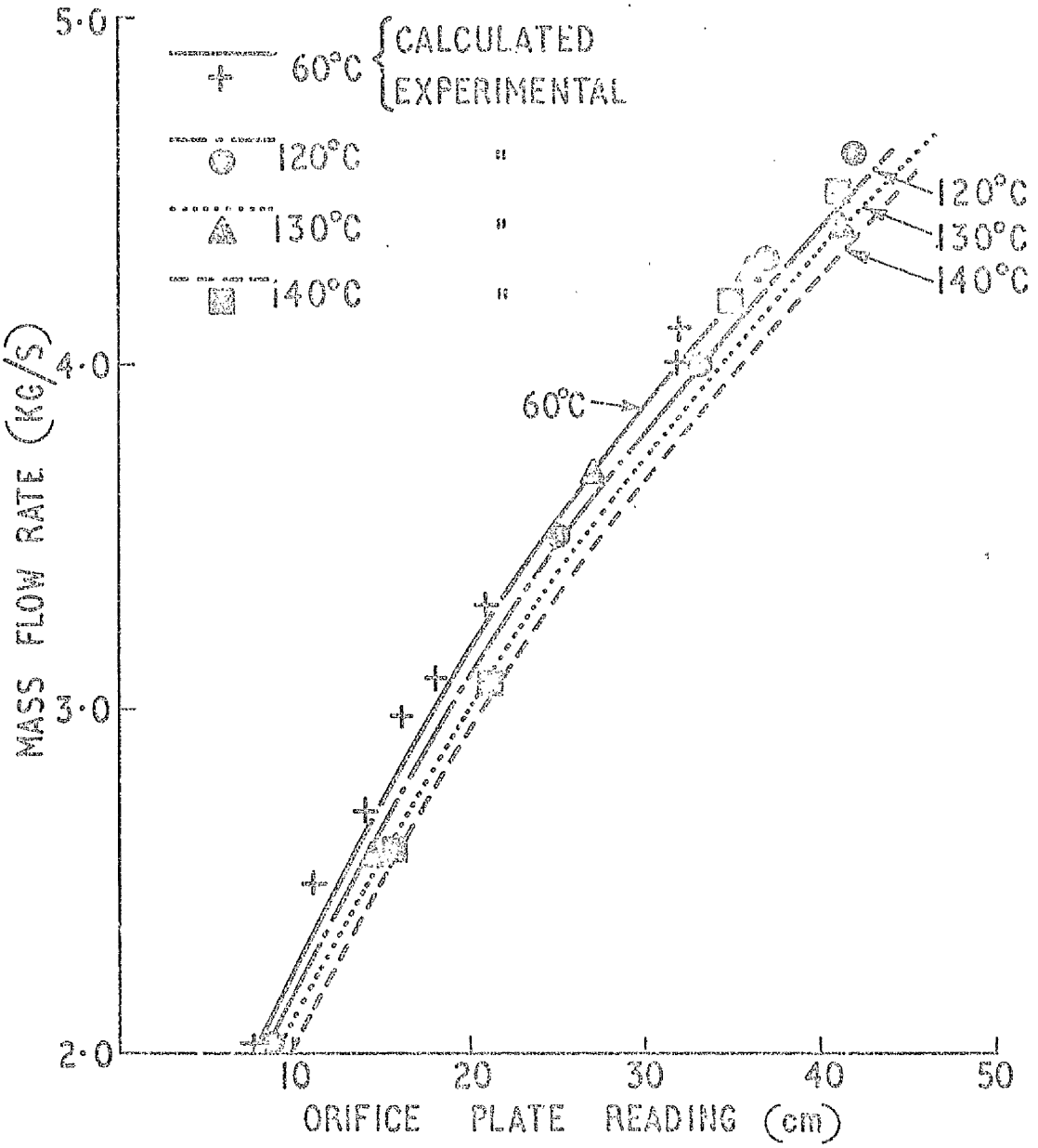

Calibration for 1·236 In Orifice Plate

Thermometer Calibration

The thermometers used were Griffin and George type GP150c/100. These thermometers are a general purpose type conforming to B.S. 1704 and designed for partial immersion to a depth of 100 mm. The temperature range for this type of thermometer is - 5 ^{o}C to + 150 ^{o}C by 1 ^{o}C stages with a maximum error of 0.8 ^{o}C.

The thermometers were set in a thermometer pocket inserted $2\frac{3}{8}$" (60 mm) into the flow, perpendicular to the axis. The total length of the thermometer pocket is $4\frac{1}{4}$" (106 mm). The pocket is constructed of copper tubing $\frac{1}{4}$" (6 mm) internal diameter and wall thickness $\frac{1}{8}$" (3 mm). The pocket is filled with oil to a depth of 100 mm (4"). The thermometer pocket will introduce an error in the thermometer reading. B.S.1704 refers to correction tabulated in "Der Chemie Ingeneur" Vol 2 p98.

From this reference it would seem that the error introduced by the use of this thermometer pocket will be less than 0.2 ^{o}C.

For this reason the error in temperature measurement was taken as 1 ^{o}C for all readings.

The large thermal capacity of the thermometer and thermometer pocket will introduce a response lag for temperature variations. Although the lag will vary with the magnitude of temperature variation, from the tests on the rig it was found that a time allowance of 30 secs was sufficient for the thermometer system to register temperature changes.

Pressure Gauge Calibration

The pressure gauges used were pressure test gauges of Bourdon tube type reading in the range 0 to 7.0 bar. The gauges were manufactured by the Bourdon Gauge Company and copies of the Company test certificates are included in this Annexe. These test certificates show that the gauges are accurate to $\pm$ 0.01 bar. The use to which the particular gauges were put is shown on the test certificate. The calibrations were checked on a dead-weight tester after the experimental programme was complete and were found to be unchanged with 0.01 bar

However since the estimated error on the theoretical calibration is 2% and on the experimental values at least 5%: the two calibrations were held to be consistent and the theoretical calibrations used throughout the experimental work.

The error on pressure gauge readings was taken as 0.05 bar and no corrections were made to nominal values.

The Winkler Test

In a flashing-flow situation, the presence of dissolved gases in the liquid phase may affect the flow rate. As the local pressure on the liquid surface is reduced some of the dissolved gas will come out of solution, thus increasing the voidage of the flow. For this reason measurements of the quantities of dissolved gases were made. These dissolved gases are, of course, a mixture of nitrogen, oxygen, carbon dioxide, and traces of other gases.

For given conditions of temperature, pressure and diffusivity coefficients, it is possible to analyse the sample purely for oxygen and relate this to total gas content. The method used was a modified version of the classical Winkler method, which makes use of the fact that a suspension of manganous hydroxide is rapidly oxidised by dissolved oxygen to a mangano-manganic hydroxide, which in acid solution, reacts with potassium iodide to liberate iodine, the latter being measured by titration with sodium thiosulphate in the presence of starch as an indicator.

For reasonably accurate measurement of dissolved oxygen, the normal Winkler method has three important sources of inaccuracy:

(i) dissolved oxygen introduced by the reagents;

(ii) the starch/iodine blue complex does not appear until an appreciable concentration of iodine is present;

(iii) it makes no allowance for the presence of oxidising or reducing agent in the test sample.

The Winkler reactions may be expressed as

(a) $2\ Mn(22) + 4OH^- \rightarrow 2\ Mn\ (OH)_2$

(b) $2\ Mn(OH)_2 + \frac{1}{2}O_2 + H_2O \rightarrow 2\ Mn(OH)_3$

(c) $2\ Mn(OH)_3 + 2I^- + 6H^+ \rightarrow 2\ Mn(11) + I_2 + 6H_2O.$

The iodine released is therefore proportional to the dissolved oxygen originally present in the solution, and the actual oxidised form of the manganese does not

affect the amount of iodine liberated.

For the analysis, the reagents consisted of the following:-

reagent (A) Potassium hydroxide
Potassium iodide } (dissolved in water)
Sodium Azide

reagent (B) Manganous chloride (dissolved in water)

reagent (C) Analar sulphuric acid.

In this case reagents A and B were used in the form of proprietary solution sealed in 2 ml glass ampoules. The solutions are made up with "air-free" distilled water by the manufacturers; British Drug Houses Ltd.

The most serious problem encountered with the classical Winkler method was the interference caused by oxidising agents present in the water which resulted in an increase in the final iodine concentration, and hence high estimations of dissolved oxygen content.

This problem was overcome by the employment of the reversed reagents technique. In the ordinary Winkler method, the reagents were added in the order (A) - (B) - (C). In the reversed reagents technique two samples are taken, one of which serves as a blank. The first one (the sample) is treated as above, the second (the blank) has the reagents added in the order (A) - (C) - (B). The equations of the Winkler reactions show that

iodine produced in sample = dissolved oxygen + (effect of oxidising agents + reagent impurities)

iodine produced in blank = effect of oxidising agents + effect of reagent impurities

This is because no manganous hydroxide is formed in the blank and the dissolved oxygen reactions are therefore eliminated. Therefore a measure of the dissolved oxygen alone should be obtained when the second titration is subtracted from the first.

This double titration is also a method of reducing the error arising from the use of starch as an end-point indicator. If the concentration of iodine needed to develop the blue colour is constant then the error would be expected

to cancel. The concentration of oxygen(in p.p.m.) dissolved in the sample is calculated by the following method:-

Using reaction equations:

(b) $2\ Mn(OH)_2 + \frac{1}{2}O_2 + H_2O \rightarrow 2\ Mn(OH)_3$

(c) $2\ Mn(OH)_3 + 2I^- + 6H^+ \rightarrow 2\ Mn + I_2 + 6H_2O.$

From the above equations it can be seen that for each mole of oxygen present in the sample, two moles of iodine are liberated.

The equation for the reaction of sodium thiosulphate with iodine is

(d) $2\ Na_2S_2O_3 + I_2 \rightarrow Na_2\ S_4\ O_6 + 2NaI.$

From this equation it can be seen that one mole of iodine is acted upon by two moles of thiosulphate.

By combining equations (b); (c) and (d) it can be seen that each mole of thiosulphate used for titration represents the initial presence of one-quarter of a mole of dissolved oxygen in the sample. The sodium thiosulphate used for titration had a normality of 0.001 N.

1 mole of sodium thiosulphate represents the presence of 0.25 mole of O_2.

$\therefore$ 0.001 moles of sodium thiosulphate represents the presence of 0.25×10^{-3} moles of O_2.

$\therefore$ 0.000001 " " " " " " " " 0.25×10^{-6} moles of O_2.

If the quantity of thiosulphate used is Y ml.,

then quantity of O_2 present is $0.25 \times Y \times 10^{-6}$ moles.

$\therefore$ weight of O_2 present $= 0.25 \times 32 \times Y \times 10^{6}$ gm.

$= 8 \times Y \times 10^{-6}$ gm.

If this contained in Z ml of sample, then concentration of oxygen

$$= \frac{8 \times Y \times 10^{-6} \times 10^{3}}{Z} \text{ gm/litre}$$

$$= \frac{8 \times Y \times 10^{-3}}{Z} \text{ gm/litre.}$$

1 litre of water weighs 1000 gm.

$\therefore$ concentration of oxygen in p.p.m. $= \frac{8 \times Y \times 10^{-3} \times 10^{3}}{Z} = \frac{8 \times Y}{Z}$ p.p.m.

Calibration of the test apparatus is, of course, difficult but a set of 4 analyses of tap water at atmospheric pressure gave dissolved oxygen values of 4 p.p.m., which is within the normal range of values. This was taken as indicating that the analysis technique was acceptable. No further "calibration" was carried out.

Chapter 7 - Presentation of Data from the Experimental Study

7.1 Introduction

The apparatus described in Chapter 6 was used to provide experimental data on the critical flashing flow of water. In this chapter the experimental data obtained in this study is presented and discussed in sections 7.2,7.3,7.4,7.5, together with more detailed notes on the methods used to obtain the data.

7.2 Critical Flow Rates

Studies were carried out on the effect on rates of critical flashing flow of (1) water temperature,

(2) nozzle entrance shape,

(3) nozzle $\frac{L}{D}$ ratio,

using the sets of metal and glass nozzles described in section 6.2 of Chapter 6. The procedure used to obtain values of the critical flow rate is detailed in the next paragraph.

When the desired water temperature had been obtained in the main pressure tank, the tank pressure was set to 4.5 to 5 bar and a 60 to 100 s run carried out as described in section 6.4, the readings on the orifice plate manometer, the thermometer and the pressure on the gauges upstream and downstream of the nozzle test section all being noted. The pressure in the main tank was then increased for the second 100 s run noting the same parameters. This increase in main tank pressure produces an increase in pressure drop across the nozzle. For each run the calculated mass flow rate from the orifice plate reading is plotted against the pressure drop across the nozzle. As the runs are continued with various pressure drops across the nozzle this graph begins to take the form shown in Fig 7.1. As the pressure drop across the nozzle increases the mass flow rate increases up to a limiting value. By examining the plot of the data, the region in which the mass flow rate reaches the limiting value can be noted. The criteria used being that the values of mass flow rate do not increase by more than 5% for a pressure increase of 0.5 bar. All the values of mass flow rate, for pressure drops above the estimated minimum for the limiting mass flow region, are used to calculate a mean and standard deviation. This mean value

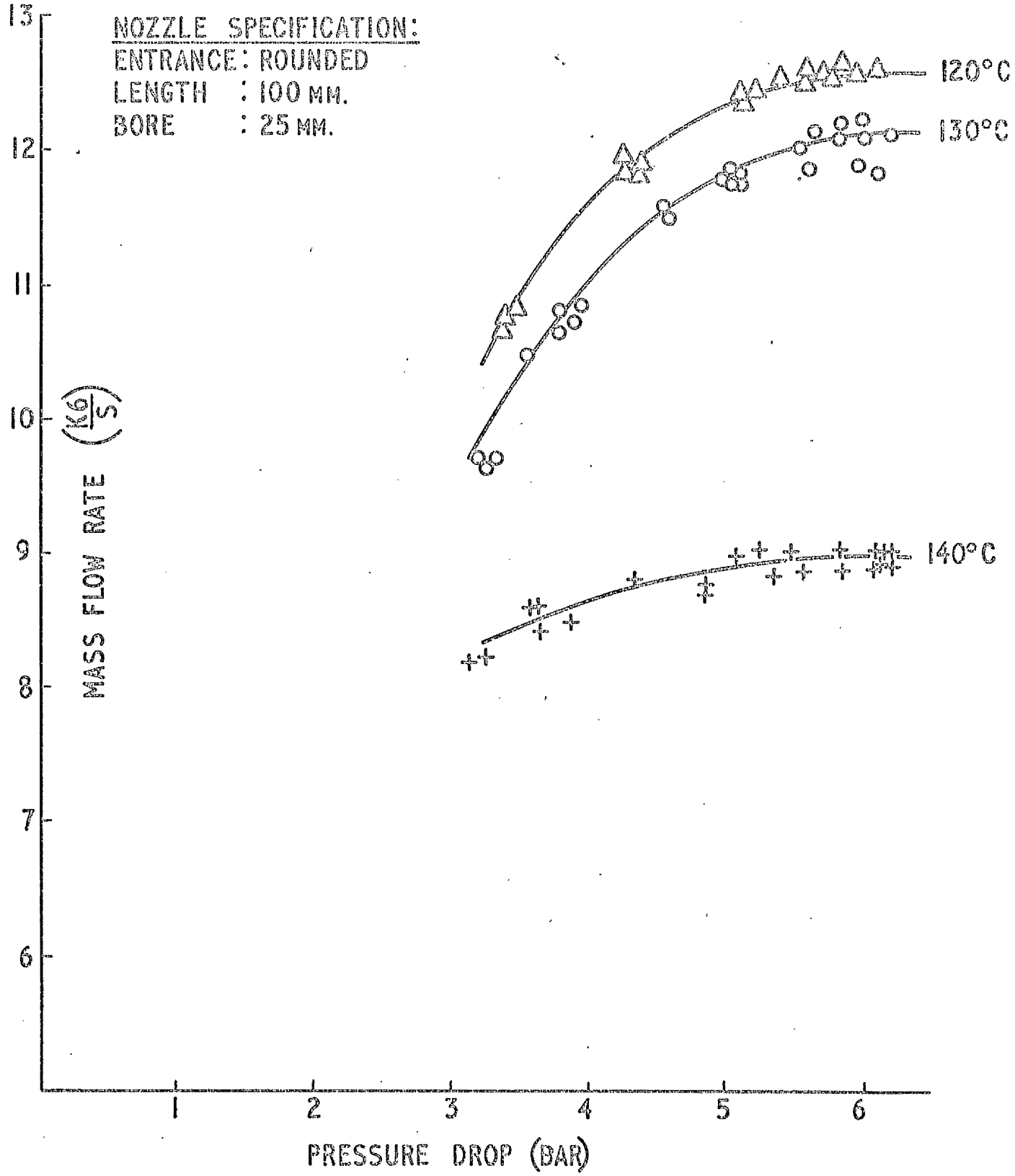

Fig. 7.1. Typical Variation of Mass Flow Rate with Pressure Drop.
[Exit Pressure – Atmospheric]

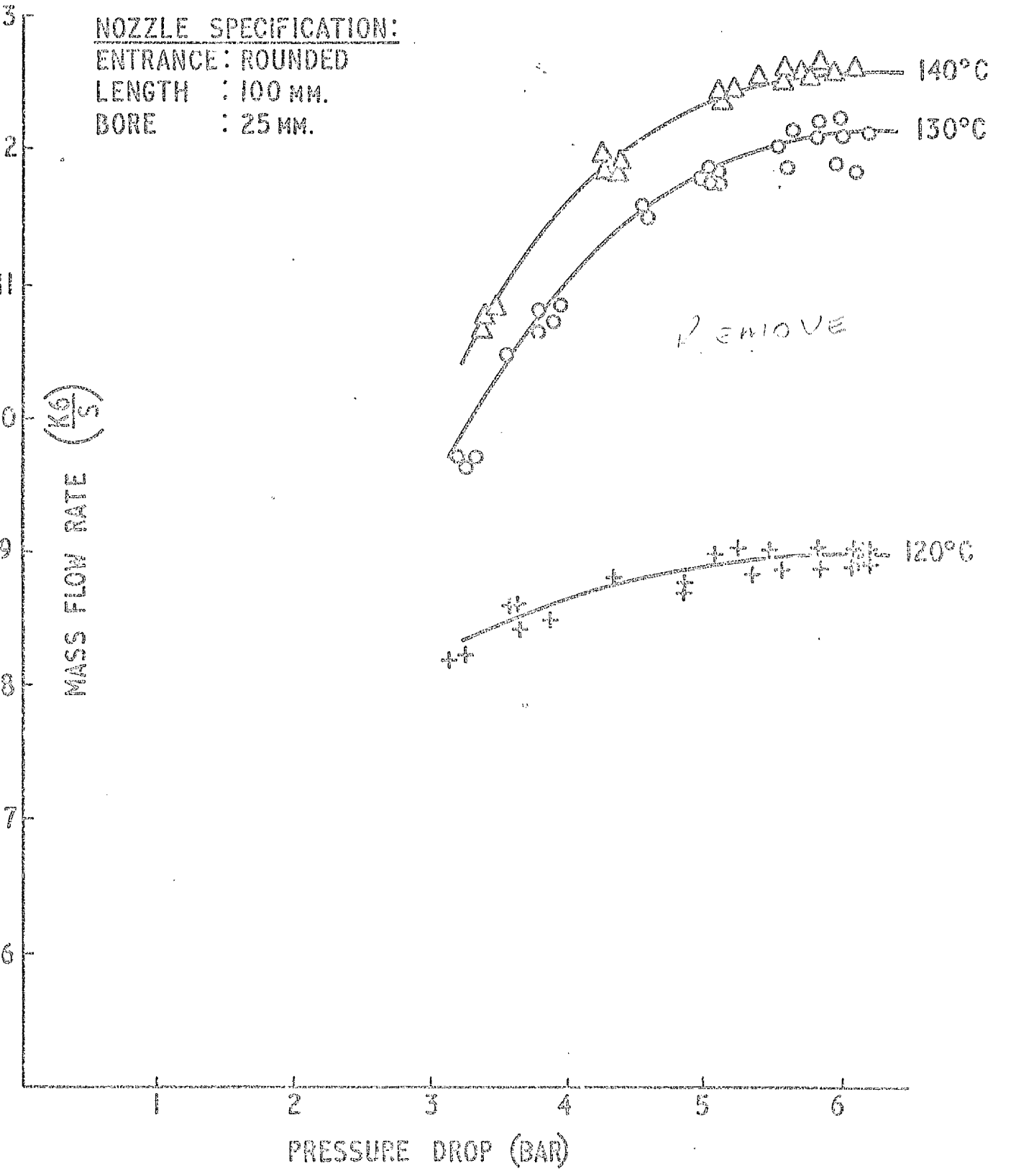

Fig 7.1 Typical Variation of Mass Flow Rate with Pressure Drop.
[Exit Pressure – Atmospheric]

is regarded as the critical mass flow rate for the nozzle at the particular water temperature. In each case the local atmospheric pressure was noted.

In this manner critical flow rates were established for the sets of metal and glass nozzles at water temperatures of 120 ^{o}C, 130 ^{o}C and 140 ^{o}C. The minimum pressure drop for critical flow was in the region 5 to 5.2 bar in all cases. Cold flow values were also established for each nozzle by noting the flow rate of water at 60 ^{o}C for a pressure drop of 5.25 bar.

The mean critical flow rates are recorded in tables 7.1 for metal nozzles and tables 7.2 for glass nozzles. These tables show the nozzle entrance profile and bore, together with the $^{\text{length}}$/diameter ratio and record the actual flow rates, with the derived specific mass flow for the temperatures of 60 ^{o}C, 120 ^{o}C, 130 ^{o}C, 140 ^{o}C. The number of values used in calculating the mean flow rates and the local barometric pressure are also shown.

Apart from the usual sources of error, this method will tend to show errors where the critical flow region must be estimated. These will be especially marked where the individual values show a large variation. Errors will also be found where the critical flow rates are large and give readings near the end of the manometer scale. For this reason, as a rule, the smaller the critical flow value, the more accurate it will be.

The critical flow values obtained are plotted against $^{\text{length}}$/diameter ratio in Figures 7.2 for Tables 7.1 and Figures 7.3 for Tables 7.2. Error flags are <u>not</u> indicated on these plots.

Theoretical curves calculated from the model presented in Chapter 4, equation (4.16), are also shown in Figures 7.2 and 7.3.

Comparison of the plots on Fig 6.2 with the values obtained from references (3),(4),(13) and (61) shown in Figures 4.2 and 4.3 indicate that the experimental values obtained in the present set of experiments are of at least the correct order of magnitude. In addition comparison of the values of critical flow rate for metal and for glass nozzles show closely similar values and trends except in the case of square entrance nozzles.

From Figures 7.2 and 7.3 certain trends can clearly be noted in the

FIGURES 7.2

CRITICAL FLOW RATES FOR METAL NOZZLES

NOTATION

■	Throat Diameter (D)	= 1" (2.54 cm)
●	- " -	= 0.5" (1.27 cm)
◆	- " -	= 1.5" (2.81 cm)
▲	- " -	= 0.75"(1.91 cm)
———	Theoretical Curve (Eqn 4.14)	

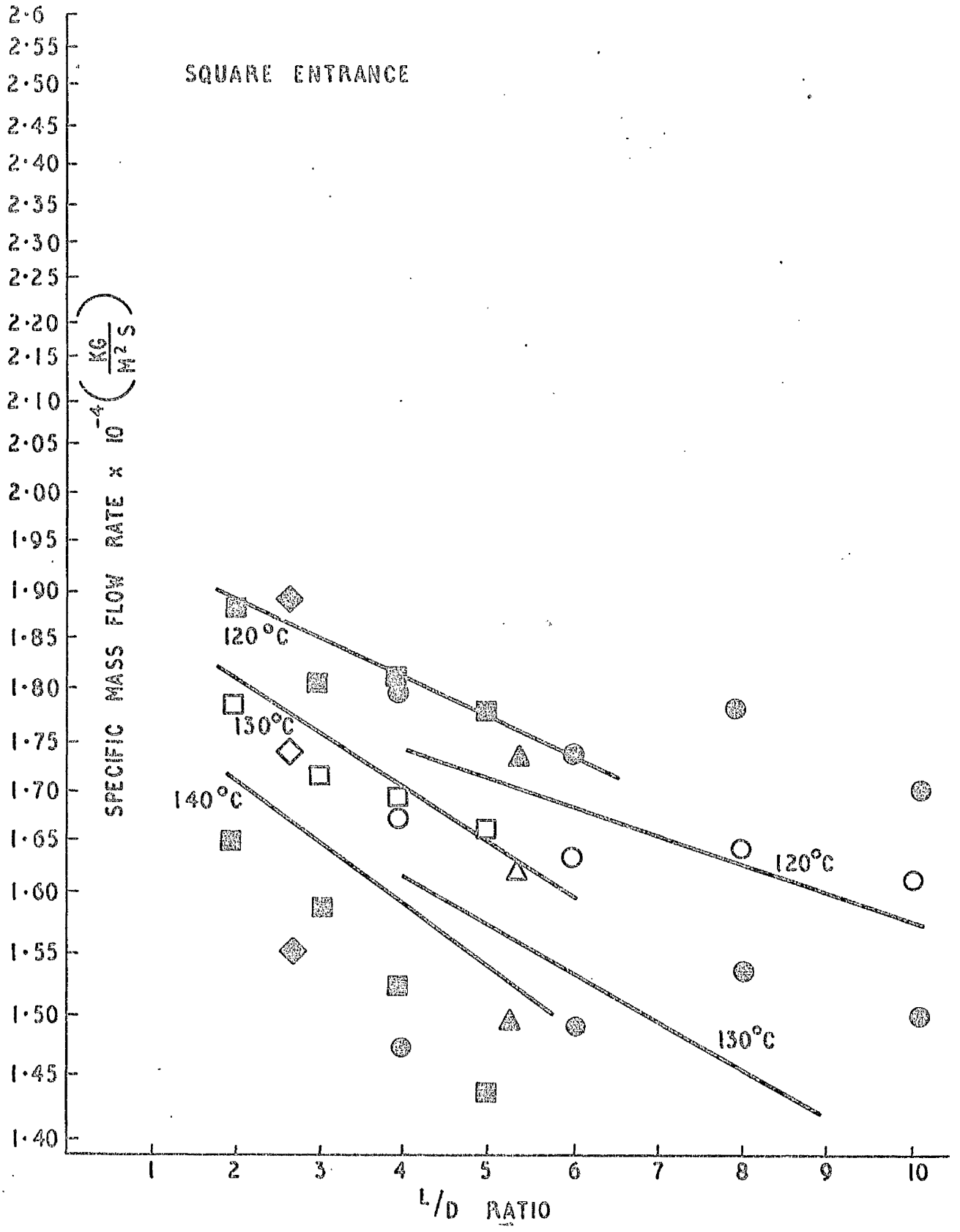
SQUARE ENTRANCE
SPECIFIC MASS FLOW RATE x 10^{-4} $\left(\frac{KG}{M^2 S}\right)$
2·6
2·55
2·50
2·45
2·40
2·35
2·30
2·25
2·20
2·15
2·10
2·05
2·00
1·95
1·90
1·85
1·80
1·75
1·70
1·65
1·60
1·55
1·50
1·45
1·40
120°C
130°C
140°C
120°C
130°C
1
2
3
4
5
6
7
8
9
10
L/D RATIO

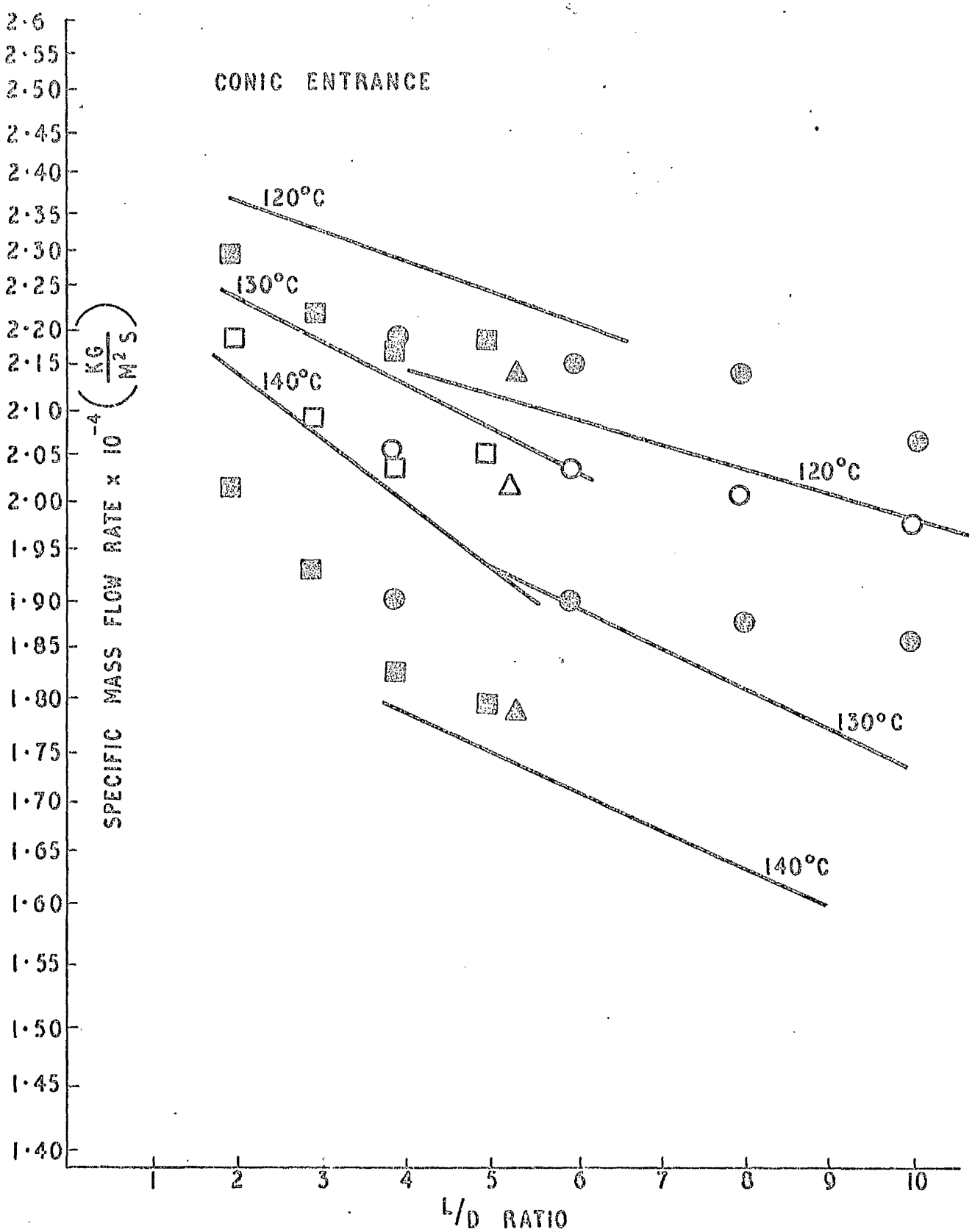
CONIC ENTRANCE
120°C
130°C
140°C
120°C
130°C
140°C
SPECIFIC MASS FLOW RATE x 10^-4 (KG/M²S)
L/D RATIO
2·6
2·55
2·50
2·45
2·40
2·35
2·30
2·25
2·20
2·15
2·10
2·05
2·00
1·95
1·90
1·85
1·80
1·75
1·70
1·65
1·60
1·55
1·50
1·45
1·40
1
2
3
4
5
6
7
8
9
10

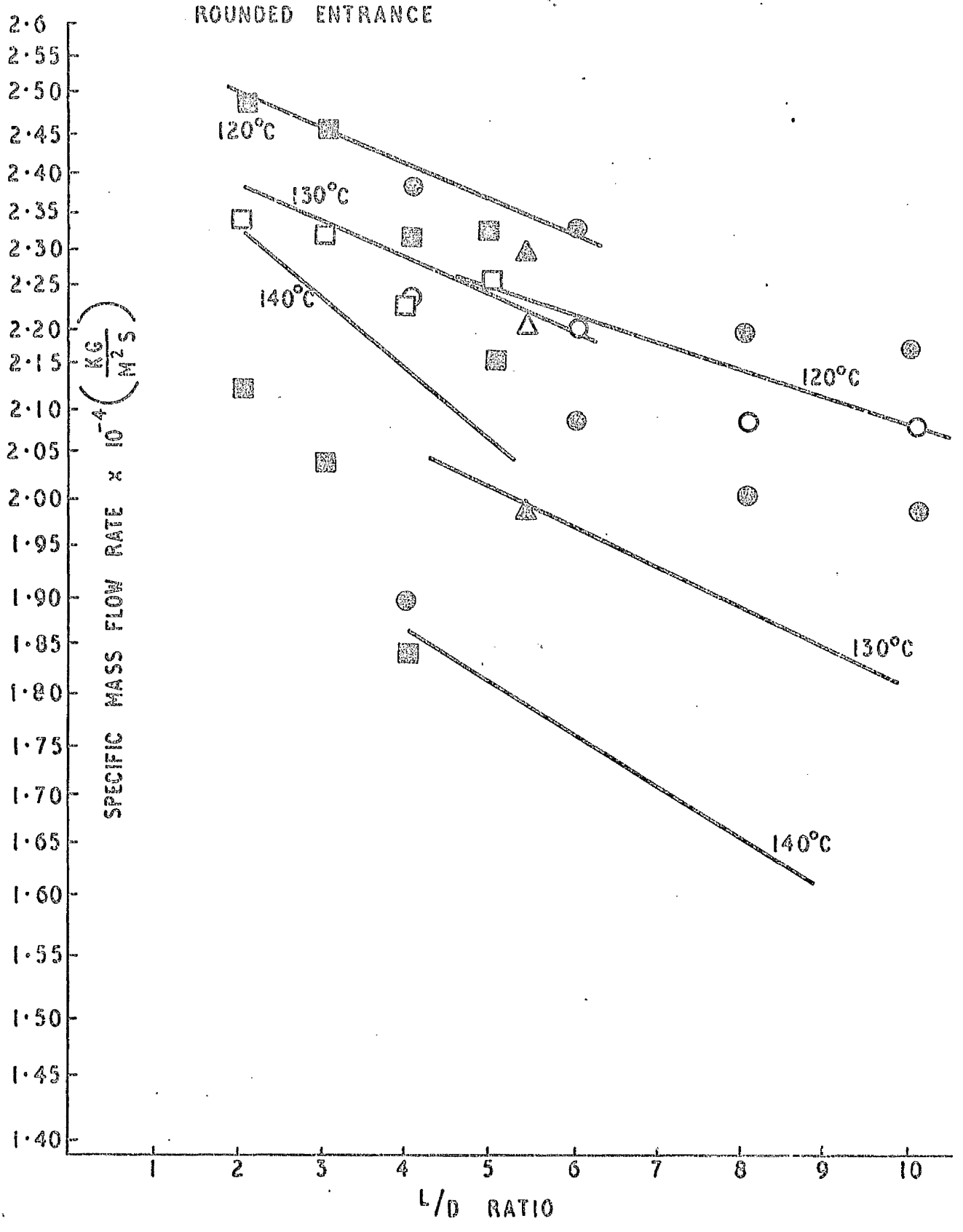
ROUNDED ENTRANCE
2·6
2·55
2·50
2·45
2·40
2·35
2·30
2·25
2·20
2·15
2·10
2·05
2·00
1·95
1·90
1·85
1·80
1·75
1·70
1·65
1·60
1·55
1·50
1·45
1·40
SPECIFIC MASS FLOW RATE × 10^{-4} $\left(\frac{KG}{M^2 S}\right)$
120°C
130°C
140°C
120°C
130°C
140°C
1
2
3
4
5
6
7
8
9
10
L/D RATIO

Tables 7.1

Critical Flow Rates for Metal Nozzles

CRITICAL FLOW RATES FOR METAL NOZZLES

Nozzle Entrance Profile: Square Bore: 3.81 cm.

Length/ Diameter	Water Temp. (°C)	Mean Critical Flow Rate (kg/s)	Mean Specific Critical Flow Rate (kg/m^2)	No. of Values Used in Mean	Barometric Pressure
2.66	120 °C	9.62 ± 0.08	1.90 ± 0.02	4	1.010
	130 °C	8.82 ± 0.04	1.74 ± 0.01	4	1.015
	140 °C	7.90 ± 0.07	1.56 ± 0.02	5	1.012
Nozzle Entrance Profile: Square				Bore:	1.91 cm.
5.33	120 °C	9.68 ± 0.04	1.91 ± 0.01	4	1.015
	130 °C	8.77 ± 0.07	1.73 ± 0.02	3	1.015
	140 °C	7.85 ± 0.09	1.55 ± 0.01	4	1.015
Nozzle Entrance Profile : Conic				Bore :	1.91 cm.
5.33	120 °C	10.84 ± 0.04	2.14 ± 0.01	5	1.009
	130 °C	10.19 ± 0.04	2.01 ± 0.01	4	1.009
	140 °C	9.02 ± 0.04	1.78 ± 0.01	4	1.009
Nozzle Entrance Profile: Rounded				Bore:	1.91 cm.
5.33	120 °C	11.80 ± 0.04	2.33 ± 0.01	6	1.010
	130 °C	11.30 ± 0.04	2.23 ± 0.01	4	1.010
	140 °C	10.13 ± 0.04	2.00 ± 0.01	6	1.006

CRITICAL FLOW RATES FOR METAL NOZZLES

Nozzle Entrance Profile: Square Bore: 1.27 cm.

Length/ Diameter	Water Temp. (°C)	Mean Critical Flow Rate (kg/s)	Mean Specific Critical Flow Rate ($kg/m^2s \times 10^{-4}$)	No. of Values Used in Mean	Barometric Pressure
10	60 °C	2.64 ± 0.02	2.08 ± 0.02	6	1.010
	120 °C	2.15 ± 0.03	1.70 ± 0.03	6	1.005
	130 °C	2.05 ± 0.04	1.62 ± 0.04	4	1.005
	140 °C	1.90 ± 0.04	1.50 ± 0.03	3	1.005
8	60 °C				
	120 °C	2.28 ± 0.02	1.80 ± 0.02	10	1.010
	130 °C	2.09 ± 0.01	1.65 ± 0.01	10	1.010
	140 °C	1.95 ± 0.02	1.54 ± 0.02	9	1.015
6	60 °C	2.52 ± 0.02	2.07 ± 0.02	6	1.010
	120 °C	2.22 ± 0.02	1.75 ± 0.02	6	1.010
	130 °C	2.08 ± 0.03	1.64 ± 0.03	4	1.010
	140 °C	1.90 ± 0.02	1.50 ± 0.02	5	1.010
4	60 °C	2.65 ± 0.02	2.09 ± 0.02	6	
	120 °C	2.28 ± 0.02	1.80 ± 0.02	4	1.014
	130 °C	2.13 ± 0.02	1.68 ± 0.02	4	1.015
	140 °C	1.92 ± 0.02	1.52 ± 0.02	5	1.015

CRITICAL FLOW RATES FOR METAL NOZZLES

Nozzle Entrance Profile: Square Bore: 2.54

Length/ Diameter	Water Temp. (°C)	Mean Critical Flow Rate (kg/s)	Mean Specific Critical Flow Rate $(kg/m^2s)10^{-4}$	No. of Values Used in Mean	Barometric Pressure
2	60 °C	10.94 ± 0.02	2.15 ± 0.01	5	0.995
	120 °C	9.41 ± 0.04	1.86 ± 0.01	8	1.013
	130 °C	9.02 ± 0.03	1.78 ± 0.01	9	1.013
	140 °C	8.33 ± 0.04	1.65 ± 0.01	8	1.013
3	60 °C	10.50 ± 0.02	2.07 ± 0.01	7	0.994
	120 °C	9.22 ± 0.05	1.82 ± 0.01	5	0.992
	130 °C	8.67 ± 0.05	1.71 ± 0.01	7	0.983
	140 °C	8.04 ± 0.05	1.58 ± 0.01	8	0.992
4	60 °C				
	120 °C	9.16 ± 0.04	1.81 ± 0.01	4	1.010
	130 °C	8.63 ± 0.06	1.70 ± 0.01	5	1.005
	140 °C	7.46 ± 0.06	1.47 ± 0.01	4	1.001
5	60 °C	10.39 ± 0.03	2.05 ± 0.01	4	0.998
	120 °C	9.07 ± 0.1	1.79 ± 0.03	5	1.003
	130 °C	8.5 ± 0.1	1.68 ± 0.02	5	1.005
	140 °C	7.3 ± 0.1	1.42 ± 0.02	6	1.005

CRITICAL FLOW RATES FOR METAL NOZZLES

Nozzle Entrance Profile: Conic Bore: 1.27 cm.

Length/ Diameter	Water Temp. (°C)	Mean Critical Flow Rate (kg/s)	Mean Specific Critical Flow Rate $(kg/m^2)_{\times 10^4}$	No. of Values Used in Mean	Barometric Pressure
10	60 °C				
	120 °C	2.59 ± 0.01	2.05 ± 0.04	7	1.008
	130 °C	2.49 ± 0.01	1.97 ± 0.03	8	1.009
	140 °C	2.34 ± 0.02	1.85 ± 0.03	7	1.009
8	60 °C				
	120 °C	2.70 ± 0.02	2.13 ± 0.03	9	0.995
	130 °C	2.53 ± 0.01	2.00 ± 0.02	7	0.995
	140 °C	2.37 ± 0.02	1.87 ± 0.03	8	1.003
6	60 °C	3.19 ± 0.02	2.52 ± 0.02	4	0.995
	120 °C	2.71 ± 0.03	2.14 ± 0.03	7	0.990
	130 °C	2.57 ± 0.02	2.03 ± 0.02	7	0.990
	140 °C	2.41 ± 0.02	1.90 ± 0.03	6	0.990
4	60 °C	3.20 ± 0.02	2.52 ± 0.02	6	1.005
	120 °C	2.76 ± 0.01	2.18 ± 0.02	8	1.006
	130 °C	2.60 ± 0.01	2.05 ± 0.02	5	1.006
	140 °C	2.42 ± 0.05	1.91 ± 0.01	7	1.005

CRITICAL FLOW RATES FOR METAL NOZZLES

Nozzle Entrance Profile: Conic **Bore:** 2.54 cm.

Length/ Diameter	Water Temp. (^{o}C)	Mean Critical Flow Rate (kg/s)	Mean Specific Critical Flow Rate (kg/m^2)x10^{-4}	No. of Values Used in Mean	Barometric Pressure
2	60 ^{o}C	12.83 ± 0.02	2.52 ± 0.01	4	1.010
	120 ^{o}C	11.50 ± 0.03	2.27 ± 0.01	6	1.003
	130 ^{o}C	11.05 ± 0.04	2.18 ± 0.02	3	1.003
	140 ^{o}C	10.20 ± 0.05	2.01 ± 0.01	5	1.003
3	60 ^{o}C	12.78 ± 0.03	2.51 ± 0.01	5	
	120 ^{o}C	11.20 ± 0.02	2.21 ± 0.04	7	1.003
	130 ^{o}C	10.54 ± 0.05	2.08 ± 0.01	6	1.003
	140 ^{o}C	9.78 ± 0.05	1.93 ± 0.01	5	1.003
4	60 ^{o}C				
	120 ^{o}C	10.89 ± 0.06	2.15 ± 0.02	7	1.010
	130 ^{o}C	10.34 ± 0.05	2.04 ± 0.01	4	1.015
	140 ^{o}C	9.17 ± 0.04	1.81 ± 0.01	6	1.013
5	60 ^{o}C	12.75 ± 0.02	2.51 ± 0.01	5	1.014
	120 ^{o}C	10.99 ± 0.08	2.17 ± 0.02	5	1.013
	130 ^{o}C	10.39 ± 0.05	2.05 ± 0.01	5	1.014
	140 ^{o}C	9.02 ± 0.02	1.78 ± 0.04	6	1.014

CRITICAL FLOW RATES FOR METAL NOZZLES

Nozzle Entrance Profile: Rounded **Bore:** 1.27 cm.

Length/ Diameter	Water Temp. (°C)	Mean Critical Flow Rate (kg/s)	Mean Specific Critical Flow Rate (kg/m^2)	No. of Values Used in Mean	Barometric Pressure
10	60 °C	3.68 ± 0.01	2.90 ± 0.01	4	
	120 °C	2.75 ± 0.05	2.17 ± 0.04	6	1.012
	130 °C	2.61 ± 0.05	2.06 ± 0.05	7	1.012
	140 °C	2.48 ± 0.04	1.96 ± 0.04	6	1.010
8	60 °C				
	120 °C	2.76 ± 0.02	2.19 ± 0.02	8	1.008
	130 °C	2.61 ± 0.03	2.06 ± 0.03	6	1.012
	140 °C	2.51 ± 0.03	1.99 ± 0.02	8	1.008
6	60 °C	3.69 ± 0.02	2.91 ± 0.02	6	
	120 °C	2.93 ± 0.04	2.32 ± 0.03	4	1.007
	130 °C	2.79 ± 0.02	2.20 ± 0.02	3	1.010
	140 °C	2.61 ± 0.03	2.06 ± 0.02	4	1.010
4	60 °C				
	120 °C	3.02 ± 0.03	2.38 ± 0.03	4	1.010
	130 °C	2.82 ± 0.03	2.23 ± 0.02	5	1.015
	140 °C	2.41 ± 0.02	1.90 ± 0.02	7	1.014

CRITICAL FLOW RATES FOR METAL NOZZLES

Nozzle Entrance Profile: Rounded **Bore:** 2.54 cm.

Length/ Diameter	Water Temp. (°C)	Mean Critical Flow Rate (kg/s)	Mean Specific Critical Flow Rate $(kg/m^2)x10^{-4}$	No. of Values Used in Mean	Barometric Pressure
2	60 °C	14.87 ± 0.03	2.93 ± 0.01	4	0.995
	120 °C	12.51 ± 0.03	2.47 ± 0.01	4	1.003
	130 °C	11.91 ± 0.04	2.35 ± 0.01	4	1.003
	140 °C	10.69 ± 0.04	2.11 ± 0.01	5	1.003
3	60 °C	14.72 ± 0.02	2.90 ± 0.01	4	0.995
	120 °C	12.42 ± 0.04	2.45 ± 0.01	4	1.013
	130 °C	11.73 ± 0.08	2.32 ± 0.02	4	1.013
	140 °C	10.29 ± 0.02	2.03 ± 0.01	4	1.013
4	60 °C				
	120 °C	11.62 ± 0.07	2.29 ± 0.01	4	1.010
	130 °C	11.29 ± 0.06	2.23 ± 0.01	4	1.015
	140 °C	9.21 ± 0.03	1.82 ± 0.01	5	1.009
5	60 °C	14.31 ± 0.03	2.82 ± 0.01	5	0.995
	120 °C	11.80 ± 0.04	2.33 ± 0.01	3	1.003
	130 °C	11.40 ± 0.04	2.25 ± 0.01	6	1.003
	140 °C	10.89 ± 0.04	2.15 ± 0.01	5	1.003

FIGURES 7.3

CRITICAL FLOW RATES FOR GLASS NOZZLES

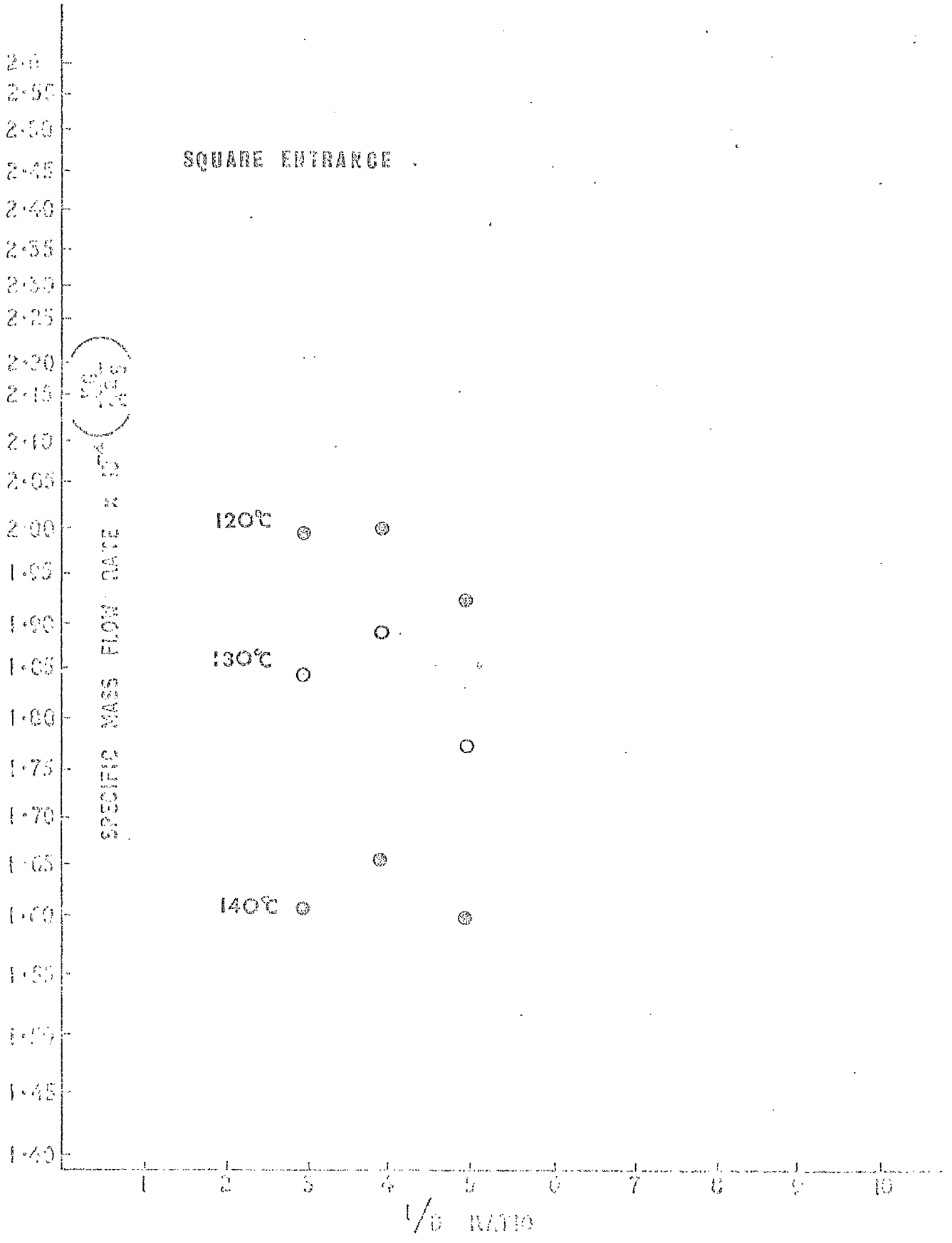
SQUARE ENTRANCE
SPECIFIC MASS FLOW RATE kg/s/m²
2·60
2·55
2·50
2·45
2·40
2·35
2·30
2·25
2·20
2·15
2·10
2·05
2·00
1·95
1·90
1·85
1·80
1·75
1·70
1·65
1·60
1·55
1·50
1·45
1·40
120°C
130°C
140°C
1
2
3
4
5
6
7
8
9
10
l/b RATIO

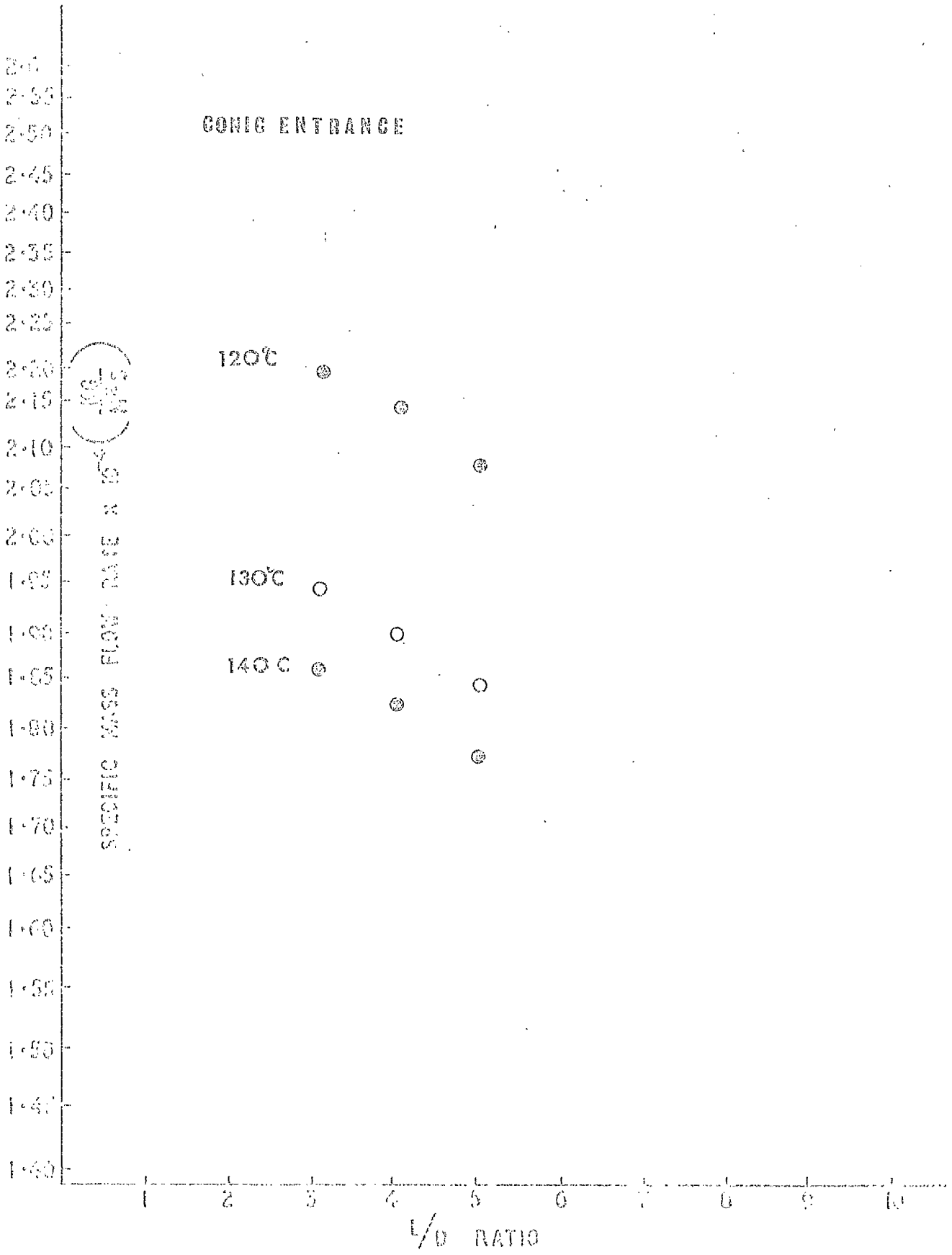
CONIC ENTRANCE
120°C
130°C
140°C
SPECIFIC MASS FLOW RATE
L/D RATIO

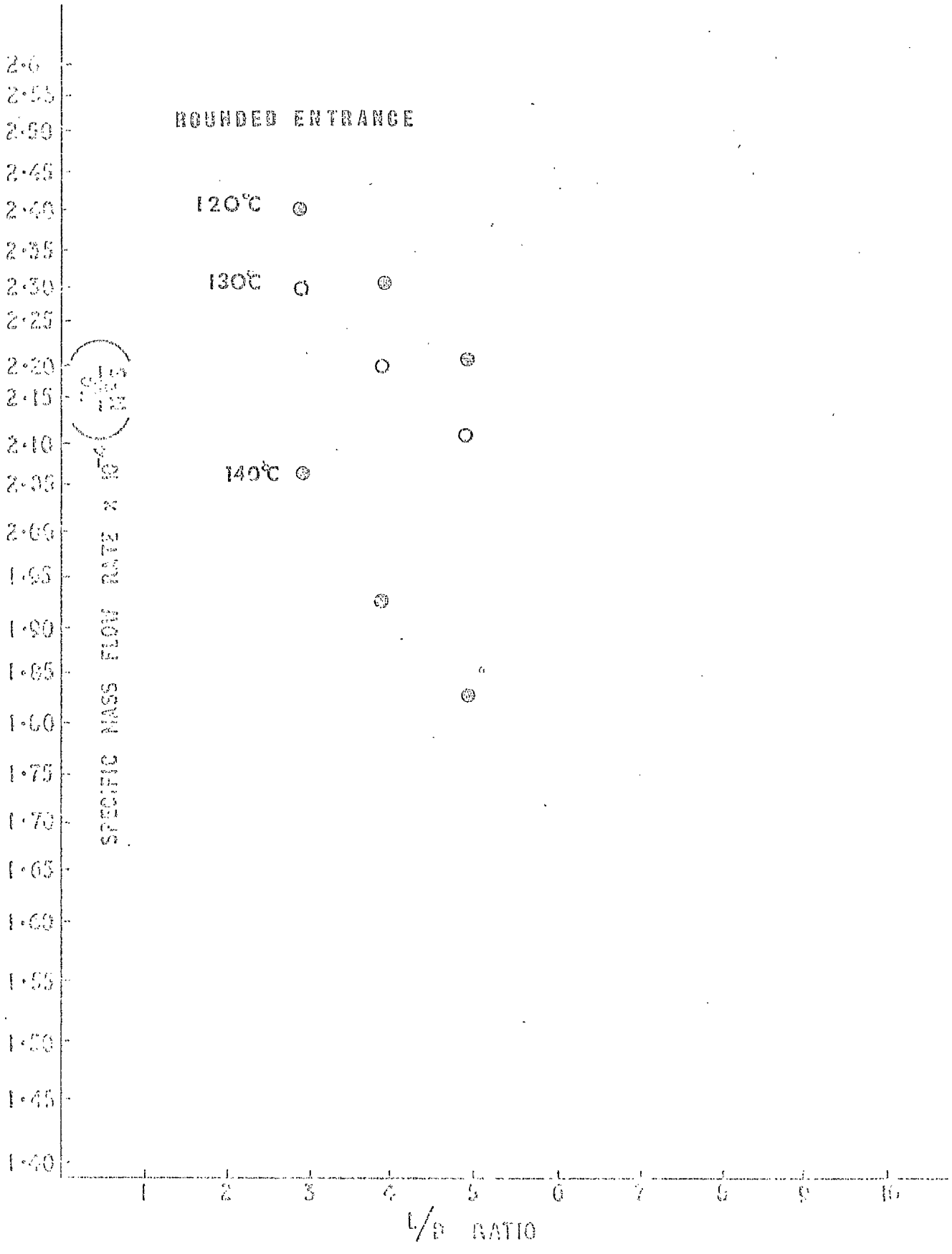
ROUNDED ENTRANCE
120°C
130°C
140°C
SPECIFIC MASS FLOW RATE
L/D RATIO
2·60
2·55
2·50
2·45
2·40
2·35
2·30
2·25
2·20
2·15
2·10
2·05
2·00
1·95
1·90
1·85
1·80
1·75
1·70
1·65
1·60
1·55
1·50
1·45
1·40
1
2
3
4
5
6
7
8
9
10

Tables 7.2

Critical Flow Rates for Glass Nozzles

CRITICAL FLOW RATES FOR GLASS NOZZLES

Nozzle Entrance Profile: Square Bore: 2.54 cm.

Length/ Diameter	Water Temp. (^{o}C)	Mean Critical Flow Rate (kg/s)	Mean Specific Critical Flow Rate (kg/m^2)$\times 10^{-4}$	No. of Values Used in Mean	Barometric Pressure
3	60 ^{o}C	10.40 ± 0.04	2.05 ± 0.01	4	0.996
	120 ^{o}C	10.15 ± 0.03	2.00 ± 0.01	10	1.003
	130 ^{o}C	9.49 ± 0.05	1.84 ± 0.01	6	1.003
	140 ^{o}C	8.03 ± 0.06	1.59 ± 0.01	9	1.003
4	60 ^{o}C				
	120 ^{o}C	10.07 ± 0.04	1.99 ± 0.01	7	1.003
	130 ^{o}C	9.53 ± 0.06	1.88 ± 0.01	8	1.003
	140 ^{o}C	8.33 ± 0.04	1.64 ± 0.01	7	1.003
5	60 ^{o}C	10.41 ± 0.04	2.06 ± 0.01	5	0.998
	120 ^{o}C	9.80 ± 0.2	1.94 ± 0.05	4	1.013
	130 ^{o}C	8.99 ± 0.04	1.77 ± 0.04	6	1.013
	140 ^{o}C	8.02 ± 0.07	1.58 ± 0.01	6	1.013

CRITICAL FLOW RATES FOR GLASS NOZZLES

Nozzle Entrance Profile: Conic

Bore: 2.54 cm.

Length/ Diameter	Water Temp. (^{o}C)	Mean Critical Flow Rate (kg/s)	Mean Specific Critical Flow Rate (kg/m^2)	No. of Values Used in Mean	Barometric Pressure
3	60 ^{o}C	12.50 ± 0.04	2.48 ± 0.02	3	1.011
	120 ^{o}C	11.07 ± 0.08	2.20 ± 0.02	7	1.005
	130 ^{o}C	9.76 ± 0.05	1.94 ± 0.01	4	1.005
	140 ^{o}C	9.30 ± 0.06	1.85 ± 0.02	6	1.005
4	60 ^{o}C				
	120 ^{o}C	10.80 ± 0.03	2.15 ± 0.01	7	1.003
	130 ^{o}C	9.49 ± 0.05	1.88 ± 0.01	6	1.003
	140 ^{o}C	9.20 ± 0.1	1.82 ± 0.01	6	1.003
5	60 ^{o}C	12.49 ± 0.04	2.46 ± 0.02	4	1.014
	120 ^{o}C	10.67 ± 0.05	2.12 ± 0.01	7	1.003
	130 ^{o}C	9.19 ± 0.04	1.83 ± 0.01	6	0.993
	140 ^{o}C	8.85 ± 0.03	1.76 ± 0.01	6	1.003

CRITICAL FLOW RATES FOR GLASS NOZZLES

Nozzle Entrance Profile: Rounded **Bore:** 2.54 cm.

Length/ Diameter	Water Temp. (°C)	Mean Critical Flow Rate (kg/s)	Mean Specific Critical Flow Rate (kg/m^2)$\times 10^{-4}$	No. of Values Used in Mean	Barometric Pressure
3	60 °C	14.20 ± 0.05	2.76 ± 0.02	4	
	120 °C	12.40 ± 0.05	2.44 ± 0.02	9	1.023
	130 °C	11.73 ± 0.02	2.32 ± 0.01	7	1.023
	140 °C	10.31 ± 0.08	2.07 ± 0.01	5	1.023
4	60 °C			7	
	120 °C	11.72 ± 0.07	2.32 ± 0.02	7	0.992
	130 °C	11.05 ± 0.09	2.18 ± 0.02	7	0.983
	140 °C	9.69 ± 0.03	1.91 ± 0.01	6	0.983
5	60 °C	14.28 ± 0.04	2.80 ± 0.01	4	0.996
	120 °C	11.10 ± 0.01	2.20 ± 0.01	6	1.004
	130 °C	10.78 ± 0.04	2.13 ± 0.01	5	1.003
	140 °C	9.23 ± 0.06	1.82 ± 0.01	6	1.003

experimental data.

Firstly, for all nozzles the critical flow rate decreases with $\frac{L}{D}$ ratio and with liquid temperature, while from Tables 6.1 cold-flow results show no such tendency.

Secondly, the critical flow rate shows a marked dependence on nozzle entrance profile.

The apparent general shape of these curves is similar for all nozzles and temperature differences, with a discontinuity in gradient between the results for 1" (2.54 cm) bore nozzles and 0.5" (1.27 cm) bore nozzles.

From these trends examination in detail shows that the critical flow rates show a variation with $\frac{L}{D}$ ratio which is consistent with an exponential variation, with any additional variation with bore. The variation with temperature is also non-linear.

The theoretical predictions of equation (4.16) are plotted on Fig 7.2 for the relevant parameters. The discharge coefficients used being, square entrance: 0.62, rounded 0.93, conic 0.78, the latter two being derived from cold flow results.

Examination of these predictions shows that while the model gives generally good predictions for the critical flows in 1" (2.54 cm) bore nozzles, the model underpredicts for 0.5" (1.27 cm) nozzles by up to 20%.

The predictions of $\frac{L}{D}$ variation, (i.e. curve gradient) seem accurate for all critical flows.

Agreement with experiment is best for flows at 120 ^{o}C and 130 ^{o}C, with over-prediction up to 10% for 140 ^{o}C, consistent with the observations in Chapter 4, that the model worked best for low liquid superheats. This overprediction may be due to the assumption in equation (4.16) that the critical flow rate is inversely proportional to the difference in saturation temperature at exit and liquid bulk temperature. This variation is shown by experimental data to be non-linear.

The failure to predict the form of the discontinuity between the results for two different bores is more disturbing. Equation (4.16) includes a factor

which would predict such a discontinuity but suggests that the experimental values should be lower than the equivalent values for the same $\frac{L}{D}$ but for larger nozzle bores. This is, of course, not borne out by experiment.

Since, for the annular flow pattern used in the theoretical model, the ratio of surface to volume increases as the throat diameter decreases, then, assuming that the mass transfer rate per unit is constant, the flow quality should be greater for nozzles with smaller throat diameters. This effect suggests that the form of the discontinuity observed with change of throat diameter or bore, can be due only to (a) systematic error presumably in the orifice plate system;

(b) a different flow pattern from the annular pattern assumed.

The calibration and comparison procedure for the orifice plate discounts (a), but although flow patterns for 1" (2.54 cm) nozzles were observed, using glass nozzles, no observations were made of flows in 0.5" (1.27 cm) nozzles.

In conclusion, the variations of critical flow rate would seem to be consistent with the variations predicted by the critical flow model of Chapter 4.

7.3 Flow Patterns

The use of glass nozzles enabled observations to be made of flow patterns in the nozzles. These observations are, of course, only for 1" (2.54 cm) nozzles. In general these seemed to conform to the pattern of an annulus of vapour surrounding a central liquid core as suggested in references (13),(14),(15). Examination of the flow pattern for the glass nozzles with the pressure probes inserted showed no apparent alteration in flow pattern.

The flow patterns were photographed on Ilford HP4 film using a Praktica FX2 camera with a Zeiss, Jena, Tessar 1:28 f 50 lens. Photographs were taken with the lens at a distance of approximately 200 mm from the nozzle centre line with exposures of 0.02 sec. These photographs are reproduced as Plates 7.1 and show typical flow patterns for various nozzle lengths and entrance profiles at various temperatures. The photographs are included merely to illustrate the type of flow pattern observed.

FLOW DIRECTION

SQUARE

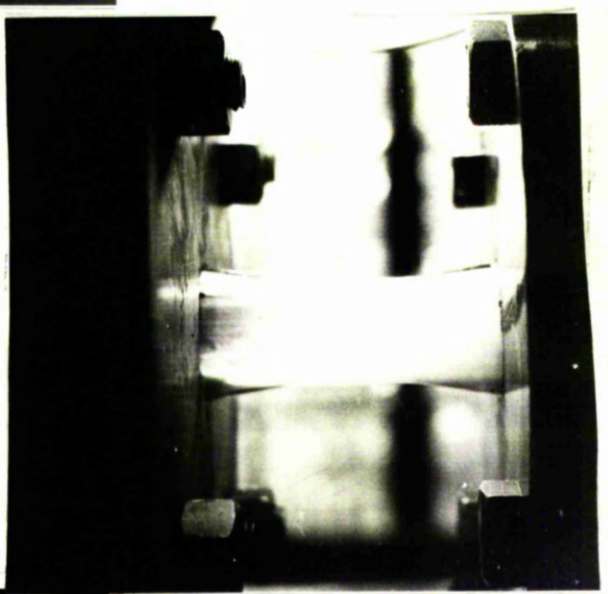

CONIC

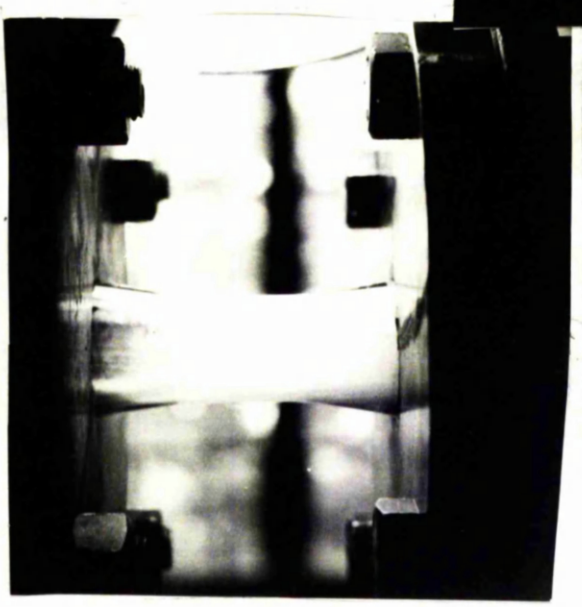

ROUNDED

PI 7.1 FLOW PATTERNS FOR VARIOUS ENTRANCES

(4" Nozzle at 140°C)

FLOW

DIRECTION

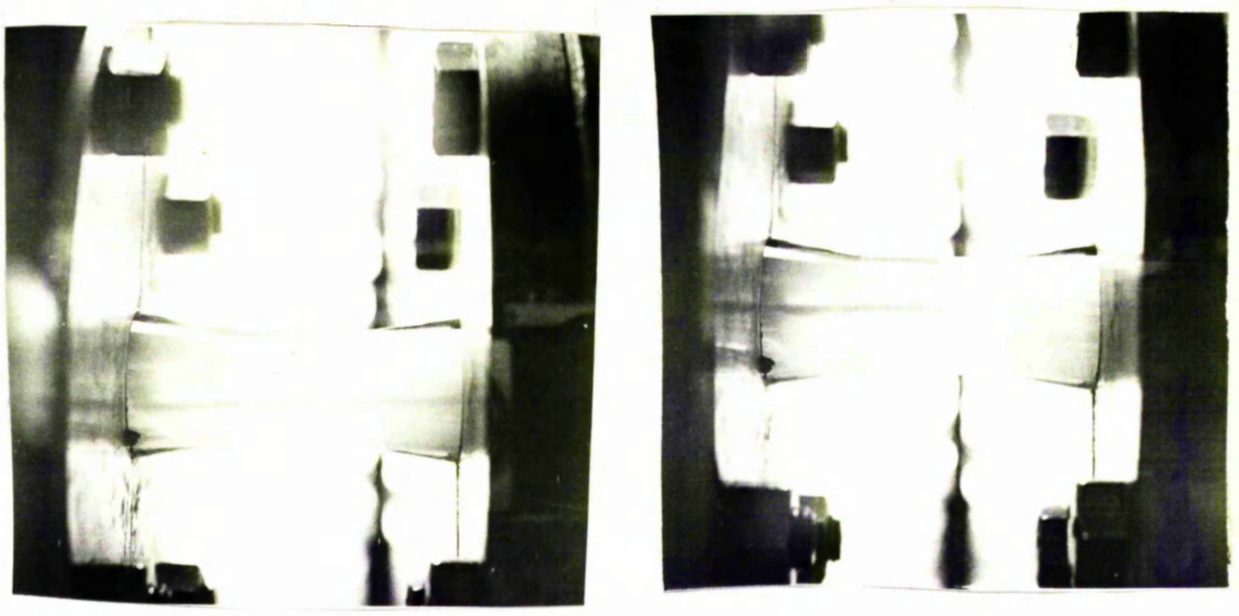

5″ LONG

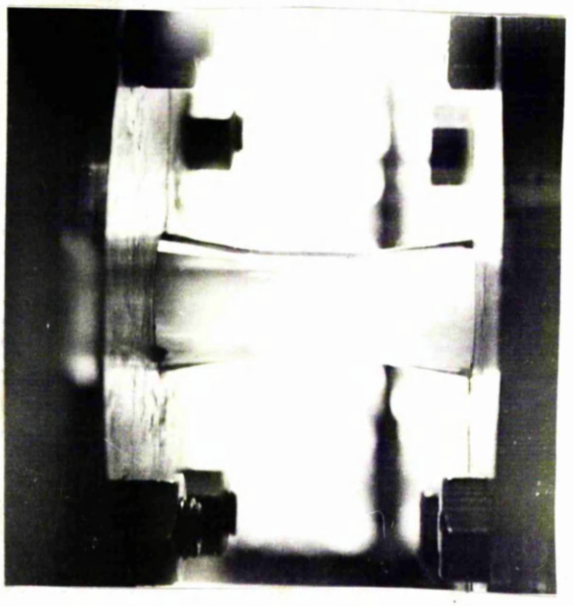

4″ LONG

PI 7.2 EFFECT OF AXIAL PROBES ON FLOW PATTERN

NOTE WAKE AT PROBE

(ROUNDED ENTRANCE 130°C)

DIRECTION

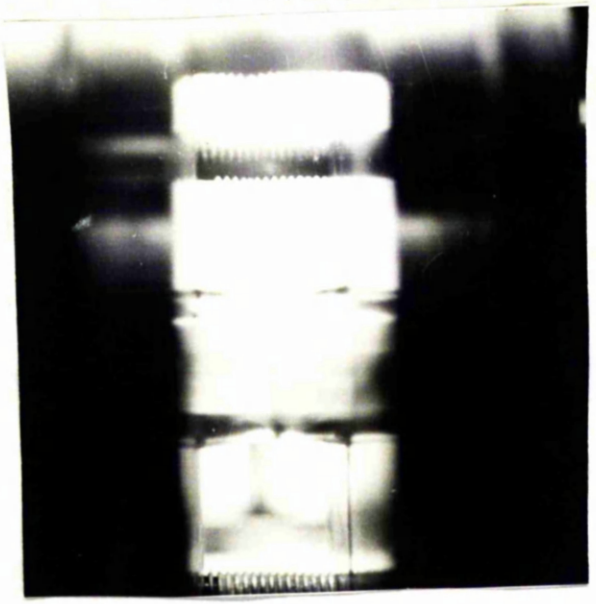

120°C

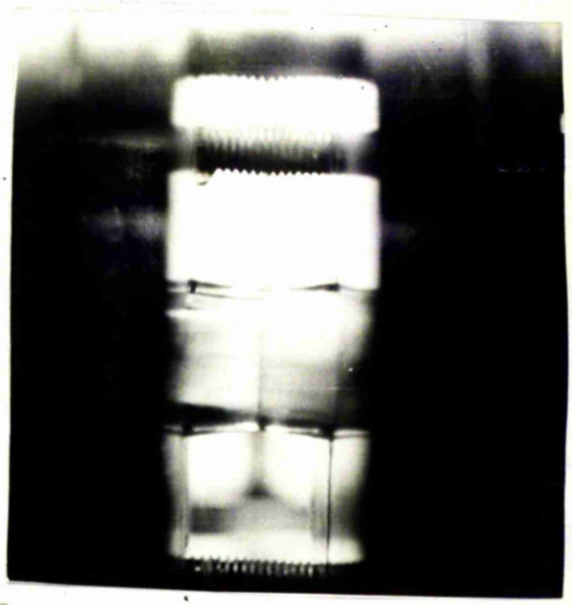

130°C

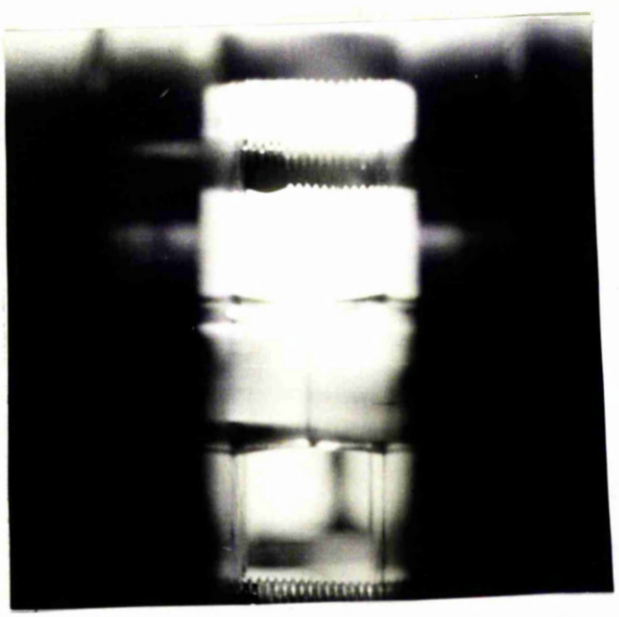

140°C

PI 7.3 EFFECT OF TEMPERATURE ON FLOW

(CONIC ENTRANCE 3" LONG)

7.4 Pressure Profiles in the Flow

Pressure profiles were obtained only for the set of glass nozzles. The pressure probes described in section 6.3 of Chapter 6 were used in this determination. The probes were fitted in the traversing mechanism and could be moved only in a vertical plane.

With the pressure drop across the test section set at 5.25 bar, pressure readings were taken with the probes, on the axis, 0.5 cm and 1 cm above and below the axis. At each point at least two readings were taken and the flow normally ran for 60 s before readings were taken, and for 30 s after probe repositioning.

Various sets of probes were used to give traverses at various distances upstream of the exit plane of the nozzles. From these sets of pressure readings the pressure profiles for the flow in the nozzles could be determined. Profiles were obtained for all none glass nozzles, each of 3 profiles at $\frac{L}{D}$, 3,4,5, for flows at 120 ^{o}C, 130 ^{o}C, 140 ^{o}C.

The pressure readings of gauge 'pressures' obtained are given in Table 7.3 and graphs of the pressure profiles are drawn from these results as Fig 7.4.

The critical flow rates found with the probes inserted were found to be about 1% less than these without probes. This is of the order of the standard deviation in flow rates for the results of Table 7.2.

To confirm that the apparent pressure gradients across the nozzle exits and entrances were not an effect of the system runs were carried out for a 4" (101 mm) length square entrance nozzle with 90^{o} and 180^{o} rotations of nozzle and nozzle and upstream pipe-section together. No variation in pressure profile was observed, after allowing for gauge reading errors. Thus the pressure profiles would not seem to be affected by the flow system.

Examination of Figs.7.4 shows a basic similarity in all the profiles. In each case the profile consists of a large pressure drop within the first 20 mm, a flat region where the axial pressure gradient is small and a further large pressure drop in the last 20 mm to the exit. (Note that the pressures are gauge pressures and the nominal exit pressure is zero.)

FIGURES 7.4

PRESSURE PROFILES IN GLASS NOZZLES

———— Probe on centre line

— — — — Probe 1 cm above centre line

—— - —— Probe 1 cm below centre line

PRESSURE DISTRIBUTION IN GLASS NOZZLES.

SQUARE ENTRANCE PROFILE

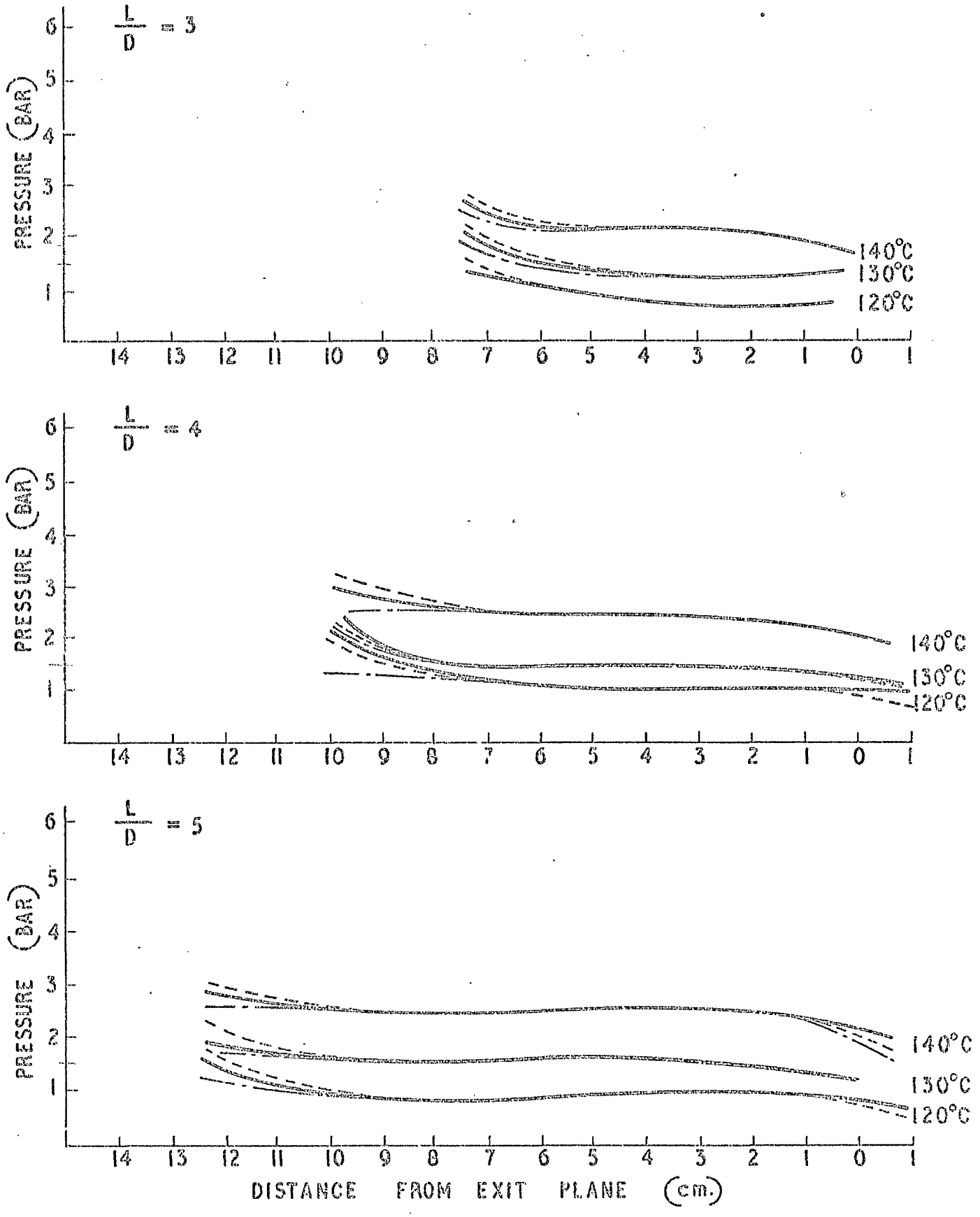

PRESSURE DISTRIBUTION IN GLASS NOZZLES.

CONIC ENTRANCE PROFILE

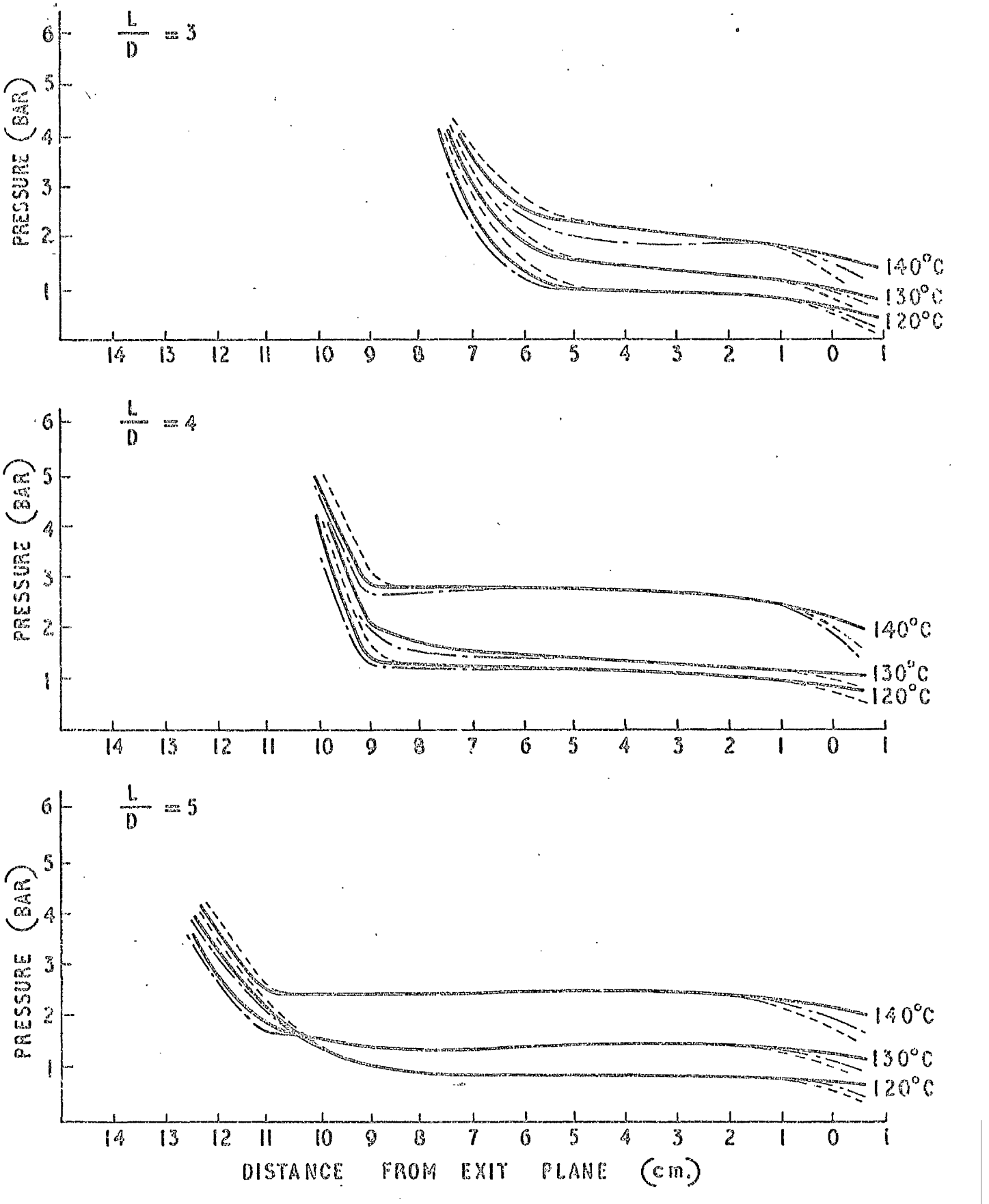

PRESSURE DISTRIBUTION IN GLASS NOZZLES.

ROUNDED ENTRANCE PROFILE

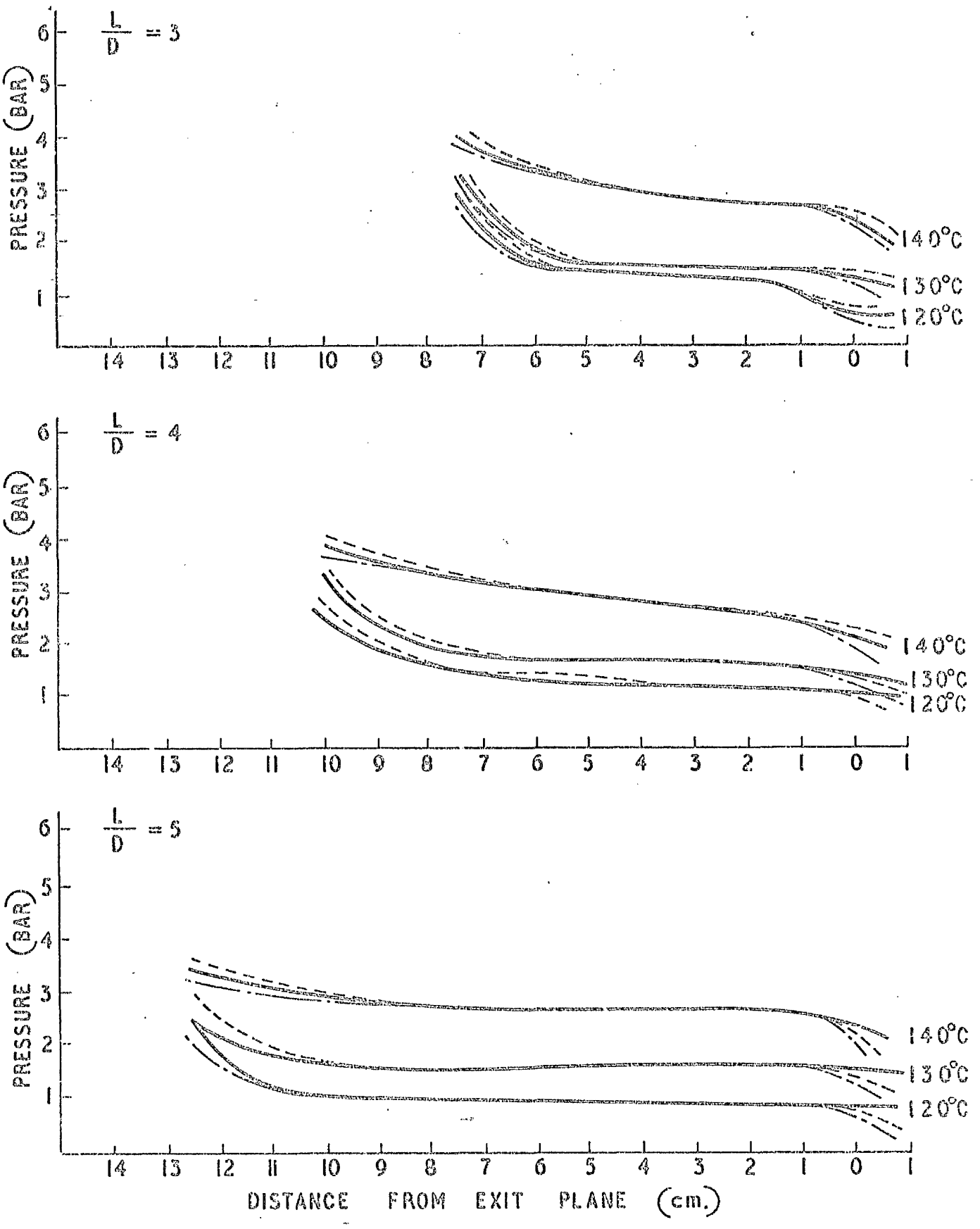

Tables 7.3

Pressure Profiles for Glass Nozzles

NOZZLE PRESSURE DISTRIBUTION - GLASS NOZZLES

Nozzle Entrance Profile: Square

$\frac{\text{Length}}{\text{Diameter}} \left(\frac{L}{D}\right) 3$

Length: 7.6 cm. Bore: 2.5 cm.

Temperature: 140 °C

Distance from Exit plane (cm)	Probe Pressure: Above Centre Line 1 cm	Above Centre Line 0.5 cm	On Centre Line	Below Centre Line 0.5 cm	Below Centre Line 1 cm	Mean Flow Rate (kg/s)	Barometric Pressure (bar)
7.5	2.80	2.75	2.77	2.70	2.62		0.996
6	1.90	1.93	2.00	1.90	1.90		0.996
2	2.20	2.20	2.15	2.20	2.12		0.993
0.7	1.90	1.88	1.90	1.90	1.90		0.993
-0.5							

Temperature: 130 °C

Distance from Exit plane (cm)	Probe Pressure: Above Centre Line 1 cm	Above Centre Line 0.5 cm	On Centre Line	Below Centre Line 0.5 cm	Below Centre Line 1 cm	Mean Flow Rate (kg/s)	Barometric Pressure (bar)
7.5	2.17	2.12	2.10	2.03	1.92		0.996
6	1.28	1.40	1.47	1.37	1.27		0.996
2	1.37	1.38	1.35	1.40	1.40		0.993
0.7	1.37	1.40	1.37	1.38	1.35		0.993
-0.5							

Temperature: 120 °C

Distance from Exit plane (cm)	Probe Pressure: Above Centre Line 1 cm	Above Centre Line 0.5 cm	On Centre Line	Below Centre Line 0.5 cm	Below Centre Line 1 cm	Mean Flow Rate (kg/s)	Barometric Pressure (bar)
7.5	1.62	1.50	1.38	1.37	1.40		0.996
6	0.83	0.88	0.97	0.90	0.85		0.996
2	0.80	0.78	0.77	0.80	0.78		0.993
0.7	0.80	0.80	0.80	0.80	0.80		0.993
-0.5							

NOZZLE PRESSURE DISTRIBUTION - GLASS NOZZLES

Nozzle Entrance Profile: Square

$\frac{\text{Length}}{\text{Diameter}} \left(\frac{L}{D}\right) 4$

Length: 10.1 cm. Bore: 2.5 cm.

Temperature: 140 °C

Distance from Exit plane (cm)	Probe Pressure: Above Centre Line 1 cm	Above Centre Line 0.5 cm	On Centre Line	Below Centre Line 0.5 cm	Below Centre Line 1 cm	Mean Flow Rate (kg/s)	Barometric Pressure (bar)
10	3.15	3.4	3.25	3.2	2.5	8.41	1.019
9	3.05	3.05	3.00	3.05	3.05	8.41	1.019
6	2.50	2.50	2.49	2.50	2.50	8.26	1.021
2	2.60	2.55	2.50	2.55	2.60	8.41	1.021
0.7	2.60	2.58	2.41	2.52	2.58	8.26	1.006
-0.5	2.00	2.08	2:10	2.08	1.90	8.41	0.993

Temperature: 130 °C

Distance from Exit plane (cm)	Probe Pressure: Above Centre Line 1 cm	Above Centre Line 0.5 cm	On Centre Line	Below Centre Line 0.5 cm	Below Centre Line 1 cm	Mean Flow Rate (kg/s)	Barometric Pressure (bar)
10	2.4	2.75	2.6	2.55	2.25		1.019
9	1.51	1.60	1.60	1.60	1.55		1.019
6	1.50	1.50	1.50	1.50	1.50		1.021
2	1.50	1.50	1.46	1.50	1.48		1.021
0.7	1.41	1.34	1.30	1.35	1.45		1.006
-0.5	0.98	1.12	1.04	1.00	0.90		0.993

Temperature: 120 °C

Distance from Exit plane (cm)	Probe Pressure: Above Centre Line 1 cm	Above Centre Line 0.5 cm	On Centre Line	Below Centre Line 0.5 cm	Below Centre Line 1 cm	Mean Flow Rate (kg/s)	Barometric Pressure (bar)
10	1.85	2.4	2.16	2.1	1.31		1.019
9	1.16	1.32	1.31	1.35	1.25		1.019
6	1.10	1.10	1.10	1.10	1.10		1.021
2	1.00	0.95	1.00	0.95	0.98		1.021
0.7	0.90	0.94	0.98	1.02	0.94		1.006
-0.5	0.75	0.85	0.90	0.90	0.82		0.993

NOZZLE PRESSURE DISTRIBUTION - GLASS NOZZLES

Nozzle Entrance Profile: Square

$\frac{\text{Length}}{\text{Diameter}} \left(\frac{L}{D}\right)_5$

Length: 12.7 cm. Bore: 2.5 cm.

Temperature: 140 °C

Distance from Exit plane (cm)	Probe Pressure					Mean Flow Rate (kg/s)	Barometric Pressure (bar)
	Above Centre Line		On Centre Line	Below Centre Line			
	1 cm	0.5 cm		0.5 cm	1 cm		
12.5	3.04	3.25	3.01	2.84	2.78	8.12	1.008
11	2.75	2.75	2.75	2.75	2.75	7.98	1.014
9	2.75	2.74	2.71	2.75	2.75	7.98	1.013
6	2.76	2.75	2.76	2.78	2.82	8.12	1.014
2	2.25	2.25	2.3	2.25	2.25	7.98	1.020
0.7	2.45	2.45	2.42	2.45	2.43	8.12	1.020
-0.5	1.68	2.00	2.00	2.00	1.81	8.12	1.017

Temperature: 130 °C

Distance from Exit plane (cm)	Probe Pressure					Mean Flow Rate (kg/s)	Barometric Pressure (bar)
	Above Centre Line		On Centre Line	Below Centre Line			
	1 cm	0.5 cm		0.5 cm	1 cm		
12.5	2.48	2.25	2.01	1.78	1.75	9.00	1.008
11	1.50	1.50	1.50	1.50	1.50	9.00	1.014
9	1.68	1.70	1.68	1.66	1.66	9.13	1.013
6	1.75	1.75	1.75	1.75	1.75	9.26	1.014
2	1.80	1.75	1.75	1.80	1.80	9.26	1.020
0.7	1.50	1.48	1.50	1.50	1.50	9.26	1.020
-0.5							

Temperature: 120 °C

Distance from Exit plane (cm)	Probe Pressure					Mean Flow Rate (kg/s)	Barometric Pressure (bar)
	Above Centre Line		On Centre Line	Below Centre Line			
	1 cm	0.5 cm		0.5 cm	1 cm		
12.5	1.70	2.08	1.75	1.25	1.25	9.76	1.008
11	1.08	1.10	1.10	1.07	1.07	9.88	1.014
9	0.90	0.90	0.90	0.90	0.90	10.00	1.013
6	1.03	1.03	1.02	1.08	1.08	10.00	1.014
2	1.03	1.03	1.01	1.01	1.05	9.88	1.020
0.7	0.90	0.90	0.90	0.90	0.93	10.68	1.020
-0.5	0.68	0.75	0.78	0.75	0.66	10.47	1.017

NOZZLE PRESSURE DISTRIBUTION - GLASS NOZZLES

Nozzle Entrance Profile: Conic

Length / Diameter (L / D) 3

Length: 7.6 cm. Bore: 2.54 cm.

Temperature: 140 °C

Distance from Exit plane (cm)	Probe Pressure (Bar)					Mean Flow Rate (kg/s)	Barometric Pressure (bar)
	Above Centre Line		On Centre Line	Below Centre Line			
	1 cm	0.5 cm		0.5 cm	1 cm		
7.5	4.7	4.6	4.52	4.5	4.47		0.995
6	2.8	2.68	2.62	2.53	2.30		0.995
2	2.05	2.0	2.02	2.02	2.0		0.977
0.7	1.75	1.75	1.75	1.75	1.75		0.987
-0.5	0.85	1.3	1.5	1.45	1.2		0.987

Temperature: 130 °C

Distance from Exit plane (cm)	Probe Pressure (Bar)					Mean Flow Rate (kg/s)	Barometric Pressure (bar)
	Above Centre Line		On Centre Line	Below Centre Line			
	1 cm	0.5 cm		0.5 cm	1 cm		
7.5	4.5	4.4	4.31	4.3	4.27		0.995
6	2.2	2.0	1.94	1.65	1.6		0.995
2	1.25	1.2	1.2	1.22	1.2		0.977
0.7	1.23	1.22	1.2	1.25	1.22		0.987
-0.5	0.5	0.85	0.92	0.8	0.65		0.987

Temperature: 120 °C

Distance from Exit plane (cm)	Probe Pressure (Bar)					Mean Flow Rate (kg/s)	Barometric Pressure (bar)
	Above Centre Line		On Centre Line	Below Centre Line			
	1 cm	0.5 cm		0.5 cm	1 cm		
7.5	4.42	4.3	4.3	4.3	4.27		0.995
6	1.72	1.6	1.38	1.1	1.0		0.995
2	0.7	0.7	0.7	0.7	0.7		0.977
0.7	0.83	0.8	0.85	0.85	0.8		0.987
-0.5	0.32	0.4	0.5	0.42	0.4		0.987

NOZZLE PRESSURE DISTRIBUTION - GLASS NOZZLES

Nozzle Entrance Profile: Conic

Length / Diameter (L / D) 4

Length: 10.1 cm. Bore: 2.5 cm.

Temperature: 140 °C

Distance from Exit plane (cm)	Probe Pressure					Mean Flow Rate (kg/s)	Barometric Pressure (bar)
	Above Centre Line		On Centre Line	Below Centre Line			
	1 cm	0.5 cm		0.5 cm	1 cm		
10	5.07	5.04	4.89	4.87	4.80		0.993
9	2.85	2.90	2.93	2.77	2.70		0.980
6	2.90	2.90	2.85	2.90	2.93		0.980
2	2.48	2.50	2.49	2.45	2.50		0.980
0.7	2.40	2.5	2.5	2.35	2.40		0.996
-0.5	1.54	1.75	1.87	1.65	1.40		0.996

Temperature: 130 °C

Distance from Exit plane (cm)	Probe Pressure					Mean Flow Rate (kg/s)	Barometric Pressure (bar)
	Above Centre Line		On Centre Line	Below Centre Line			
	1 cm	0.5 cm		0.5 cm	1 cm		
10	4.54	4.40	4.35	4.34	4.25		0.993
9	1.98	2.05	2.00	1.85	1.70		0.980
6	1.50	1.50	1.50	1.50	1.50		0.980
2	1.38	1.37	1.30	1.35	1.40		0.980
0.7	1.28	1.25	1.26	1.30	1.28		0.996
-0.5	0.75	1.03	1.20	0.95	0.74		0.996

Temperature: 120 °C

Distance from Exit plane (cm)	Probe Pressure					Mean Flow Rate (kg/s)	Barometric Pressure (bar)
	Above Centre Line		On Centre Line	Below Centre Line			
	1 cm	0.5 cm		0.5 cm	1 cm		
10	4.48	4.40	4.34	4.30	4.17		0.993
9	1.33	1.32	1.25	1.00	0.95		0.980
6	1.28	1.25	1.25	1.27	1.30		0.980
2	1.03	1.03	1.02	1.00	1.05		0.980
0.7	0.83	0.80	0.80	0.82	0.85		0.996
-0.5	0.65	0.7	0.84	0.72	0.62		0.996

NOZZLE PRESSURE DISTRIBUTION - GLASS NOZZLES

Nozzle Entrance Profile: Conic

Length / Diameter (L / D) 5

Length: 12.7 cm. Bore: 2.5 cm.

Temperature: 140 °C

Distance from Exit plane (cm)	Probe Pressure					Mean Flow Rate (kg/s)	Barometric Pressure (bar)
	Above Centre Line		On Centre Line	Below Centre Line			
	1 cm	0.5 cm		0.5 cm	1 cm		
12.5	4.72	4.65	4.50	4.50	4.37	9.08	1.019
11	-	-	2.27	-	-	8.95	1.016
9	2.48	2.50	2.50	2.46	2.48	-	1.019
6							
2	2.60	2.60	2.60	2.60	2.60	8.95	1.017
0.7	2.45	2.31	2.25	2.40	2.45	8.95	1.019
-0.5	1.42	2.25	2.20	2.25	1.75	8.95	1.019

Temperature: 130 °C

Distance from Exit plane (cm)	Probe Pressure					Mean Flow Rate (kg/s)	Barometric Pressure (bar)
	Above Centre Line		On Centre Line	Below Centre Line			
	1 cm	0.5 cm		0.5 cm	1 cm		
12.5	4.48	4.37	4.20	4.10	4.03	10.07	1.019
11	-	-	1.81	-	-		1.016
9	1.55	1.60	1.60	1.58	1.56	9.71	1.019
6							
2	1.60	1.60	1.60	1.60	1.60	9.71	1.017
0.7	1.43	1.50	1.50	1.41	1.41	9.71	1.019
-0.5	0.91	1.26	1.25	1.25	1.01	9.71	1.019

Temperature: 120 °C

Distance from Exit plane (cm)	Probe Pressure					Mean Flow Rate (kg/s)	Barometric Pressure (bar)
	Above Centre Line		On Centre Line	Below Centre Line			
	1 cm	0.5 cm		0.5 cm	1 cm		
12.5	4.31	4.20	4.10	4.00	3.94	10.69	1.019
11	-	-	1.25	-	-		1.016
9	1.05	1.05	1.05	1.05	1.05	10.80	1.019
6							
2	1.01	1.00	1.00	1.01	1.01	10.47	1.017
0.7	0.98	0.95	0.90	0.90	0.94	10.69	1.019
-0.5	0.41	0.81	0.80	0.86	0.65	10.69	1.019

NOZZLE PRESSURE DISTRIBUTION - GLASS NOZZLES

Nozzle Entrance Profile: Rounded

Length / Diameter (L / D) 3

Length: 7.6 cm. Bore: 2.5 cm.

Temperature: 140 °C

Distance from Exit plane (cm)	Probe Pressure: Above Centre Line 1 cm	Above Centre Line 0.5 cm	On Centre Line	Below Centre Line 0.5 cm	Below Centre Line 1 cm	Mean Flow Rate (kg/s)	Barometric Pressure (bar)
7.5	4.20	4.10	4.00	3.95	3.87		0.989
6	3.30	3.30	3.28	3.25	3.28		0.976
2	2.66	2.68	2.71	2.68	2.74		0.977
0.7	2.7	2.68	2.68	2.68	2.7		0.977
-0.5	2.12	1.9	1.87	2.05	1.48		0.985

Temperature: 130 °C

Distance from Exit plane (cm)	Probe Pressure: Above Centre Line 1 cm	Above Centre Line 0.5 cm	On Centre Line	Below Centre Line 0.5 cm	Below Centre Line 1 cm	Mean Flow Rate (kg/s)	Barometric Pressure (bar)
7.5	3.45	3.40	3.30	3.22	3.05		0.989
6	1.68	1.70	1.74	1.68	1.68		0.976
2	1.60	1.60	1.60	1.60	1.60		0.977
0.7	1.6	1.58	1.55	1.6	1.62		0.977
-0.5	1.33	1.30	1.17	0.90	0.50		0.985

Temperature: 120 °C

Distance from Exit plane (cm)	Probe Pressure: Above Centre Line 1 cm	Above Centre Line 0.5 cm	On Centre Line	Below Centre Line 0.5 cm	Below Centre Line 1 cm	Mean Flow Rate (kg/s)	Barometric Pressure (bar)
7.5	3.24	3.10	3.05	2.90	2.78		0.989
6	1.42	1.40	1.42	1.42	1.40		0.976
2	1.40	1.40	1.40	1.40	1.40		0.977
0.7	0.80	0.80	0.80	0.80	0.80		0.977
-0.5	0.88	0.80	0.75	0.68	0.38		0.985

NOZZLE PRESSURE DISTRIBUTION - GLASS NOZZLES

Nozzle Entrance Profile: Rounded

$\frac{\text{Length}}{\text{Diameter}} \left(\frac{L}{D}\right) 4$

Length: 10.1 cm. Bore: 2.5 cm.

Temperature: 140 °C

Distance from Exit plane (cm)	Probe Pressure: Above Centre Line 1 cm	Above Centre Line 0.5 cm	On Centre Line	Below Centre Line 0.5 cm	Below Centre Line 1 cm	Mean Flow Rate (kg/s)	Barometric Pressure (bar)
10	4.16	4.10	4.00	4.00	3.90		0.996
9	3.80	3.80	3.80	3.80	3.80		0.995
6	3.25	3.24	3.20	3.22	3.22		0.997
2	2.4	2.4	2.4	2.43	2.43		0.997
0.7	2.52	2.50	2.48	2.52	2.50		0.997
-0.5	2.1	2.05	2.0	1.6	1.25		0.997

Temperature: 130 °C

Distance from Exit plane (cm)	Probe Pressure: Above Centre Line 1 cm	Above Centre Line 0.5 cm	On Centre Line	Below Centre Line 0.5 cm	Below Centre Line 1 cm	Mean Flow Rate (kg/s)	Barometric Pressure (bar)
10	3.67	3.60	3.47	3.40	3.30		0.996
9	2.38	2.3	2.31	2.38	2.33		0.995
6	2.02	1.82	1.75	1.72	1.7		0.997
2	1.70	1.70	1.70	1.68	1.70		0.997
0.7	1.60	1.60	1.59	1.60	1.60		0.997
-0.5	1.17	1.5	1.45	1.4	1.08		0.997

Temperature: 120 °C

Distance from Exit plane (cm)	Probe Pressure: Above Centre Line 1 cm	Above Centre Line 0.5 cm	On Centre Line	Below Centre Line 0.5 cm	Below Centre Line 1 cm	Mean Flow Rate (kg/s)	Barometric Pressure (bar)
10	2.87	2.82	2.75	2.70	2.62		0.996
9	1.90	1.90	1.90	1.90	1.90		0.995
6	1.52	1.42	1.35	1.34	1.28		0.997
2	1.20	1.17	1.18	1.20	1.17		0.997
0.7	0.90	0.90	0.85	0.85	0.90		0.997
0.5	0.75	0.80	0.90	0.85	0.75		0.997

NOZZLE PRESSURE DISTRIBUTION - GLASS NOZZLES

Nozzle Entrance Profile: Rounded

Length / Diameter (L / D) 5

Length: 12.7 cm. Bore: 2.5 cm.

Temperature: 140 °C

Distance from Exit plane (cm)	Probe Pressure					Mean Flow Rate (kg/s)	Barometric Pressure (bar)
	Above Centre Line		On Centre Line	Below Centre Line			
	1 cm	0.5 cm		0.5 cm	1 cm		
12.5	3.5	3.68	3.50	3.02	3.22	12.21	1.008
11	3.25	3.27	3.27	3.28	3.28	12.21	1.015
9	2.95	2.95	2.95	2.95	2.95	12.21	1.016
6	2.82	2.83	2.80	2.85	2.85		1.000
2	3.02	3.03	3.01	3.03	3.03		0.998
0.7	2.75	2.75	2.75	2.75	2.75		0.998
-0.5	1.07	1.25	2.15	1.25	0.88		0.998

Temperature: 130 °C

Distance from Exit plane (cm)	Probe Pressure					Mean Flow Rate (kg/s)	Barometric Pressure (bar)
	Above Centre Line		On Centre Line	Below Centre Line			
	1 cm	0.5 cm		0.5 cm	1 cm		
12.5	3.25	3.20	2.60	2.98	2.61	10.64	1.009
11	1.80	1.75	1.75	1.80	1.80		1.016
9	1.78	1.80	1.75	1.80	1.80	10.64	1.016
6	1.80	1.78	1.78	1.77	1.78	10.64	1.013
2	1.70	1.72	1.70	1.73	1.70	10.64	0.998
0.7	1.80	1.80	1.80	1.80	1.88	10.75	0.998
-0.5	0.75	1.20	1.75	1.26	0.901	10.64	0.977

Temperature: 120 °C

Distance from Exit plane (cm)	Probe Pressure					Mean Flow Rate (kg/s)	Barometric Pressure (bar)
	Above Centre Line		On Centre Line	Below Centre Line			
	1 cm	0.5 cm		0.5 cm	1 cm		
12.5	2.55	2.75	2.50	2.24	2.08	9.46	1.009
11	1.08	1.10	1.10	1.10	1.10	9.34	1.016
9	1.02	1.00	1.02	1.02	1.02	9.34	1.016
6	1.30	1.30	1.27	1.30	1.30	9.34	1.013
2	1.00	0.95	0.96	0.98	0.98	9.34	0.998
0.7	1.00	1.02	1.00	1.00	1.03	9.34	0.998
-0.5	0.62	0.83	0.85	0.77	0.32	9.46	0.977

Both exit and entrance regions show marked radial pressure gradients suggesting some swirling of the water at both exit and entrance. Similar radial pressure gradients were noted in references (16) and (17), for the exit region. The existence of a radial gradient at the entrance of the nozzles does not seem to have been previously reported, although reference (3) includes indications consistent with such a gradient.

The extent of these gradients is affected by water temperature and entrance profile but for a fixed condition, shows no variation with nozzle length. For a given entrance profile the pressure profiles at exit and entrance show a marked similarity and differ from those for other entrance profiles. The flow at the entrance can be regarded as subcooled, single-phase water.

The flat central region is unaffected by exit profile but varies in length with nozzle length and profile. The pressure in this section is slightly (~0.5 bar) below the saturation pressure corresponding to the liquid bulk temperature. No radial pressure gradient was observed.

This experimental evidence suggests a number of conclusions. Firstly the evolution of vapour in the flow will be strongly affected by the nozzle length.

Secondly the entrance profile will affect such flow rates only by its effects on residence time, due to swirling and other features of the flow, associated with subcooled flows. No flashing takes place in the entrance region.

Thirdly, the effects of entrance profile affect the flow at the exit of the nozzle.

Although the theoretical studies in the first part of this thesis do not attempt to describe in detail the flow patterns for critical flow in short nozzles, an interesting comparison can be made with some of the assumptions used in developing the theory and the conclusions drawn in this section.

The assumption in the theory that the liquid phase behaved as a subcooled liquid is borne out by the observations of the effects of entrance profile, but the theoretical assumptions of liquid core surface temperature are not consistent with the experimental evidence on pressures in the main flat region of the pressure profiles.

7.5 Dissolved Oxygen in the Water Samples

Water samples were analysed using the procedure set out in section 6.3. All the samples were taken at the end of the nozzle test programme.

Typical sampling pressure was 4 bar, and samples were taken of water which had not been steam-heated, water which had been heated to 120 ^{o}C, to 140 ^{o}C and water which had been heated to 140 ^{o}C cycled once through the system and then reheated to 140 ^{o}C.

In all cases the system was pressurised using the air-compressor system.

In all cases two separated analyses were carried out, using 0.001 N sodium thiosulphate, and the calculation of oxygen content carried out in accordance with Annexe A to Chapter 6.

The results of these analyses are expressed in Table 7.4. The designation of sample titrations is that given in Annexe A to Chapter 6. The errors in titration are taken as $\pm$ 0.5 ml, giving a final oxygen content error of $\pm$ 0.1 ppm.

From these results it is clear that for this experimental system even a single heating cycle markedly reduces the quantity of dissolved oxygen in the water used, while successive cycles have much less effect.

Although this set of samples is by no means conclusive, the results quoted in Table 6.4 do suggest that for all the experimental runs quoted in this chapter, the dissolved oxygen content in the water used was less than 0.5 ppm.

Recent studies of nucleation processes (63) have emphasised the importance of the presence of dissolved gases in promoting nucleation. In much of the present work the possibility of nucleation in flashing flows has been ignored. If the low values for concentrations of dissolved oxygen, found here, are representative, and the work of reference (63) accurately describes the nucleation process, then it would seem that for the flows studied here the assumption that bubble formation plays no part in the process of vapour evolution is acceptable.

Table 7.4

Dissolved Oxygen Content for Water Samples

Table 7.4

Water Sample	Sample Volume	First Titration (Dissolved Oxygen)	Second Titration (Dissolved Oxidents)	Oxygen Conc. (ppm)
Cold (No heating)	105 ml	52 ml	11 ml	3
- " -	102 ml	50 ml	11 ml	3
Heated once to 120°C	98 ml	15 ml	10 ml	0.4
- " -	102 ml	15 ml	11 ml	0.3
Heated once to 140°C	105 ml	16 ml	12 ml	0.3
- " -	103 ml	16 ml	13 ml	0.2
Heated twice to 140°C	96 ml	16 ml	13 ml	0.2
- " -	104 ml	15 ml	13 ml	0.2

In these experiments no attempt was made to determine the quantities or sizes of suspended solid particles in the water used. Although the water appeared clear and free of suspended solids, it is likely that some small particles existed in suspension. These small particles would offer nucleation sites, however, it has recently been shown (63) that water samples containing small particles of size about 30 microns will show considerable delays in nucleation if the quantity of dissolved oxygen is less than about 0.3 ppm. This oxygen content is greater than that found for the water used here and it is unlikely that the presence of solid particles would enhance nucleation in this case.

7.6 Chapter Review

The data presented in this chapter, provides a small addition to the mass of information available on two-phase critical flows. Like the rest of this thesis the experimental study is confined to initial subcooled flows.

In the chapter the experimental values obtained in the programme have been presented in the form of tables and graphs, but discussion has been confined to detailed description of the apparent trends of the data. The policy in this part of the thesis has been to present the data and to avoid interpretation, since the data is certain, but interpretation is subjective.

However the prediction of the theoretical model set out in Chapter 4 have been examined using this data.

Section 5.2 of Chapter 5 set out four requirements for the experimental study and the experimental data presented in this chapter meets those requirements. These were, the determination of (1) variation of critical flow rate with liquid superheat;

(2) variation of critical flow rate with entrance profile;

(3) variation of critical flow rate with $\frac{L}{D}$ ratio;

(4) pressure gradients in the nozzles.

All of these variations have been examined at one time or another by

various experimenters and the previous work is discussed in Chapter 1, but never before were all these variations examined together for low pressure critical flows.

Similarly the experimental apparatus was in no way unusual, though most similar systems have been rather more sophisticated, but no system has been used to obtain information on the effects of all four parameters mentioned above.

The data presented here, and indeed, the experimental study, is unique only in that never before have critical flow rates and pressure distribution been determined on a single system for a set of nozzles, incorporating so many varying parameters. For this reason, comparisons and deductions of effects from varying parameters have been made much easier. Conversely this examination of a wide range of variations on standard parameters has introduced certain restrictions in the utility of the results. These are that

(i) only initial subcooled flows have been examined;

(ii) only very simple nozzle forms have been tested.

Within the limits imposed by the experimental design this comprehensive set of data on low pressure critical flows should prove to be of considerable value, offering direct comparison of the effects of certain parameters on rates of critical flashing flow.

To summarise, Chapter 7 presents a set of data on low pressure critical flows, drawn from experiments on a single set of nozzles on a single experimental apparatus.

The work complements and extends those by previous experimenters in that it covers a wide variation of standard parameters, indeed although the data presented does not extend the area of knowledge of two-phase critical flashing flows, it confirms and deepens that knowledge.

Chapter 8 - General Discussion of Present Work and Suggestions for Further Developments

8.1 Introduction

The previous chapters of this thesis fall into two parts. The first is devoted to the exposition of a new theoretical model of critical flashing flows, while the second part describes experimental investigation of certain aspects of these flows.

This chapter is intended to discuss the relationship between those parts. The discussion will illustrate the contributions from the work and identify the limits of the presentation. An attempt will be made to suggest areas of the present work which might be fruitfully extended in future studies. Detailed comments on the various parts of this work have been previously made and will not be repeated here.

8.2 Summary of the Contributions of this work

The work presented in this these, whether experimental or theoretical, owes much to the efforts of previous authors, whose works are reviewed in Chapter 1. Despite this obvious debt, it is claimed that this present contribution to the knowledge of two-phase critical flows, is significant.

On the theoretical side the model proposed offers adequate predictions of critical flow rates within the known limits of the model, the limits being introduced by certain of the assumptions used in the formulation of the model. The model is built around a new method of calculating mass transfer rates between phases at short time intervals, but also incorporates concepts first proposed by earlier authors. Although these earlier concepts are used, this combination, in the present model, is unique.

The experimental studies are original in two senses. Firstly the experimental system was specifically built for these studies and the system was designed from basic principles, although influenced by previous similar systems. Hence the data produced here must be regarded as unique.

Secondly, and more importantly, the data produced by the experimental study

form a unique integrated set of results showing the effect of controlled variation of certain parameters on critical flow rates of initially subcooled water.

Comparison of the theoretical predictions and experimental data has been made in Chapter 7, but some of the important points in the comparison may be recapitulated here.

This comparison shows that, while the model gives reasonable predictions of flow rates, at least one theoretical assumption, namely that of liquid core surface temperature, is not consistent with the observed local pressure for critical flows in glass nozzles. On the other hand the predictions of the theoretical model threw doubt on the magnitude and direction of the discontinuity in flow rate curves between nozzles with 1" (2.54 cm) and 0.5" (1.27 cm) diameters.

These two examples illustrate the interdependence of the theoretical and experimental studies if both studies are designed from the start to examine similar flows. Thus a knowledge of experimental data, refines the theoretical model, while a theoretical model may help to indicate areas of possible error, or further experimental interest in an experimental study.

8.3 The Limitations of the Work, Suggestions for Future Studies

To say that no research work is ever complete may be a common cliche, but nevertheless the cliche contains considerable truth. This section sets out some of the known limitations of the present work and makes suggestions for possible future extensions.

Most of the limitations were introduced in the design of the experimental system or in the assumptions made in developing the theoretical model. Four limitations appear to be noteworthy. These are:

(a) Both experimental and theoretical studies are confined to flows of water in systems where the maximum pressure is less than 8 bar, and the maximum temperature is less than 150 ^{o}C.

(b) These studies are confined to flows where the water upstream of the nozzle entrance is initially subcooled.

(c) Both studies apply only to flows in nozzles of simple form.

(d) Critical flow has been obtained only by increasing upstream pressures.

Of these four limitations, the first does not restrict the utility of the work, either as a contribution to the academic study of equilibration rates and flashing flows, or, indeed, as a possible source of information to the designer of more practical systems, since some flashing flows found in engineering applications take place at such low temperatures.

The second, third and fourth limitations do restrict the utility of the work, and efforts should be made to extend the studies described here to overcome these limitations. It is these possible extensions which form the bulk of the suggested possible future work together with an addition to the parameters observed.

Before discussing this future work it may be noted that the simple instrumentation employed on the experimental system seems to have performed adequately for the studies reported here. This performance does not preclude the introduction of more sophisticated measuring instruments to give a continuous record of various parameters, for example the use of pressure transducers in place of pressure gauges, thermocouples etc., all connected to some electronic data-logging system.

In addition to the present system, since these critical flow studies are much concerned with rates of equilibration and the possible existence of metastable states at points in the flow, it would be of value to add some thermocouple system to the pressure probes. This would enable the simultaneous observation of pressure and temperature profiles in the flows and, although problems arise in identifying to which phase the observation applies, such simultaneous profiles would assist in determining the existence of regions in which the liquid phase was superheated.

The modification of the experimental system to overcome the second and third limitation would be comparatively simple. The internal shapes of the nozzles could be modified, from the present simple form, perhaps by building up a "sandwich" of detachable entrances, exits, and throats. The critical flow tests could be carried out in the manner described in Chapter 7.

To examine cases in which the flow at the nozzle entrance was not single phase, some steam, or air, injector could be fitted upstream of the nozzle test section. The design of this injector should ensure that the injected phase was distributed in a known pattern and the flow pattern upstream of the nozzle would assume increased importance. Problems might also arise in fitting the injector if the present orifice plate system was retained for flow measurements

With regard to the theoretical model, considerable problems may arise in attempting to produce predictions of the critical flow observations which would be obtained in an extended experimental programme of this type. At present the model assumes a flow pattern which has been observed only for critical flows of initial subcooled water, however some of the techniques used might be of value in formulating a revised model to describe the observations of the extended programme

To examine the critical flow rates found if the pressure drop across the nozzles were altered by changing the back pressure, a throttle could be introduced in the 8" (203 mm) line from the deflector box to the main receiving tank. By this means the back pressure at the nozzle could be altered.

The reasons for not incorporating this modification initially were discussed in Chapter 5. However comparison of critical flow rates obtained by varying the back pressure with those corresponding flow rates given in Table 7.1 would help to resolve the problem of distinguishing between experimental methods in determinations of critical flow rates. Hence such comparisons carried out on the same set of test nozzles would be of considerable interest.

8.4 Closure

The previous remarks in this chapter have discussed the theoretical

and experimental work presented in this thesis. Some ideas have been set forth for possible future work on this type of flow situation using the present work as a foundation.

Assessing the contribution of a thesis of this type is always difficult, but the combination of theoretical model and experimental data for critical flashing flows of this type offers a definite contribution to knowledge of two-phase critical flashing flows. There are, of course, areas where further work could profitably be carried out, but although this present work must stand or fall on its own merits, it is clear that it has added something to the understanding of two-phase critical flashing flows.

References

(1) WALLIS, G.B. "Two Phase Flow and Heat Transfer".
Notes for a Summer Course, Dept. of Mechanical Engineering, Stanford University, Stanford, California, (1967).

(2) SILVER, R.S. "Temperature and Pressure Phenomena in the Flow of Saturated Liquids",
Proc. Roy. Soc. A vol.194 (1948), p.464.

(3) SILVER, R.S. and MITCHELL, J.A. "The Discharge of Saturated Water Through Nozzles",
Trans. N.E.Coast Inst. Engrs. and Shipb. Vol.62 (1946) p.51.

(4) ZALOUDEK, F.R. "The Critical Flow of Hot Water Through Short Tubes",
Report HW77594 Hanford Laboratories 1963.

(5) BOTTOMLEY, W.T. "Flow of Boiling Water Through Orifices and Pipes",
Trans.N.E.Coast Inst. Engrs. and Shipb. vol.53 (1936) p.65.

(6) BENJAMIN, M.W. and MILLER, J.C. "The Flow of Saturated Water Through Throttling Orifices",
Trans A.S.M.E. vol.63 (1941) p.410.

(7) BENJAMIN, M.W. and MILLER, J.C. "The Flow of Flashing Mixtures of Water and Steam Through Pipes",
Trans.A.S.M.E. vol.64 (1942) p.657.

(8) STUART, M.C. and YARNALL, D.R. "Fluid Flow Through Two Orifices in Series".
Trans. A.S.M.E. vol.66 (1944) p.387.

(9) CRUVER, J.E. "Metastable Critical Flow of Steam-Water Mixtures",
Ph.D., Dept. of Chemical Engineering,
University of Washington (1963).

(10) CHRISTENSEN, H. and SOLBERG, K.O. "Incomplete Thermal Equilibrium in Two-Phase Flow", Proc. of a Symp. on Two-Phase Flow,
University of Exeter, Paper H.3 (1965).

(11) PLESSET, M.S. and ZWICK, S.A. "Growth of Vapour Bubbles in Superheated Liquids".
J. App. Physics vol.25 (1959) p.493.

(12) BAILEY, J.F. "Metastable Flow of Saturated Water",
Trans. A.S.M.E. vol.73 (1951) p.1100.

(13) FAUSKE, H.K. "The Discharge of Saturated Water through Tubes", Chem. Eng. Prog. Symp. Series Vol.61 (1965) p.21.

(14) MIN, T.C., FAUSKE, H.K. and PETRICK, M. "Effect of Flow Passages on Two-Phase Critical Flow", I and E.C. Fundamentals vol.5 (1966) p.50.

(15) HESSON, J.C. and PECK "Flow of Two-Phase Carbon Dioxide through Orifices A.I.Ch.E.Journ. vol.4 (1958) p.207.

(16) HENRY, R.E. "A Study of One- and Two-Component, Two-Phase Critical Flows at Low Qualities", Report ANL-7430 Argonne National Laboratory (1968).

(17) KLINGEBIEL, W.J. "Critical Flow Slip Ratios of Steam-Water Mixtures", Ph.D.Thesis, Department of Chemical Engineering, University of Washington (1964).

(18) EDMONDS, D.K. and SMITH, R.V. "Comparison of Mass Limiting Two-Phase Flow in a Straight Tube and in a Nozzle", Proceedings of a Symp. on Two-Phase Flow, University of Exeter, Paper G.4 (1965).

(19) FAUSKE, H.K. "Two-Phase, Two- and One-Component Critical Flow", Proceedings of a Symp. on Two-Phase Flow, University of Exeter, Paper G.1 (1965).

(20) CIMORELLI L. and EVANGELISTI, R. "Experimental Determination of the "Slip Ratio" in a Vertical Boiling Channell under Adiabatic Conditions at Atmospheric Pressure", Int. J. Heat Mass Transf vol.12 (1969) p.713.

(21) ISBIN, H.S., MOY, J.E., DA CRUZ, J.R. "Two-Phase, Steam-Water Critical Flow", A.I.Ch.E.Journ. vol.3 (1957)p.361.

(22) FALETTI, D.W. "Two-Phase Critical Flow of Steam-Water Mixtures", Ph.D. Thesis, Dept. of Chemical Engineering, University of Washington (1959).

(23) MURAOKA, J. "Steam-Water Critical Flow Test-Design Test 1040", Report HW-69488 Hanford Laboratories (1961).

(24) CHISHOLM, D. "Critical Conditions During the Flow of Two-Phase Mixtures Through Nozzles", Proc. Inst. Mech. Engrs. vol.182 Pt 3H (1967) p.145.

(25) SILVER, R.S. "Procedure in Industrial Physics and Its Implication for Education", Brit. J. Appl. Phys. vol.2 (1951) p.241.

(26) HENRY, R.E. and FAUSKE, H.K. "The Two-Phase Critical Flow of One-Component Mixtures in Nozzles, Orifices, and Short Tubes", Journ. Heat Transf. Trans. A.S.M.E.(C) vol. (1971) p.179.

(27) SIMPSON, H.C. and SILVER, R.S. "Theory of On-Dimensional, Two-Phase, Homogeneous Non-Equilibrium Flow", Proc. Inst. Mech. Engrs. vol. (1962) p.45.

(28) MOODY, F.J. "Maximum Flow Rate of a Single Component, Two-Phase Mixture", Journ. Heat Transf. Trans.A.S.M.E.(C) vol.87 (1965) p.134.

(29) ZIVI, S.M. "Estimation of Steady-State Steam Void Fraction by Means of the Principle of Minimum Entropy Production", Journ. Heat Transf. Trans.A.S.M.E.(C) vol.86 (1964) p.247.

(30) FAUSKE, H.K. "Some Ideas About the Mechanism Causing Two-Phase Critical Flow", Appl. Sc. Res. Section A vol.13 (1963) p.149.

(31) STUART, D.O. and MURPHY, G. "Prediction of Critical Pressure for the Two-Phase Flow of Saturated Water in Pipes", A.S.M.E.Paper No.58-A-112 (1958).

(32) ZALOUDEK, F.R. "The Low Pressure Critical Discharge of Steam-Water Mixtures from Pipes", Report HW-68934 REV Hanford Laboratories (1961).

(33) REYNOLDS, O. "On the Extent and Action of the Heating Surface of Steam Boilers", Papers on Mechanical and Physical Subjects Vol.I paper 14, Cambridge University Press (1901).

(34) PRANDTL, L. "Bericht über Untersuchungen zur ausgebildeten Turbulenz", ZAMM 5 (1925) p.136.

(35) PRANDTL, L. "Uber ein neues Formelsystem für die ausgebildete Turbulenz" Nachrichten von der Akad. der Wissenschaften in Göttingen (1945) p.6, Van den Loeck of Ruprecht, Göttingen.

(36) SPALDING, D.B. "Notes on the Solution of the Navier-Stokes Equations for Steady, Two-Dimensional, Turbulent Flow by Numerical Techniques", Imperial College Mech.Eng.Dept. Report No.SF/TN/S (1967).

(37) PATANKAR, S.V. "Heat and Mass Transfer in Turbulent Boundary Layer", Imperial College Mech. Eng. Dept. Report TWF/R/S.

(38) SILVER, R.S. "Application of the Reynolds Analogy to the Combustion of Solid Fuels", Nature vol.165 (1950) p.725.

(39) SILVER, R.S. "Theoretical Treatment of Combustion in Fuel Beds, I Gas Composition and Heat Release; II Temperature attained in Combustion", Fuel vol.32 (1953) p.121.

(40) SILVER, R.S. "An Approach to a General Theory of Surface Condensers", Proc. Instn. Mech. Engrs. vol.178 (1963) p.339.

(41) WALLIS, G.B. "Use of the Reynolds Flux Concept for Analysing One-Dimensional Two-Phase Flow", Int. J. Heat and Mass Transfer vol.11 (1968) p.445.

(42) SPALDING, D.B. "Convective Mass Transfer", Edward Arnold, London (1963).

(43) TYLDESLEY, J.R. and SILVER, R.S. "The Prediction of the Transport Properties of a Turbulent Fluid", Int. J. Heat Mass Transfer vol.11 (1968) p.1325.

(44) WEIR, R.S.L. "Turbulent Diffusion in Single- and Two-Phase Flows", Ph.D. Thesis, University of Glasgow (1972).

(45) TYLDESLEY, J.R. and MORONES ESCOBAR, R. "Turbulent Diffusion of Heat, Mass, Momentum in Solid Suspensions", Proc. Second Int.Conf. on Hydraulic Transport of Solids in Pipes, Paper A1.

(46) SILVER, R.S. "Some Personal Views and Experiences in Heat Transfer Design", Proc. 3rd Int. Heat Transfer Conference A.J.Ch.E. Chicago (1966).

(47) DANCKWERTS, P.V. "Significance of Liquid-Film Coefficients in Gas Absorption", Ind. Eng. Chem. vol. 43 (1951) p.1460.

(48) MICKLEY, H.S. and FAIRBANKS, D.F. "Mechanism of Heat Transfer in Fluidised Beds", A.I.Ch.E.J. vol. 1 (1955) p.374.

(49) THOMAS, L.C., CHUNG, B.T.F. and MAHALDAR, S.K. "Temperature Profiles for Turbulent Flow of High Prandtl Number Fluids", Int.J.Heat and Mass Transfer vol.14 (1971) p.1465.

(50) CARSLAW, H.S. and JAEGER, J.C. "Conduction of Heat in Solids", Oxford (1947).

(51) MORSY, M. and SILVER, R.S. "A Theorem on Reynolds Flux and Boundary Layers", Privately Circulated by Glasgow University 1972.

(52) THOMAS, L.C. and FAN, L.T. "Heat and Momentum Transfer Analogy for Incompressible Boundary Layer Flow", Int. J. Heat Mass Transfer vol.14 (197) p.715.

(53) CRANK, J. "The Mathematics of Diffusion", Oxford (1956).

(54) LAUFER, J. "The Structure of Turbulence in Fully Developed Pipe Flow", N.A.C.A.Reprint 1174 (1954).

(55) WELLS, C.S., HARKNESS, J. and MEYER, W.A. "Turbulence Measurements in Pipe Flow of a Drag Reducing Non-Newtonian Fluid", A.I.A.A.Jn. vol.6 (1967) p.250.

(56) HICKMAN, J. et al "Behaviour of Liquid Surfaces During Evaporation or Condensation", O.S.W., R & D Progress Report No. 392 (1969).

(57) JAMIESON, D.T. "The Condensation Coefficient of Water", Nature, vol.202 (1964) p.483.

(58) SILVER, R.S. "Heat Transfer Coefficients in Surface Condensers", Engineering, Vol. (1946) p.1.

(59) RUSHTON, E. and LESLIE, D.C. "A Reappraisal of Silver's Model for Saturated Water Flow Through Nozzles", Brit. Chem. Eng. vol.14 (1969) p.319.

(60) BATCHELOR, G.K. "Introduction to Fluid Mechanics", Cambridge (1967).

(61) BURNELL, J.G. "Flow of Boiling Water through Nozzles, Orifices and Pipes", Engineering, vol.164 (1947) p.572.

(62) MAYHEW, Y.R. and ROGERS, G.F.C. "Thermodynamics and Transport Properties of Fluids, S.I. Units", Second Edition, Oxford - Basil Blackwell 1968.

(63) HANBURY, W.T. "Bubble Nucleation in Flash Boiling of Water", Pan Arab Symposium on Desalination, Cairo (1972).

BRITISH STANDARDS

The following British Standards were used in the design of the experimental apparatus.

B.S.10 (1962) "Flanges and Bolting for Pipes, Valves and Fittings".

B.S.1041 (1943) "Temperature Measurement".

B.S.1041 (1969) Section 2.1. "Liquid in Glass Expansion Thermometers".

B.S.1042 (1943) "Flow Measurement".

B.S.1500 (1958) "Fusion Welded Pressure Vessels".

B.S.1704 (1951) "General Purpose Thermometers".

B.S.2598 (1966) "Specification for Glass Pipelines and Fittings".

ANNEXE A1

Int. J. Heat Mass Transfer. Vol 15, pp. 1284–1287. Pergamon Press 1972. Printed in Great Britain

REYNOLDS FLUX AND DANCKWERTS SURFACE RENEWAL THEORY

G. M. THOMSON and R. S. SILVER

Department of Mechanical Engineering, The University of Glasgow, Glasgow, Scotland

(*Received* 21 *July* 1971)

NOMENCLATURE

A, dA,	area of surface;
C,	concentration;
C_p,	specific heat at constant pressure;
D,	diffusion coefficient;
h,	heat-transfer coefficient;
h_D,	mass transfer coefficient;
K,	thermal conductivity;
t,	time;
U,	velocity of fluid;
R,	entity size parameter;
α,	thermal diffusion coefficient;
ε,	Reynolds flux;
μ,	dynamic viscosity;
ν,	kinematic viscosity;
ρ	density;
τ,	shear stress;
θ,	temperature difference between fluid and transfer surface.

Subscripts

∞,	in bulk fluid;
0,	at transfer surface.

A THEORY of the observed correlation between convective heat transfer and convective momentum transfer appears first to have been suggested by Reynolds [1].* Reynolds theory assumed that both such processes were due to the motion of fluid particles in lateral directions relative to the mean axial flow of the fluid. In 1950, Silver [2] suggested that by deducing the amount of lateral motion from known experimental results of heat transfer *or* of frictional resistance the limit rates of mass transfer access to a surface could be calculated. From 1950 to 1954 this was applied by him to the calculation of combustion rates of fuel particles and in fixed beds [3, 4], and later to the calculation of condensation rates and associated pressure drop [5]. Meanwhile similar applications of Reynolds theory had been developed by Spalding [6] who coined the term Reynolds Flux as a name for the assumed lateral motion of fluid particles. Both Silver and Spalding recognised that they were developing a concept initiated by Reynolds.

However, in 1951 Danckwerts [7] in discussing gas absorption in liquid films suggested a process of replacement of liquid surface by lateral flow of fresh liquid, and Mickley, Fairbanks [8] adapted this to a discussion of heat transfer in fluidized beds. Danckwerts coined the term "surface renewal mechanism" to describe his idea. There is no doubt, however, that the underlying concept is an assumed lateral flux, yet neither Danckwerts nor Mickley and Fairbanks appear to have recognized the identity of this concept with that of Reynolds. The explanation of this may have been that, as discussed in the Reynolds Centenary volume [9], Reynolds actual theoretical model was largely neglected because of the loose term "Reynolds Analogy" which had been commonly used to describe his ideas, and it was only from [2] onwards (1950), that interest was directed to the flux concept. Alternatively it may simply illustrate the common difficulty of "information transfer" from one field of study to another.

We have examined several references to surface renewal theory [10–12] including one very recently in this journal and in no case have we found comment on its relation to Reynolds theory.

It seems therefore worthwhile to point this out briefly.

Where Reynolds referred to "non-molecular fluid particles", Danckwerts speaks of "eddies exposing fresh surface" from the interior of the fluid, and Silver adopts the general term "entities" to describe the elements whose lateral motion constitutes the lateral flux.

In Reynolds original theory, the lateral flux was assumed to reach equilibrium with wall surface conditions instantaneously on reaching the wall. This simple assumption was on the whole maintained in the further work by Silver and by Spalding, although in 1966 Silver [13] discussed the possibility that the return flux from the wall might not have reached equilibrium with wall conditions. Danckwerts, however, included the possibility of incomplete equilibration of flux with wall conditions right from the start.

A duration time of the entity while in contact with the surface is postulated, and diffusion equations for energy, mass, or momentum can be applied for these duration times. A statistical mean life and corresponding mean transfer rates can be assessed. This has been the pattern of development of surface renewal theory.

It is seen therefore that essentially surface renewal theory is one form of refinement of Reynolds theory, using the same basic concept of a lateral flux, but permitting adjustments through the concept of extent of equilibration with wall conditions.

We have therefore used the ideas of surface renewal to develop an improved two parameter form of the Reynolds theory. We retain the Reynolds Flux (ε) as one parameter but introduce a size parameter R which physically corresponds to a normal dimension of the "eddies" or "entities" in contact with the transport surface or wall. As in Danckwerts formulation [8] molecular transport occurs to the entities in contact with the solid surface.

Thus the transport processes within fluid *elements* are defined by:

$$\left.\begin{aligned} \alpha\frac{\partial^2\theta}{\partial x^2} &= \frac{\partial\theta}{\partial t} && \text{—heat transfer}\\ \nu\frac{\partial^2 U}{\partial x^2} &= \frac{\partial U}{\partial t} && \text{—momentum transfer}\\ D\frac{\partial^2 C}{\partial x^2} &= \frac{\partial C}{\partial t} && \text{—mass transfer} \end{aligned}\right\} \quad (1)$$

* Footnote: This is I think correct, although Thomson (Lord Kelvin) was on the same track earlier. In 1856 commenting on a paper by Joule he referred to "clogging of the water caused by the heating particles not being quickly enough carried away and replaced by cooler ones". —R.S.S.

with boundary conditions

$$t = 0\ x \geqslant 0\ \theta = \theta_\infty\ U = U_\infty\ C = C_\infty$$
$$t > 0\ x = 0\ \theta = 0\quad U = 0\quad C = C_0$$
$$x = \infty\ \theta = \theta_\infty\ U = U_\infty\ C = C_\infty$$

The solutions of these equations give instantaneous transport coefficients at the solid surface.

$$\left.\begin{aligned} h &= \left[\frac{K\rho C_p}{\pi t}\right]^{\frac{1}{2}} && \text{—heat transfer}\\ \tau &= \left[\frac{\mu^2 U^2}{\pi \nu t}\right]^{\frac{1}{2}} && \text{—momentum transfer}\\ h_D &= \frac{D}{[\pi D t]^{\frac{1}{2}}} && \text{—mass transport.}\end{aligned}\right\} \quad (2)$$

To obtain average values of these coefficients it is necessary to obtain some surface age distribution $\phi(t)$. It is at this point that our presentation diverges from that of Danckwerts [8].

The mass of surface dA, having an age between t and $t + dt$ is simply $\rho R\ dA\ \phi(t)\ dt$.

Also the rate of decrease of surface of any age is equal to the rate at which surface of that age is replaced.

Rate of replacement of surface of age t to $t + dt$ is $\varepsilon\ \phi(t)\ dt$ whence

$$-\frac{d\phi(t)}{dt}\rho R = \varepsilon\phi(t). \quad (3)$$

This gives the distribution function

$$\phi(t) = \frac{\varepsilon}{\rho R}\exp\left(\frac{-\varepsilon}{\rho R}t\right). \quad (4)$$

Now the heat transfer coefficient for the surface is the average of all the local coefficients

$$h = \left[\frac{K\rho C_p}{\pi}\right]^{\frac{1}{2}}\frac{\varepsilon}{\rho R}\int_0^\infty t^{-\frac{1}{2}}\exp\left(\frac{-\varepsilon}{\rho R}t\right)dt = \left[\frac{KC_p\varepsilon}{R}\right]^{\frac{1}{2}}. \quad (5a)$$

$$\left.\begin{aligned} &\text{Similarly } \tau = U_\infty\left[\frac{\mu\varepsilon}{R}\right]^{\frac{1}{2}}\\ &\text{and } h_D = \left[\frac{D\varepsilon}{\rho R}\right]^{\frac{1}{2}}.\end{aligned}\right\} \quad (5b)$$

The mean age of entities at the surface is

$$\bar{t} = \int_0^\infty t\,\phi(t)\,dt = \frac{\rho R}{\varepsilon}. \quad (6)$$

The parameter R in this model represents a surface layer depth and since the diffusion equations have been solved for semi-infinite boundary conditions it would seem that R must be greater than the depth to which the molecular diffusion process has penetrated, i.e.

$$\left.\begin{aligned} R &> (\nu t)^{\frac{1}{2}}\\ R &> (\nu t)^{\frac{1}{2}}\\ R &> (D t)^{\frac{1}{2}}\end{aligned}\right\} \quad (7)$$

Substituting for $\bar{t}$ from (6)

$$\left.\begin{aligned} R &> \frac{K}{C_p\varepsilon}\\ \text{or } R &> \frac{\mu}{\varepsilon}\\ \text{or } R &> \frac{D_p}{\varepsilon}.\end{aligned}\right\} \quad (8)$$

If these are substituted into the corresponding transport coefficients we obtain

$$\left.\begin{aligned} h &= \left[\frac{KC_p\varepsilon}{R}\right]^{\frac{1}{2}} < \varepsilon C_p\\ \tau &= U_\infty\left[\frac{\mu\varepsilon}{R}\right]^{\frac{1}{2}} < \varepsilon U\\ h_D &= \left[\frac{D\varepsilon}{\rho R}\right]^{\frac{1}{2}} < \frac{\varepsilon}{\rho}.\end{aligned}\right\} \quad (9)$$

Equations (9) merely indicate that the normal Reynolds Theory transport coefficients represent the maximum possible values obtainable.

Physically R might be taken as the depth of the laminar sublayer in turbulent flow. However, the theory of turbulence by Tyldesley and Silver [14] utilizes the entity concept with an entity size related to the microscale of the turbulence as one of the parameters describing the turbulence, and it may later be possible to introduce R in that context.

Experimentally the data from anemometry experiments by Laufer [15] and Wells Harkness, and Meyer [16] suggest that in ducts or pipes both the depth of laminar sublayer and the turbulent microscale near the walls of the duct are of same order.

REFERENCES

1. O. Reynolds, On the extent and action of the heating surface of steam boilers, Papers on Mechanical and Physical subjects, Vol. I, Paper 14. Cambridge University Press (1901)
2. R. S. Silver, Application of the Reynolds analogy to the combustion of solid fuels, *Nature* 165, 725 (May 1950).
3. R. S. Silver, Theoretical treatment of combustion in fuel beds, I. Gas composition and heat release. II Temperature attained in combustion, *Fuel* 32, 121–159 (1953).
4. R. S. Silver and R. W. Maclay, Mass transfer theories of fuel bed combustion, *Br. J. Appl. Phys* 6, 267–271 (1955).
5. R. S. Silver, An approach to a general theory of surface condensers, *Proc. Instn Mech. Engrs* 178, 339–376 (1963–64).
6. D. B. Spalding, *Convective Mass Transfer*, Edward Arnold, London (1963).
7. P. V. Danckwerts, Significance of liquid-film coefficients in gas absorption, *Ind. Engng Chem.* 43, 1460 (1951).
8. H. S. Mickley and D. F. Fairbanks, Mechanism of heat transfer in fluidised beds, *A.I.Ch.E. Jl* I, 374 (1955).
9. R. S. Silver, Reynolds flux concept in heat and mass transfer, *Proceedings of the Osborne Reynolds Centenary Symposium*, Manchester University Press (1970).
10. C. Judson-King, Turbulent liquid phase mass transfer at a free gas–liquid interface, *I/EC Fundls* 5, 8 (1966).
11. J. C. Deni, The calculation of convective and condensation heat transfer coefficients to surfaces held in an acoustic field or subjected to Mechanical oscillations, Ph.D. Thesis Loughborough University of Technology (1969)
12. L. C. Thomas and L. T. Fan, Heat and momentum transfer analogy for incompressible boundary layer flow, *Int. J. Heat Mass Transfer* 14, 715–717 (1971).
13. R. S. Silver, Some personal views and experiences in heat transfer design, Proceedings of 3rd International Heat Transfer Conference, A.I.Ch.E. Chicago (1966)
14. J. R. Tyldesley and R. S. Silver, The prediction of the transport properties of a turbulent fluid, *Int. J. Heat Mass Transfer* 11, 1325–1340 (1968).
15. J. Laufer, The structure of turbulence in fully developed pipe flow, N.A.C.A. Reprint 1174 (1954)
16. C. S. Wells, J. Harkness and W. A. Meyer, Turbulence measurement in pipe flow of a drag reducing non-Newtonian fluid, *AIAA Jl* 6, 250–257 (1967).

ANNEXE A2

AN APPROACH TO THE CALCULATION OF EQUILIBRATION RATES IN FLASHING FLOWS

Gordon M. Thomson

Department of Mechanical Engineering

The University of Glasgow

Glasgow. G12 8QQ

September, 1972

1. Introduction

The phenomenon of flashing flows in short nozzles and orifices has been the subject of many experimental and theoretical investigations. In such flows mass transfer takes place between phases. Since the rate of flow of two-phase mixture is affected by the quality of the flowing mixture, a knowledge of the rate of mass transfer between phases is necessary for the accurate description of flashing flows.

Mass transfer between phases is a time-dependent process and, although in the case of critical flashing flows certain authors have had some success in assuming thermodynamic equilibrium between phases, in general some lack of equilibration between phases may exist. This departure from thermodynamic equilibrium should be most marked in flows where the residence time for the flashing mixture in the flow passage is very short. Experimental evidence of this phenomena can be found in the experimental studies of Stuart and Yarnall (1) for discharges through orifices, and of Cruver (2). In both cases simultaneous measurements were made of liquid phase temperature and local pressure. These studies showed that the liquid phase temperature could be considerably in excess of the saturation temperature corresponding to the local pressure, suggesting that the liquid phase was in some metastable state.

This short paper presents a method of calculating rates of evaporation (and condensation) from the surface of liquids exposed to changes of local pressure for short time intervals. This method is derived from a simple model of turbulent flow, the Danckwerts' surface renewal model (3).

2. The Danckwerts Surface Renewal Model

The surface renewal model proposed by Danckwerts (3) describes heat transfer between a liquid and its boundary surface in terms of a liquid surface film constantly renewed by a lateral flux of lumps, or eddies, of fluid (Fig. 1).

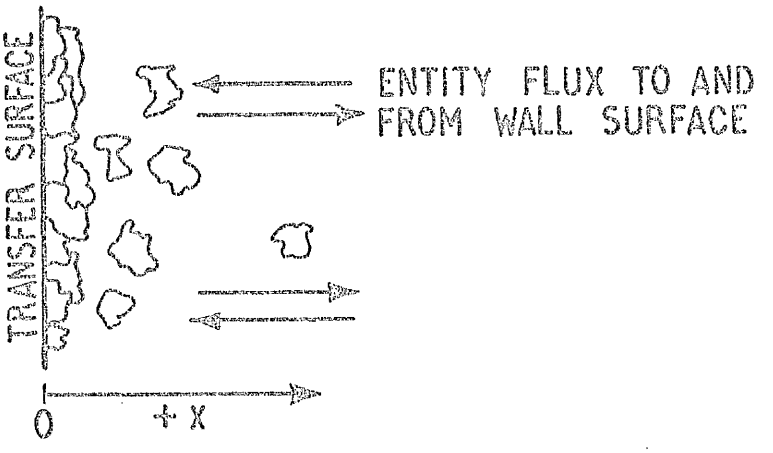

FIG 1

Heat transfer at the surface is assumed to take place solely by conduction and for the coordinate system of Fig. 1 can be described by the conventional uni-directional form.

$$\alpha \frac{\partial^2 \theta}{\partial x^2} = \frac{\partial \theta}{\partial t} \qquad (1)$$

If (1) is solved for semi-infinite boundary conditions

i.e.

$\underline{t = 0}$	$x = 0$	$\theta = \theta_\infty$
$\underline{t > 0}$	$x = 0$	$\theta = 0$
	$x = \infty$	$\theta = \theta_\infty$

(2)

where t is the time for which an entity is in contact with the surface. Then the solution is standard and may be found for example in Carslaw and Jaeger (4).

The instantaneous heat transfer coefficient for an entity of age t is

$$h_i = \left[\frac{k \rho C_p}{\pi t} \right]^{\frac{1}{2}} \qquad (3)$$

However the entities in contact with the surface have ages in the range $t = 0$ to $t = \infty$ for a steady state situation. Hence the effective heat transfer coefficient over the surface is given by the instantaneous values weighted by an entity surface age distribution $\phi(t)$,

i.e. $$\bar{h} = \frac{\int_0^\infty h_1 \, \phi(t) \, dt}{\int_0^\infty \phi(t) \, dt} \qquad (4)$$

The distribution $\phi(t)$ can be evaluated.

Let the number of entities striking the surface per unit time be S. The rate of decrease of surface of any age is equal to the rate at which it is replaced. The rate of replacement of surface of age t to t + dt is $S\phi(t)\,dt$ per unit area.

The number of entities per unit area having ages between t and t + dt is $\phi(t)\,dt$.

Whence

$$-\frac{d\phi(t)}{dt} = S\phi(t) \qquad (5)$$

with solution for $\phi(t)$

$$\phi(t) = (\text{const}) \exp(-St) \qquad (6)$$

Now impose on $\phi(t)$ the condition

$$\int_0^\infty \phi(t) \, dt = 1 \qquad (7)$$

Then combining (6) and (7) and solving for constant

$$\phi(t) = S \exp(-St) \qquad (8)$$

Substituting (3) and (8) in (4)

$$\bar{h} = \left[\frac{k \rho c_p}{\pi}\right]^{\frac{1}{2}} \int_0^\infty t^{-\frac{1}{2}} S \exp(-St) \, dt \qquad (9)$$

3. Extension of Danckwert's Model to Prediction for Short Exposure Time

Consider now the case where the liquid flow takes place with no heat transfer. Although no heat transfer takes place a surface film of entities will still exist at the liquid boundary and will still be renewed. The entity age distribution will then have the form given in equation (8). Suppose then that heat transfer instantaneous commences at the surface at t = 0. Then

if exposure times are limited to times τ of order $\frac{1}{S}$ the upper limit of the integrals in (4) must be set at τ and the effective heat transfer rate after time τ is given by

i.e.
$$h_t = \frac{\int_0^\tau h_1 \, \phi(t) \, dt}{\int_0^\tau \phi(t) \, dt} \qquad (10)$$

6. Evaporation Rates at Short Time Intervals.

Consider a plane liquid-vapour interface with the phases in equilibrium. Let the liquid bulk temperature be T_b and let the pressure acting on the surface be P_b.

Suppose that the pressure acting on the liquid surface is now suddenly reduced at time $t = 0$ to a value P_2 with corresponding saturation temperature T_{sat} such that $T_{sat} < T_b$ The liquid is suddenly taken into a metastable state and will return to thermodynamic equilibrium by evaporation of the liquid at some rate $\dot{m}_t$ per unit area.

Heat transfer takes place at a rate $\dot{q}_f$ from the bulk liquid to the interface surface and at rate $\dot{q}_g$ from the surface into the vapour. The heat transfer to the liquid surface is assumed to be due to a lateral motion of entities to the surface.

For energy balance at the surface

$$\dot{q}_g + m_\tau H_g = \dot{q}_f \qquad (11)$$

and $\dot{q}_f = h_\tau (T_b - T_s)$ $\qquad T_s$ = surface temperature.

Provided the heat loss from the vapour to its surroundings is small then the temperature gradient in the vapour phase may be neglected. If this is done then

$$T_s \doteq T_{sat}$$

and $$\dot{q}_g \doteq 0$$

Whence equation (11) can be written as

$$\dot{m}_\tau = \frac{h_t (T_b - T_{sat})}{H_{fg}}$$

$$= \frac{x}{C_p} h_t \qquad (12)$$

where $x = \dfrac{C_p (T_b - T_{sat})}{H_{tg}}$

Substituting for h_t from (10) in (12)

$$\dot{m}_\tau = \frac{x}{C_p} \frac{\int_0^\tau h_j \, \phi(t) \, dt}{\int_0^\tau \phi(t) \, dt} \qquad (13)$$

The mean value of $\dot{m}_\tau$ over the period from t = 0 to t = τ is

$$\bar{\dot{m}} = \frac{\int_0^\tau \dot{m}_\tau dt}{\tau} \qquad (14)$$

Writing $\dot{m}_\tau$ in the form of (13) into (14), and substituting for h_1 and (t)

$$\bar{\dot{m}} = \frac{x}{C_p} \left[\frac{k \rho C_p}{\pi}\right]^{\frac{1}{2}} \frac{1}{\tau} \int_0^\tau dt \; \frac{\int_0^\tau St^{-\frac{1}{2}} \cdot \; \text{[illegible]} \; dt. \exp(-St) \, dt}{\int_0^\tau \text{[illegible]} \; dt. \; S \exp(-St) \, dt} \qquad (15)$$

Integrals of this form can be evaluated analytically only with extremely difficulty if at all. However if $\tau \ll \frac{1}{S}$ then exp (- St) $\doteq$ 1 and the equation (15) can be evaluated as

$$\bar{\dot{m}} = \frac{4x}{C_p} \left[\frac{k \rho C_p}{\pi \tau}\right]^{\frac{1}{2}} \qquad (16)$$

The assumption $\tau \ll \frac{1}{S}$ can be justified only by showing that the predictions of equation (16) are consistent with experimental data for evaporation at short time intervals.

The assumptions made in the derivation are such that equation (16) should

be equally applicable to the prediction of condensation rates at short time intervals.

6. Comparison with Experimental Data

The predictuve equation (16) must be compared with evaporation rates at suitably short time intervals. Fortunately experimental studies exist of evaporation and condensation rates from the surface of water jets.

Hickman et al (5) examined the evaporation and condensation of water from the surface of jets at low temperatures and pressures. Pressures of order 10^{-3} bar were used with temperature differences of order $10^{o}C$. Exposure times were in the range 5×10^{-4} sec to 2×10^{-3} sec. Hickman's data is plotted in Fig. 3 together with theoretical predictions from equation (16). In general the predictions are good for exposure times of about 10^{-3} sec but over predict evaporation rates by around 10%.

Rates of condensation of water vapour on jet surfaces have also been examined experimentally by Jamieson (16). Here vapour pressures ranged from 0.185 bar to 0.98 bar with temperature differences from $30^{o}C$ to $100^{o}C$. Exposure times ranges from 2×10^{-5} sec. to 3×10^{-4} sec.

Figure 4 shows Jamieson's results compared with the values predicted by equation (16). Here agreement appears good for exposure times above 2×10^{-4} sec. but equation (16) underpredicts at shorter exposure times.

From this comparison of the prediction of equation (16) with experimental data it would seem that equation (16) provides accurate predictions of condensation rates for exposure times in the range 2×10^{-4} sec. to 2×10^{-3} sec over a wide range of pressures and temperature differences but will consistently overpredict evaporation rates by approximately 10%.

The tendency of equation (16) to overpredict evaporation rates is probably introduced by the assumption that the temperature gradient in the vapour phase was negligible. Accurate prediction of the effects of a vapour

phase temperature gradient might well require consideration of effects at the liquid vapour interface of the type discussed by Bornhorst and Hatsopoulos (7

4. Closure

The simple model discussed in this paper offers a method of predicting mass transfer rates between phases in flashing flow situations where the flashing mixture is resident in the flow passage for a short time. Situations of the type are found in the critical flashing-flow of liquids in short nozzles and orifices and an approach to prediction of evaporation rates similar to that presented here has been used in the development of a theoretical model of critical two-phase flashing flows in short nozzles(8).

Acknowledgements

The author wishes to thank Professor R.S. Silver, Mr. J.R. Tyldesley and Mr. R. Muncaster for helpful discussion of parts of the work presented in this paper.

Notation

C_p = specific heat at constant pressure

h = heat transfer coefficient

H_{tg} = enthalpy difference between liquid and vapour phases

K = thermal conductivity

$\dot{m}$ = mass flux

P = pressure

$\dot{q}$ = rate of heat transfer

T = temperature

S = entity renewal rate

α = thermal diffusion coefficient

ρ = density

τ = exposure time

Θ = temperature difference between fluid and transfer surface.

Subscripts

b = in bulk liquid

f = for liquid phase

g = for vapour phase

s = at liquid surface

sat = at saturation conditions

t, τ = at time t, τ

∞ = in bulk liquid

References

1. STUART, M.C. and YARNALL, D.R. "Fluid flow through two orifices in series". Trans. ASME Vol 66 (1944) p.387.

2. CRUVER, J.E. "Metastable critical flow of steam-water mixtures" Ph.D. Theses, Department of Chemical Engineering, University of Washington (1963).

3. DANCKWERTS, P.V. "Significance of liquid-film coefficients in gas absorption". Ind. Eng. Chem. Vol. 43 (1951) pp 1460

4. CARSLAW, H.S., and JAEGER, J.C. "Conduction of heat in solids" Oxford (1947)

5. HICKMAN, et al. "Behaviour of liquid surfaces during evaporation of condensation". O.S.W., R & D. Progress Report No. 392 (1969)

6. JAMIESON, D.T. "Condensation coefficient of water". Nature, Vol 202 (1964), p.483.

7. BORNHORST, W.J. and MATSOPOULOS, G.N. Journ. App. Mech. (1967) p.840.

8. THOMSON, G.M. "Aspects of two phase critical-flashing flow of water in short nozzles". Ph.D. Thesis, University of Glasgow, in preparation for presentation, Oct. 1972.

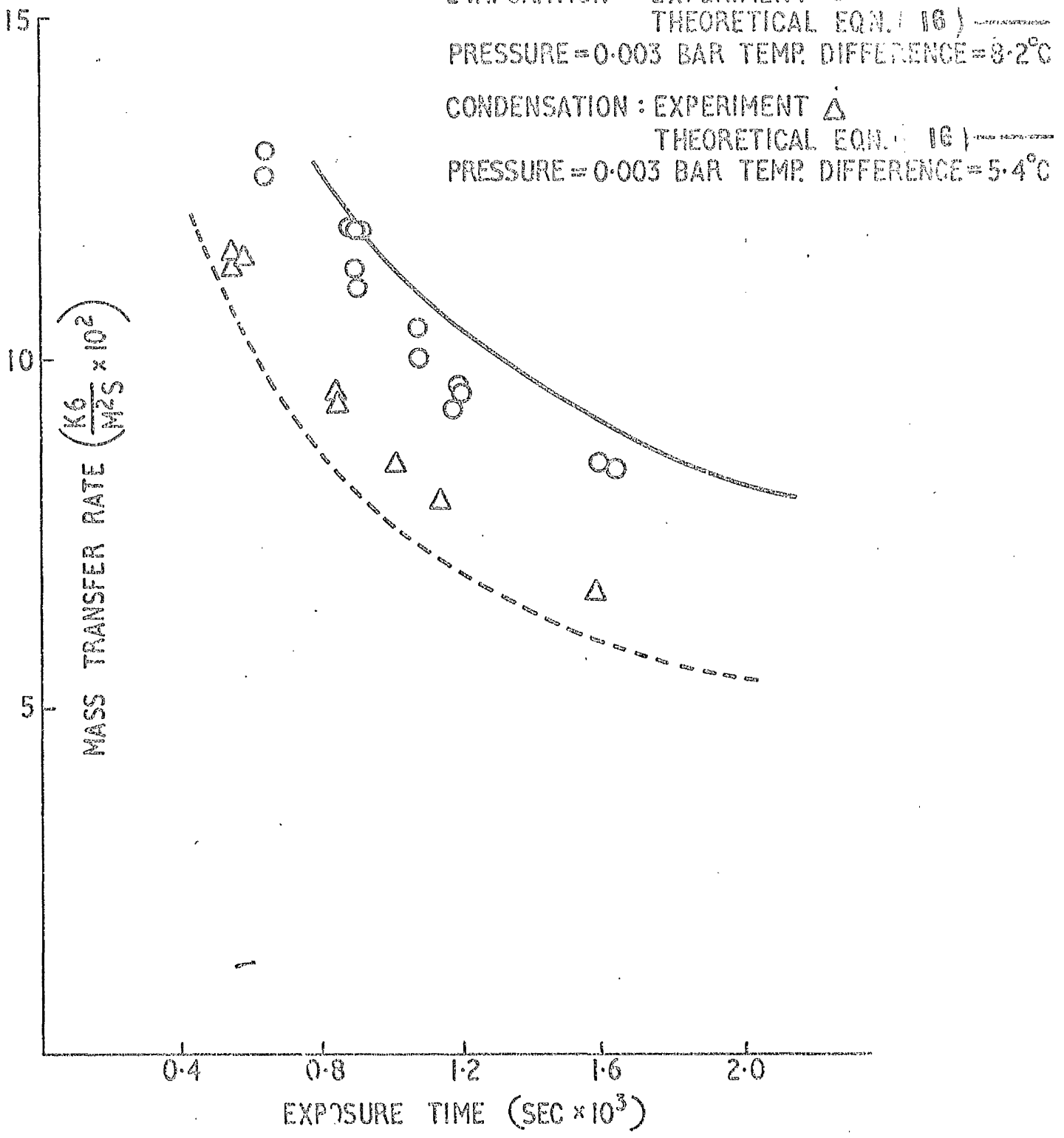

Fig. 2 Comparison of predictions of eqn.(16) Hickmans data.

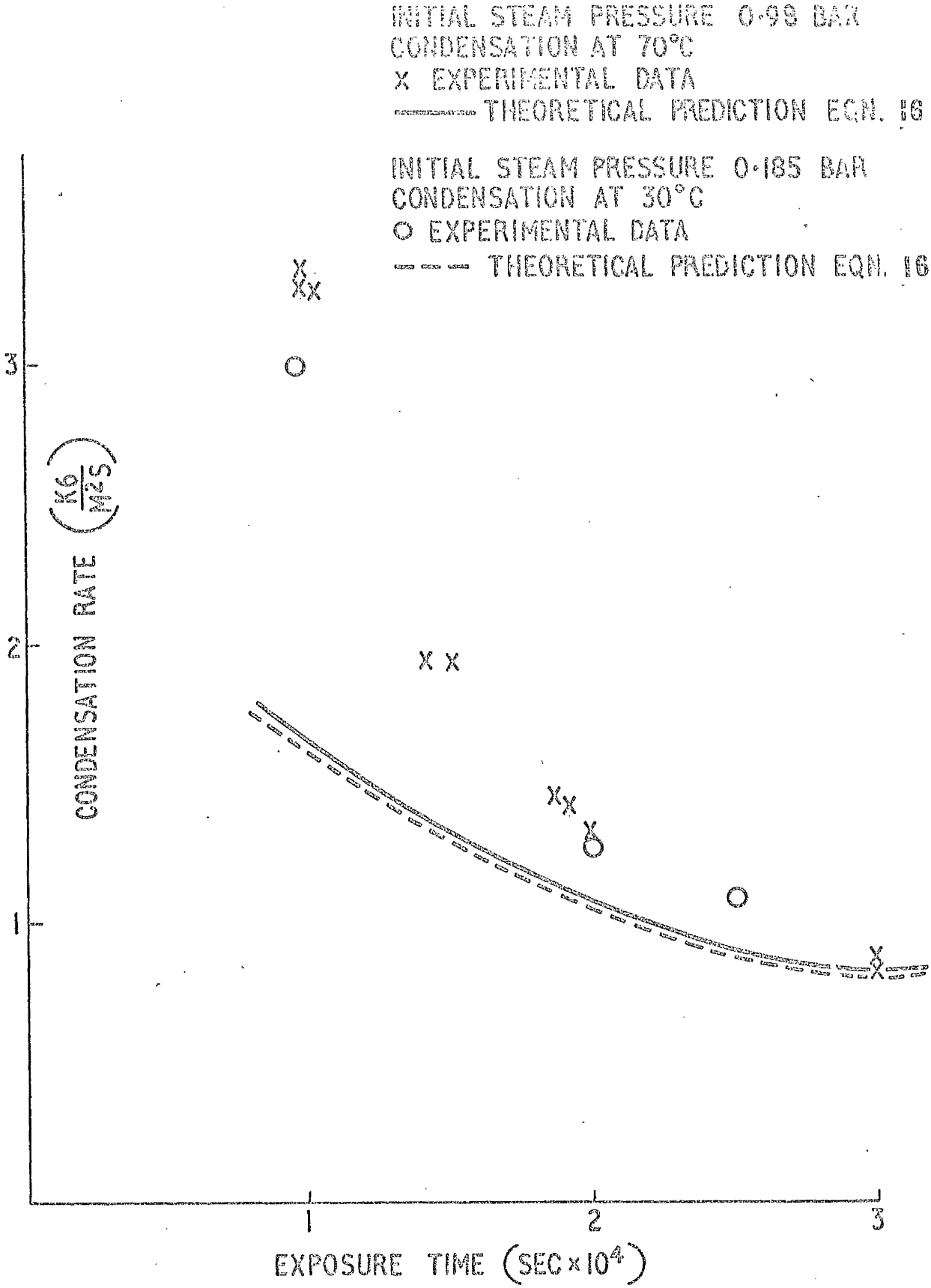

Fig. 3. Comparison of predictions of eqn. (16) with data of Jamieson

"Aspects of Two-Phase Critical Flow of Water in Short Nozzles under Flashing Conditions."

GORDON M. THOMSON, B.Sc.

SUMMARY

The phenomenon of choking or mass limiting flows of two-phase mixtures is well known. The particular case of choking two-phase flow in which mass transfer takes place between phases is designated two-phase critical flashing flow, and has been the subject of many theoretical and experimental investigations.

In this work, experimental and theoretical studies are described for critical flashing flows of water at temperatures between 120 ^{o}C and 140 ^{o}C with maximum system pressures of 10 bar.

A simple model for turbulent heat transfer is developed from the Reynolds Flux model by introducing a second parameter into the descriptive equations. This revised flux model is adapted for prediction of rates of evaporation and condensation from the surface of water jets, exposed to large variations of surface pressure for short time intervals (of order 1 millisecond). The predictive equation, for evaporation rates, is shown to be applicable to experimental situations similar to these found in certain types of critical flashing flow.

A new model of critical two-phase flashing flow is developed using this method of predicting evaporation rates.

By comparison with experimental data, the model is shown successfully to predict rates of critical flashing flow of water, in nozzles, in cases where the flow is subcooled upstream of the nozzle entrance.

For the experimental tests, initially subcooled water at temperatures up to 140 ^{o}C and pressures up to 7 bar was discharged to atmospheric conditions through test nozzles. The choking condition was obtained by varying the upstream pressure while maintaining constant downstream conditions.

The test nozzles were metal with circular cross-sections and consisted of one of three simple forms of converging entrance before a parallel section at the throat. The nozzles formed a set having lengths of 50 mm, 75 mm, 100 mm and 125 mm for each of two throat diameters of 12.5 mm and 25 mm. Nozzles were made with three different entrances for each length and diameter. Data are reported for critical flashing flow rates of water in this set of nozzles. By using one single set of nozzles on the same apparatus, the effects of variation of critical flow rate with Length/Diameter ratio could be examined with greater certainty than has previously been the case for low pressure critical flashing flows. Pressure profiles of the flow within the nozzles are reported showing the variations of pressure profiles with nozzle length and entrance profile at the choked condition. Measurements of dissolved air in the water used in the experiments are also included.

The experimental data are compared with the assumptions made in deriving the theoretical model and with the predictions made from the theoretical model.